A Comparative Computed Tomography Study of Canine Laparoscopic Abdominal Anatomy Pre- and Post-Insufflation

By

Ross Christopher Elliott

Submitted to the

Faculty of Veterinary Science

University of Pretoria

In partial fulfilment of the requirements for the degree

MMedVet (Chir) (Small Animals)

Pretoria, 2011

SUPERVISOR:

Prof. RM Kirberger

Diagnostic Imaging Section

Department of Companion Animal Clinical Studies

Faculty of Veterinary Science

University of Pretoria

TABLE OF CONTENTS

ACKNOWLEDGEMENTS

To my beloved fiancé, Shona-Lea, thank you for all your support through the late nights, turmoil and triumphs of this dissertation.

To my promoter, Prof. R. Kirberger, thank you for all your help and advice.

To Dr. K. Joubert, thank you for your help with obtaining the data and your endless encouragement.

To Sr. M. McClean and Sr T. Serfontein, thank you for all your help with the data collection and computer work.

To Prof. R. Lobetti, thank you for helping with the statistics and for your patience in explaining them time after time.

To all at the Bryanston Veterinary Hospital, thank you for your support.

LIST OF FIGURES

the left ovary to the caudal pole of the left kidney

LIST OF TABLES

LIST OF GRAPHS

LIST OF ABBREVIATIONS

CT   Computed Tomography

CTDI   Computed Tomography Dose Index

HU   Hounsfield Units

LL   Left Lateral

MRI   Magnetic Resonance Imaging

OVAH   Onderstepoort Veterinary Academic Hospital

PoI   Post-insufflation

PrI   Pre-insufflation

RL   Right Lateral

UPBRC   University of Pretoria Biomedical Research Facility

VDR   Ventro-Dorsal Routine

VDT   Ventro-Dorsal Trendelenburg

VE   Virtual Endoscopy

SUMMARY

A Comparative Computed Tomography Study of Canine Laparoscopic Abdominal Anatomy Pre- and Post-Insufflation

Elliott, RC. University of Pretoria, 2011

Laparoscopy has been shown in human medicine to have a rapid recovery time and less morbidity when compared to open abdominal surgery. It involves the insufflation of carbon dioxide into the peritoneal cavity. This creates a space for the surgeon to work in and manipulate the organs. In the normal abdominal cavity the peritoneal cavity is a potential space obliterated by the serosal contact between all the organs. The insufflation of carbon dioxide turns this potential space into a working space. This allows the introduction of an endoscope, usually through a single port, and then various instruments usually through another port into the peritoneal cavity. Multiple veterinary studies have shown the advantages of laparoscopy to decrease the morbidity of animals post surgery. The visualisation of the organs tends to be enhanced by the increased lighting and magnification provided by the laparoscopic equipment.

There are intricate attachments and associations between various abdominal organs that are responsible for maintaining organ position and orientation in the peritoneal cavity.

Computed tomography (CT) has been proven in human medicine to show excellent abdominal anatomical resolution. It is the modality of choice to detect free abdominal gas. Logically, if there is a massive insufflation of gas, it would be expected that this will enhance the ability of CT to provide real anatomical likeness to the laparoscopic image. The animals were all subjected to multiple CT scans and the scans were found to be rapid and non-invasive. There was a concern over the amount of radiation that each animal received and this was pre-empted by using a CARE 4D dose. The CT machine detected the thickness of the part of the animal being scanned and only provided the needed kV and mAs to penetrate and create an image. This was a paediatric human modality. Six beagle dogs were used and all assessed prior to the study to be clinically healthy. An abdominal ultrasound was performed to assess that they had normal abdominal anatomy. All animals had eight scans performed, four pre-insufflation (PrI) and four post-insufflation (PoI). The animals were placed in a ventro-dorsal routine (VDR), a ventro-dorsal Trendelenburg (VDT), a left lateral (LL) and a right lateral (RL) position. The scans were performed using a helical dual slice sliding gantry CT machine, Somatom Emotion (Siemens AG, Erlangen, Germany).

With the insufflation of carbon dioxide in this study, the attachments and associations change and these were shown to play a role in the movement of the abdominal organs during the manipulations and how the organs come to lie in the abdominal cavity. It was shown that together with the insufflation of carbon dioxide into the abdomen, a very

important factor in the movement of the organs was gravity. In certain organs the effect of gravity was found to be the significant factor when the positioning of the animal was changed, more so than the insufflation of the abdomen when PrI and PoI scans were compared. The effects of gravity during the changes in position and the insufflation of the abdomen were compared using a set number of measurements, of organ size and location. The size and location of the organs was compared to set landmarks in the body such as the sternum and certain vertebra, depending on the organ in question. These measurements were compared between the pre- and post-insufflation scans to evaluate the changes that occurred after insufflation with regards to the movement of certain organs and their exposure for a surgical approach. These measurements gave the data an objective value which could then be analysed statistically to determine any significant changes. The p value was set at <0.05 in determining statistical significance using a Kruskal-Wallis one way of variance (ANOVA) and the Tukey-Kramer multiple comparison test. This data was analysed and used to determine the best position to place an animal in order to perform laparoscopic surgery of certain organs.

This dissertation showed that the VDR and VDT positions proved much better laparoscopic access to the majority of the parenchymatous organs in the peritoneal cavity than the lateral positions. There were certain organs such as the kidney, the ovaries, the uterine horns and the duodenum that were visualised on CT clear of the rest of the parenchymatous organ mass on the non-dependant part in the respective lateral positions. This indicated that these organs will be easily accessible during laparoscopic surgery in the RL and LL. However no matter what position was used, no position was perfect for every organ of interest, and positions need to be combined for certain procedures. The use of positioning will not remove the need for intra-operative retraction and laparoscopic retractors are an essential part of the surgeon's arsenal when performing laparoscopic procedures.

CHAPTER 1: INTRODUCTION

1.1 Background

Laparoscopic surgery has evolved into one of the cutting edge techniques in modern surgery. This is due to the ability to magnify the operating field and perform a multitude of surgical procedures with a minimally invasive approach and provide illumination in the surgical field. This decreases patient morbidity and recovery time. However, the cost and relatively steep learning curve have made this modality less accessible to the veterinary surgeon in the past. Laparoscopic surgery has progressed in Europe and the United States in the last two decades. The use of this technique in these countries has led to a handful of experienced specialists.

In South Africa there is an increasing demand by veterinary surgeons to learn this technique. However, there is limited exposure in countries outside of Europe and the United States. To gain the experience needed to be proficient in these techniques, it is proposed that by examining the alterations in the abdominal anatomy with post-insufflation (PoI) computed tomography (CT), this will provide a learning platform for the novice surgeon.

1.2 Research Question

How does the introduction of air/gas into the peritoneal cavity alter the topographic anatomy for the laparoscopic approach to the abdominal organs?

1.3 Hypothesis

The air/gas introduced into the peritoneal cavity will fill the potential space of the peritoneal cavity and cause the organs to separate and gravitate to the side of the body in relation to the organs' suspending ligaments or mesentery.

Post-insufflation CT accurately depicts the anatomical relationship of the organs in relation to the normal organ position.

1.4 Benefits

By providing a reference of the expected anatomy during laparoscopy, this will help to teach and improve the skill of surgeons using this modality.

It is hoped that it will lead to more advanced procedures, with laparoscopy becoming common place in veterinary medicine and thus decreasing the post-operative morbidity of our patients.

It forms part of the fulfilment of the requirements of the MMedVet (Chirg) (Small Animals) degree.

CHAPTER 2: LITERATURE REVIEW

2.1 Introduction

Surgeons have long been looking for methods to decrease the degree of trauma caused by surgery. Laparoscopy has given the surgeon the tools and ability to provide similar if not better visualization of the surgical area through a much smaller approach, resulting in less tissue trauma caused by making the approach and less adhesion formation post surgery[1].

Laparoscopy is a relatively new modality in veterinary science and the visualization of the anatomy may confuse even the most experienced surgeon adapting to the modality. The surgeon must adapt to looking through a port on a monitor, at an angle ranging from 0-60˚. The peritoneal cavity is filled with carbon dioxide which displaces many organs to the dependant surface, thus altering the anatomy.

Computed tomography has been shown to be a reliable representation of anatomical topography[2]. The aim of this study was to describe the abdominal anatomy once carbon dioxide had been insufflated into the abdominal cavity. This was to determine how the topographic anatomy after insufflation with carbon dioxide differed from the anatomy prior to insufflation. It was largely affected by the position of the animal, the effect of gravity and the support of anatomic ligaments associated with the viscera in the abdomen. This will hopefully give the surgeon an insight as to what would be visible through the port of the laparoscope during surgery.

2.2 Computed Tomography

Computed tomography has proven to be the diagnostic imaging modality of choice for imaging the abdomen in human medicine[2]. The increased availability of veterinary CT means it is fast becoming the modality of choice for abdominal imaging in cats and dogs and gives a reliable representation of cross-sectional anatomy[2, 3]. Computed tomography has the ability to aid in making a diagnosis for many diseases, however the specificity can be limited. This is not due to the image quality but due to the limited number of basic pathological responses of the tissues to a disease process. For example, oedema, inflammation and neoplasia can all increase the water content of an organ and thus decrease the attenuation of the x-ray photons. This will decrease the Hounsfield units (HU) of the soft tissue[4].

Cross-sectional imaging has the advantage over conventional radiographs in that the image is depicted without the effects of superimposition and has superior soft tissue differentiation (contrast resolution) [3, 4]. The spatial resolution of CT is far superior to conventional radiographs[4]. This is due to the physics behind the formation of a CT image.

The image is made up of a number of slices, usually contiguous, through the area of interest. The image is made of differing shades of black, white and grey (the grey scale). The entire CT image is made up of tiny squares called pixels. The higher the number of pixels, the better the spatial resolution[5]. Each of these pixels represents a small volume of tissue in the final image, a voxel. The grey scale value assigned to each pixel is determined by the degree of attenuation of the x-ray beam by the tissue in question and the linear attenuation coefficient which describes the fraction of x-rays removed per unit thickness of tissue. The degree of attenuation is linked to the type of tissue and the ability of the tissue to remove x-ray photons from the beam either by scatter or absorption[4, 6, 7]. As the beam is attenuated while passing through the body, the photons are removed according to the law of exponential decay or attenuation according to the following equation: $N=N_0e^{-\mu x}$. N_0 is the initial number of photons. N is the number of photons transmitted which is measured by the detecting device. The base e is the natural logarithm, x is the thickness of the absorber and μ is the linear attenuation coefficient. All the factors are known or can be measured and thus μ can be calculated for any tissues or substances measured[7]. Similar to conventional radiography the degree of attenuation represents the relative densities of the tissue. This is the atomic number and physical density of the atoms that make up that portion of tissue. The final grey scale assigned to the pixel will represent the average of all of the above. If two differing densities fall in the same pixel the computer will take the linear attenuation coefficient and average them to give the final grey scale value for that pixel[5, 6, 7]. The spatial resolution is enhanced by the ability of the computer to optimize the difference in attenuation of the x-ray beam. As the x-ray tube and the detectors rotate around the patient, the detectors pick up the remnant photons representing the attenuation sum from the primary beam from multiple projection angles. The intensity as it leaves the x-ray tube is measured, so it is known for the computerized calculations [5, 7]. In the detectors there are scintillation crystals that the photons fall on. These crystals emit light in response to the photons. The amount of light produced by the detector depends on the number of photons striking it. The light then strikes the photocathode of the photomultiplier tube and this produces electrons which in turn create an electric current. The electrical current is measured, amplified and converted to digital numbers directly proportional to the number of photons striking the detectors[7]. With all the factors in the equation of linear decay being known or measured, the computer can then process all the raw data[5]. This enables the computer to reconstruct an image from the attenuation profiles representative of the tissues in their topographic positions. This is termed filtered backprojection[7]. This is the back bone of image reconstruction and involves complex mathematical equations.

Once all the information of the scan has been collected, the computer will transfer all the information received into an image, assigning each pixel a grey scale value based on the degree of attenuation of the portion of tissue in that area. This is the primary image construction. Each grey scale value is assigned a HU[6, 7]. The computer assigns each pixel a number which carries the representative grey scale value for the degree of attenuation of

that portion of tissue. These units or numbers can be changed to increase the resolution of the scan. This is called manipulating the window width. Bone carries a HU of +1000, water 0 and air -1000. The window width represents the range of HU above and below the window level, which is the central HU in the window used for the reconstruction[4, 5]. With a wide window width the grey scale has to represent a large number of densities giving a low contrast. With a narrow window width a large number of HUs has to represent few differing densities thus allowing more shades of grey available to represent different tissue. Tissues outside of the window will be shown as black or white with few shades of grey assigned to them. This allows tissues with small differences in density to be visualized as the highest number of HU are assigned to the tissues of interest. This gives the image a high contrast[5, 7]. For abdominal imaging a narrow window is selected as there are many organs of similar densities in the abdominal cavity. The human eye perceives fewer shades of grey than the computer provides so the resolution is decreased further by the human factor. Thus windowing is very important in image quality and making a diagnosis. Hounsfield units are not specific for any tissue but just a quantification of the x-ray attenuation for the representative portion of tissue. However most 'normal' tissues in the body have a specific range of HU. This can be used to check the organ for pathology that may increase or decrease the HU represented by that tissue. For example, if the liver becomes oedematous the HU will drop below the normal range and it can then be quantified that the density of the liver is less when pathology is present[4]. Hounsfield units enable a viewer the potential to quantify the changes that they are seeing, rather than an objective assessment of density. Slice thickness will affect the resolution of the image in that the narrower the slice thickness, the closer the representation of the attenuation of the beam for that specific pixel[5, 6]. This gives better spatial resolution. The smaller the slice thickness, however, the longer the scanning time and thus a higher potential for motion artefacts[4, 5, 6]. Pitch or table speed can affect the resolution of the image as well as the life of the CT machine. In helical studies a continuous image is taken as the patient moves through the gantry. The image is taken in a spiral fashion related to pitch and gantry rotation time. In helical CT the patient moves through the gantry and the gantry rotates round the patient. There will be "gaps" in the data for the final image in the detectors. The lower the pitch and the faster the gantry rotation speed, the fewer "gaps" will be created by the x-ray tube and the detectors. The gaps that are present will be represented by volume averaging in the final image[8]. This will decrease the spatial resolution. However, as the scan time is increased in an effort to increase the resolution, this may create motion artefacts which will markedly decrease spatial resolution[8]. A trade-off between slice thickness, gantry rotation speed and pitch needs to be met to gain the best image for the particular study being performed. Increasing the gantry rotation speed and decreasing the pitch may cause overheating in the x-ray tube in some of the older helical machines. This has been managed by providing sophisticated cooling systems in the x-ray tube[8].

A further way to differentiate tissues is by the use of contrast media. The most commonly used media may be injected intravenously or administered orally. To highlight the intestinal system, iodinated contrast media can be used *per os*, at 10ml/kg, two hours before scanning and a further 3ml/kg just prior to scanning[9]. However this is expensive compared to barium. Oral barium contrast media are more commonly used for radiographic studies of the gastrointestinal system and are administered at 6-12ml/kg[7]. Intravenous contrast media are iodine based. These are administered prior to scanning and will highlight the arterial or venous portion of the circulation depending on when the CT is performed post injection of the contrast. Iohexol (Omnipaque, GE Medical, London, United Kingdom), a non-ionic iodinated contrast medium, is usually administered at 814mg iodine/kg. At least two scans should be done from 2 seconds to 40 seconds after injection to find the best image of the phase of interest[9, 10]. This is known as dual phase angiography. The arterial phase is visible in the initial scan right after injection and depending on the animal, the venous phase ranges from 34-40 seconds after injection[9, 10, 11]. This aids to differentiate between organs, as well as differentiate organs from vasculature. The administration of IV contrast media is not without side effects. Toxic nephrosis has been reported with use of ionic contrast media[9, 10, 11]. This has been linked to existing renal disease, hypotension and the use of high doses of contrast media. Air or carbon dioxide should provide excellent negative contrast in the abdomen once insufflated into the peritoneal cavity.

By convention the patient is placed in dorsal or sternal recumbency for the CT scan. Most procedures are done in a cranial to caudal direction, however this can affect image quality due to the movement of the thoracic cavity during respiration. Breath hold techniques to create hypocapnoea are unreliable in creating apnoea but if a thoracic scan is performed in a caudal to cranial direction there will be less affect as the scan reaches the cranial part of the thoracic cavity as movement is less in this area. For abdominal scans the reverse could be true in that there will be more effect in the cranial abdominal cavity adjacent to the diaphragm from respiration and hence this should be scanned first. In humans the image can be collected with the patient holding his or her breath. In most animals, however, it requires sedation or general anaesthesia for them to be kept still. Under anaesthesia, hyperventilation with positive pressure ventilation is used to create a period of hypocapnoea and the resultant apnoea can provide enough time to complete a scan, but this is not reliable. The use of muscle relaxants such as scopolamine can aid in decreasing respiratory motion but does complicate the anaesthetic in thoracic scans and seems unnecessary in such a potentially short procedure[8]. A simple way of creating apnoea is to hyperventilate the patient manually then inflate and hold the patient in this state for the duration of the scan. It is less of a problem in abdominal scans but one has to take movement from breathing in the cranial abdomen into consideration. The effects of peristaltic movement on image quality also has to be considered when scanning the abdomen, as having intestines filled with contrast may stimulate increased peristalsis.

The indications for CT in small animals are increasing at an amazing rate. With more practitioners having CT available to them, more information is being acquired. Computed tomography has been used commonly in the investigation of nasal disease, fractures of the skull with associated intracranial haemorrhage/ haematoma and intra-cranial neoplasia[12]. The advantage of CT over magnetic resonance imaging (MRI) for cranial studies is the speed of image acquisition in the compromised neurological patient. Computed tomography is the modality of choice for metastasis of neoplasia to the thorax and intra-thoracic masses[12]. Computed tomography is the imaging modality of choice to detect, stage and monitor pancreatic neoplasia in human medicine[13]. Computed tomography of the canine pancreas has been described using dual phase CT with intravenous iodinated contrast injection to view the arterial, parenchyma and venous supply of the pancreas[14]. This provides information on the invasion of the vasculature by pancreatic neoplasia. It has been shown that the pancreas can be detected by using the portal vein for the body of the pancreas, the descending duodenum for the right lobe and the dorsal extremity of the spleen and the gastric fundus for the left lobe. This has been shown to be more accurate than using the kidneys to locate the pancreas[15]. Computed tomography has shown accurate representation of the topographic anatomy of the canine and feline abdomen[16, 17]. The bile duct can be visualized and obstruction of this structure can be viewed. Computed tomography will provide excellent visualization of the liver and the portal vasculature[9, 11, 17, 18]. Dual phase angiography can help make a diagnosis of portal systemic shunts, arterio-venous fistulas and neoplasia[9, 10, 11, 18]. This gives a non-invasive method of making the diagnosis of a shunt[10]. The ureters which are not usually seen on conventional radiography or ultrasonography can be visualized by CT. They can be seen in pre- and post contrast images. The ureterovesicular junction can be assessed thus facilitating diagnoses in that area[19]. Excretory urography with intravenous injection of iodinated contrast can be performed with CT rather than conventional radiography to diagnose ectopic ureters. It is more sensitive and accurate than conventional radiography[19]. Computed tomography plays a major role in staging and diagnosing metastatic abdominal neoplasia and primary abdominal neoplasia[12]. This is predominantly true in the organs that are not seen on routine radiographs such as the pancreas and adrenals. Computed tomography has shown to be useful in differentiating malignant from non-malignant splenic masses in dogs. These will obviously need a biopsy to confirm, but CT can provide an idea of prognosis[12, 20]. Computed tomography will detect changes in these and all of the abdominal organs earlier than ultrasound and conventional radiography thus making therapeutic procedures more successful.

A new exciting spin off from CT is the concept of virtual endoscopy (VE). This is a three dimensional reconstruction of the CT image. The image is collected as for routine CT then processed by the computer using a reconstruction increment, usually of 1mm. The thinner the slice thickness, the higher the spatial resolution of the three dimensional reconstruction[21, 22]. This provides the benefit of a non-invasive diagnostic procedure to detect small abnormalities. The quality and accuracy of this modality has been shown in

human studies to be excellent. This allows the viewer to do a 'fly by' through the lumen of the hollow organ. A fly by gives the viewer the impression that the viewer is within the lumen of the viscus[21, 22]. The image moves through in real time giving the viewer an impression of contour and mucosal irregularities. The sensitivity has been shown to be better in the lumen of a hollow tube as this allows a straight fly through of the lumen[22]. A hollow viscus doesn't allow a straight fly through given the nature of the organ, however one can visualise the inner surface of the organ from any angle. For the best image quality it is important to have an inherent contrast. The oesophagus, for example, is a collapsed tube in its normal state[21]. To dilate the oesophagus and stomach, effervescent granules have been used in man. A stomach tube can be passed into the stomach and air introduced in this fashion. This has been used in dogs at the Onderstepoort Veterinary Academic Hospital (OVAH). Virtual endoscopy has been shown to represent the anatomy of the stomach accurately in humans, showing normal anatomy of the pylorus, gastric folds and the incisura angularis[23]. In humans, imaging of the pancreas is accomplished with insufflation of medical carbon dioxide. This has shown excellent results in detecting pancreatic neoplasia early and less invasively by means of VE[13]. This holds promise for detection of serosal abnormalities in the peritoneal cavity in dogs. If contrast can be given into the lumen of the viscus, a virtual endoscopy of the mucosal surface can be done. This has been shown to be sensitive in detecting small (1-3mm) neoplasm's of the bladder and ureter when intravenous iodinated contrast is injected and time is given for it to be concentrated in the bladder and ureter[22].

Virtual endoscopy has been used to diagnose the cause of death and investigate the mummies of ancient Egypt[24]. With the increasing quality of CT imaging the sensitivity of the diagnostic qualities in making the correct diagnosis will increase.

The levels of radiation in CT when compared to conventional radiography are substantial. Unconfirmed reports put it as 100-500 times higher per exposure. The level of radiation should be kept at the lowest dose possible. The Siemens CARE 4D scanning protocol delivers the lowest dose possible based on adaptations made to the patient's size. As the tube rotates around the patient, the tube determines adequate tube current levels according to the patient's angular attenuation profile. The tube's current modulation is based on the angular profile on the long axis of the patient attained from a single topogram (dorsoventral or lateral). This leads to the optimal intensity of radiation being delivered in real time scanning, with the patient not being exposed to unnecessary radiation[26]. The advantages of CT such as speed of scan, resolution and ability to make a diagnosis without having to do an invasive surgery, far outweigh the potential risks of increased radiation.

2.3 Laparoscopy

Laparoscopy has been shown to provide excellent visualization of the peritoneal cavity with clear video images and magnification[27]. The morbidity of the procedure appears to be less than for the same diagnostic and therapeutic procedures performed via a ventral celiotomy[27].

With the advent of laparoscopy and the increasing demand in veterinary science for less invasive procedures, it is becoming more common for veterinarians to perform laparoscopy. Once air is introduced into the peritoneal cavity, it becomes more than a potential space and the different organs separate depending on gravity and position thus making laparoscopy possible. This is called peritoneal insufflation. It is obvious that in order to do this specialized equipment is needed[27, 28].

The basic equipment needed can be used for laparoscopy as well as thoracoscopy, otoscopy, rhinoscopy and cystoscopy. The essential components are the endoscope which ranges in size from 1mm to 10mm in outer diameter. In laparoscopy the most commonly used diameter is 5mm. The larger an endoscope the more light it will transmit and the larger the images. Smaller diameter endoscopes will fit into smaller spaces but will transmit less light. The tip of the endoscope comes as a 0˚ forward viewing endoscope or 30˚ viewing angle. The 0˚ is easier to triangulate for novice surgeons but gives a smaller field of view[28, 29]. The 30˚ gives a wider field of view but this is offset by 30˚ to the centre and takes experience to triangulate while operating[28]. A light source is essential to illuminate the abdominal cavity. The most common sources are halogen and xenon. Halogen is the more economical choice, but xenon produces higher quality, more powerful light at a higher price. Xenon produces more lumens per watt energy and produces a higher colour temperature of 5700 Kelvin compared to halogen of 3000 Kelvin. This is a whiter, cleaner light compared to halogen[29]. A video imaging system is not essential but has many advantages. The video system consists of a video camera, fibre optic cables, camera control unit and a video monitor[27]. Although the region of interest can be viewed directly through the eyepiece, a video system makes performing the procedure more comfortable for the surgeon. It doesn't compromise the sterile field, it allows for documentation of the procedure and it enables the entire surgical team to view the procedure, which facilitates teaching. The camera attaches to the eyepiece. The camera head contains an objective lens, a prism assembly and one to three sensors or chips. The chip/s are responsible for sensing the image, converting it to an electrical signal and transmitting it to the monitor. Single chips transmit all three of the primary colours, whereas three chip cameras have a chip for each of the primary colours[28, 29]. The video monitor provides the final image and hence the final picture quality. However, the cable links the camera to the video monitor so in purchasing a high quality camera and monitor one needs a high quality cable to transmit the image. Depending on

whether a single chip or three chip camera is used, it must be linked to the correct cable and video monitor. Due to financial constraints, high quality single chip cameras are most commonly used in veterinary endoscopy.

In laparoscopy, an insufflator is required to induce a pneumoperitoneum to separate the abdominal organs and create a space for the surgeon to work in. The most commonly used inert gas is carbon dioxide. Room air carries a higher risk of fatal air embolism. Pure oxygen is flammable and is ill advised in the presence of cautery or surgical lasers. The recommended abdominal pressure with carbon dioxide insufflation is a maximum of 14 mm Hg which can be decreased to 10 mm Hg after the operating cannula has been introduced[27, 28]. The insufflator will maintain the pressure and regulate gas flow to maintain the pneumoperitoneum, whilst not exceeding the pressures stated above. Increased pressures above 14 mm Hg can compromise venous return and respiration[28].

The essential ancillary instrumentation needed consists of a sheath and a cannula for insufflation and a simultaneous instrument port. A sheath implies that the tube locks onto the endoscope and provides anatomical access and passage of fluid and carbon dioxide into the peritoneal cavity, whereas a cannula implies the endoscope or instruments are freely movable within the tube. Operating sheaths serve a number of functions: protection of the endoscope, preventing the operating instrument from bending, maintaining anatomical access and allowing the ingress and egress of fluids and carbon dioxide into the peritoneium[27]. There are sheaths that allow the passage of an instrument alongside the endoscope. Most instruments are passed through a separate cannula under direct visualization of the camera. Most cannulae have a trocar with a pyramidal cutting tip to facilitate piercing the body wall which provides a portal to the peritoneum. The cannula contains a Luer-lock which snaps shut once the instrument has been removed, which maintains the pneumoperitoneum during the surgery. A rubber washer provides a tight seal around the instrument when it is placed in the cannula[29]. There are newer cannulae that do not require a trocar to place. They are placed through a small skin incision and then screwed in to the abdominal wall. The fit is more secure, with less chance of the port pulling out during the procedure and there is less risk of iatrogenic damage during placement[27]. The Veress needle is a modified cannula which is used specifically for insufflation of the peritoneal cavity; it is not essential for laparoscopy but will aid insufflation. The needle is placed in the same port that will be used for the camera port placement. It is usually placed blind through a small stab incision at the chosen site, usually in the midline or the paralumbar fossa depending on the surgical procedure. The needle consists of a sharp outer spring-loaded sheath with a blunt hollow inner stylet, through which the gas passes. As the needle is passed through the abdominal wall, the spring-loaded outer sheath retracts over the blunt hollow inner tube due to the loss of pressure on the outer cannula to decrease the risk of damage to vital organs[28]. This is the described technique for placement of a Veress needle[28]. A Hasson technique can be performed without the need for a Veress needle. This entails performing a small incision into the ventral abdomen, usually in the area of the

umbilicus. The linea alba is identified and lifted up. A stab incision is made through the linea alba. This incision is just large enough to place a cannula in and this cannula is secured by screwing it through the muscle or by placing a purse string suture[27]. Hasson cannulae are available commercially but a standard cannula can be used.

The most commonly encountered problems with placement include placing the needle subcutaneously or retroperitoneal, placing the needle in the omentum or falciform fat, and penetration of a viscus. Subcutaneous placement is not fatal but will impede the technique. Penetration of the spleen will result in haemorrhage which can impede visualization but this is rarely fatal[27, 29]. However, insufflation of air into a mass, organ or vessel can lead to fatal air embolism. Once the needle is in place, the sterile tubing is placed and insufflation is begun. Abdominal pressures should be low initially (2 mm Hg) and if it rises rapidly, this indicates incorrect placement of the needle or blockage of the needle[28]. Once the abdomen is insufflated to 10-14 mm Hg through the Veress needle, the primary trocar and cannula are placed, the camera is inserted and the site of the primary cannula and Veress entry site is examined for damage[27]. Secondary cannulae are then placed under direct visualization. The tubing can then be transferred to the cannula port and the Veress needle removed[29].

There are a multitude of secondary endoscopic instruments that are available from biopsy forceps to stapling devices. Practically every routine surgical instrument has a smaller endoscopic version. Depending on the procedures being performed, the surgeon should have the available instruments[27].

Positioning of the patient depends on the procedure being performed. Liver procedures are most commonly performed in left lateral recumbency with a right lateral or a ventral approach providing better access to the ventral surface of the liver. The best approach may be obscured by the falciform fat. The first cannula is placed in the right paralumbar fossa with a secondary cannula in line but closer to the midline. This provides access to the liver, gallbladder, extra-hepatic billary system, pancreas, right kidney and 85% of the liver including the hilus. Liver, kidney and pancreatic biopsy are the most commonly performed procedures using laparoscopy. The extra-hepatic billary system can be palpated with a blunt laparoscopic probe and with experience the surgeon will gain a 'feel' for normal anatomy through the probe. Patency of the billary tract can then be assessed[30, 31]. Laparoscopic biopsies of the pancreas, kidney and liver are superior to tru-cut biopsies. There are fewer complications as the procedure is done under direct visualization and can be observed for haemorrhage[27, 30, 31]. The gold standard in diagnosis of pancreatic and liver disease is a good quality biopsy[31, 32]. Non-invasive imaging techniques can indicate pancreatic disease and together with blood tests, can point in the direction of pancreatic disease[31]. Laparoscopy has been proven to be a safe, reliable method of attaining biopsies of these organs[27, 31]. This will prognosticate the disease process. In dogs, mesenteric lymphadenography performed via laparoscopy has shown to be comparable to celiotomy performed lymphadenography. This then potentially allows a thoracoscopic thoracic duct ligation[33]. It is less invasive and

will aid in surgical assessment of dogs with chylothorax. With laparoscopy being used more commonly, many other indications have become apparent. One of the more recent advantages is prophylactic gastropexy in giant breed dogs at the time of laparoscopic ovariohysterectomy or as an elective procedure on its own using a right lateral or ventral approach. It has been shown that prophylactic gastropexy will decrease the incidence of gastric dilatation volvulus in dogs[27, 34]. The functional strength of a laparoscopic gastropexy is similar to the adhesion formed with other reported open techniques 10 weeks after surgery[35]. There was minimal alteration in gastric emptying at the same time post-operation in the reported dogs. This will prevent a gastric dilatation volvulus in dogs prone to the condition.[27, 32, 36].

Laparoscopy is one of the main methods of performing abdominal surgery in humans with dogs being used as an experimental model for humans. There are complex human procedures that are being performed on canine models as pilot studies for humans. This is exciting for veterinary surgery as we can hopefully adopt some of these procedures. Segmental liver lobe resection and complex pyloroplasty, including Heineke-Mikulicz pyloroplasty, have been done on canine models from a right lateral approach[37]. The Heineke-Mikulicz pyloroplasty has been used to correct outflow obstruction of the pylorus in dogs. This has shown success when compared to conventional pyloroplasty via abdominal surgery when evaluated with ultrasound post operatively[2, 38].

A left lateral approach would be the mirror image of the right lateral approach. This approach will provide access to the liver, spleen, left kidney and the fundus of the stomach. The indications for the approach are much the same as for the right lateral approach. Gastrotomy has been reported with the use of Endobags, a type of sterile expanding bag by which organs or masses can be removed via an expanded port. Foreign bodies have been removed from the fundus of the stomach with the Endobag[32]. This can be done via a left lateral approach or a ventral approach[27, 39].

The ventral approach with the animal in dorsal recumbency is the most commonly utilized approach. The most common indication is laparoscopic ovariohysterectomy, with most of the teaching and research on veterinary laparoscopy done as an expansion on this procedure. Full thickness intestinal biopsies and placement of gastrotomy, duodenostomy and jejunostomy feeding tubes have shown promise with laparoscopic assisted procedures[27, 39]. There have been fewer complications associated with the placement of jejunostomy tubes via laparoscopic-assisted placement and the creation of a temporary jejunostomy for faecal diversion in the case of recto-cutaneous fistulas[40, 41]. Complications for a temporary jejunostomy include mild ostomy site dermatitis and rare bile-induced dermatitis in one dog[41]. This can provide nutrition for a compromised patient in the cases of jejunostomy feeding tubes. A portion of the organ is still exteriorized through an enlarged portal to the outside for the surgeon to complete the procedure. Portal placement is slightly different for intestinal biopsies than for an ovariohysterectomy with the camera port

situated in the midline just cranial to the umbilicus and the two instrument ports placed 4-6cm lateral to the midline on either side. The portal placement for ovariohysterectomy has all three portals in the midline caudal to the umbilicus. A modification on the positioning in dorsal recumbency is where the head of the animal is placed 30˚ lower than the sacrum (Trendelenburg position)[27, 28]. This will increase access to the organs in the caudal abdomen. During ovariohysterectomy, the body will be tilted 45˚ to the left and right to gain increased access to the ovaries of the respective sides[27, 42, 43]. Ovariohysterectomy requires excellent haemostasis of the ovarian pedicles and the uterine arteries at the uterine body. Pedicle haemostasis requires dissection and cautery with specific endoscopic monopolar or bipolar grasping forceps or a harmonic scalpel[42, 43, 44, 45]. Alternatively it can be achieved with ligating clips or endoloop, a specific endoscopic device that can pass and tighten a ligature through an instrument portal. Uterine body haemostasis requires either an endoloop system or exteriorization through an enlarged caudal port with routine ligation. The advantage of laparoscopic ovariohysterectomy is that the stretching of the ovarian ligament is avoided and thereby the tearing of the peritoneum is also prevented, which can be painful[42, 43]. The surgical exposure is potentially less than routine open ovariohysterectomy. Studies have shown that the laparoscopic ovariohysterectomy is less painful than conventional ovariohysterectomy[27, 28, 42, 43, 44]. Ovariectomy can be performed as a quicker simpler procedure than ovariohysterectomy, as there is no benefit to removing the uterus and some authors report a lower morbidity and complication rate with ovariectomy[46, 47]. Ovariectomy has been performed with a single or double port technique[46]. This requires increased intra-operative skill but no significant increase in operative time. It is however essential to use a coagulating device when using a single port technique[46]. The complications seen with laparoscopic ovariohysterectomy are, however, minor and include seroma formation and herniation of omentum[43, 44]. Other procedures associated with sterilization include removal of an ovarian remnant and cryptorchidectomy[27, 28, 48]. Laparoscopic assisted cystopexy has shown promising results in removing uroliths, benign inflammatory polyps and investigating urinary tract disorders[27, 49, 50]. This is accomplished by locating the urinary bladder and creating a stoma between the skin and the ventral abdomen. This allows the surgeon to pass a cannula into the bladder and visualize the bladder lumen. Polyps can then be removed similarly to removal of calculi[49, 50]. A report of urethral sphincter mechanism incompetence in a male dog managed with a laparoscopic guided deferentopexy via a modified ventral approach has been described. After transection of the ductus deferens, the urinary bladder is retracted cranially and the ducts passed through incisions in the lateral abdominal walls[51]. Radical prostatectomy has been performed by human laparoscopic surgeons in a canine model and holds promise for canine applications in veterinary medicine with increased exposure[52]. Laparoscopic cholecystectomy is the procedure of choice for diseases of the gallbladder in humans. This can be performed with a ventral approach as described above. Cholecystectomy is indicated for chronic cholelithiasis/mucolithiasis, obstruction of the cystic duct, gallbladder neoplasia and chronic cholecystitis[27, 28, 32]. Dissection of chronic diseased gallbladders is difficult as

they become friable. Puncture of the gallbladder with leakage of the luminal contents is a common complication that should be avoided and necessitates conversion to a laparotomy[53]. Recently there has been a description of cholecystostomy tube placement to divert bile from the bile duct in cases of bile duct stenting or extrahepatic bile duct obstruction[32]. This diverts bile into the intestine in the case of temporary bile duct obstruction such as is seen in pancreatitis or choleliths[32]. Cautery is helpful to control the ooze from the fossa once the gallbladder has been removed. Vascular clips or endoloop devices can be used to ligate the proximal cystic duct[27].

Other potential applications of laparoscopy in animals are adrenalectomy in the case of adrenal tumours, correction of portosystemic shunts, nephrectomy, removal of abdominal and intestinal masses and hernia repair[27, 32].

No surgical procedure is free of complications and laparoscopy is no different. Most complications are rare and relate to surgeon's inexperience. Veress needle insertion can lead to injury of the abdominal wall, penetration of organs and perforation of a hollow viscus as mentioned above. Penetration with a Veress needle can lead to haemorrhage which is seldom fatal. If the air is insufflated whilst the needle is in the organ, there is the potential for fatal air embolism. If air embolism is suspected, place the animal in left lateral recumbency and ventilate with oxygen. This moves air bubbles away from the right ventricular outflow tract thus decreasing the potential for pulmonary embolism[27]. Given the solubility of carbon dioxide, the bubbles will dissolve rapidly and the obstruction will be resolved. Penetration of a hollow viscus is seldom a problem, as small perforations will heal up rapidly. This can be avoided by use of the more invasive Hasson or open technique. Penetration of the diaphragm can lead to pneumothorax which will need to be drained[27, 28]. Insufflation into the subcutaneous tissues leads to subcutaneous emphysema which can be painful but will resolve. With all the specialized equipment needed there is a higher potential for equipment failure. There is always a risk of bleeding from any surgical site which needs to be managed. It has been reported that the carbon dioxide used for insufflation can cause peritoneal acidosis and irritation and a potential cause of post-operative pain[27, 54]. The insufflation of carbon dioxide has been reported to increase the risk of portal site metastasis in laboratory animals that have abdominal malignancy. The risk is linked to diagnostic procedures to evaluate the malignancy such as biopsy and manipulation. Factors influencing portal site metastasis are unknown, however direct contamination, aerosolisation, chimney affect, local immune response and the establishment of a pneumoperitoneum have all been implicated[54].

Patients that have pre-existing pulmonary or cardiac disease are often less tolerant of the carbon dioxide induced pneumoperitoneum. They are susceptible to hypercarbia and hypoxia and conversion to a laparotomy is elected instead of laparoscopy. Another reason for an elective laparotomy instead of laparoscopy is obesity where intra-abdominal fat will obscure visualisation of the intra-abdominal structures[53]. The presence of intra-abdominal

adhesions from previous surgery, liver disease leading to massive ascites or aberrant abdominal anatomy, could lead a surgeon to choose a laparotomy instead of laparoscopy. During surgery, massive haemorrhage which cannot be controlled during laparoscopy requires emergency conversion to a laparotomy[53]. Perforation of a hollow viscus and equipment malfunction both require intra-operative conversion to a laparotomy.

Peritonitis, diffuse neoplasia, pregnancy and intra-cranial disease are all definitive contra-indications for performing laparoscopy. It has been noted that older human patients have a higher risk of intra-operative conversion to a laparotomy. This may affect a surgeon's decision to perform laparoscopy[53].

Laparoscopy provides a less invasive surgical method to make a diagnosis or to treat disease in animals. However, it becomes difficult to use in smaller dogs and cats. The technique can take time and patience to master but once competent, it enables the surgeon to gain excellent diagnostic information with minimal invasiveness. It has been shown in human medicine that laparoscopy potentially causes fewer adhesions than conventional abdominal surgery[1].

2.4 Abdominal Anatomy

There has been nothing published on canine abdominal anatomy after insufflation up to pressures required for laparoscopy. Once the abdomen has been insufflated, there is space for organs to gravitate into, dependent on the position of the animal. To determine where the organs will gravitate towards the attachments of the specific organs in the abdominal cavity needs to be understood.

The peritoneum plays an important role in the formation of the ligaments, mesenteries and recesses in the abdominal cavity. The peritoneum is a serous membrane made up of surface mesothelium composed of squamous cells and a connective tissue ground work called the stroma. This is attached to the fascia transversalis which internally attaches the peritoneum to the underlying muscle or bone[55]. During the embryological development of the abdominal organs, the peritoneum forms reflections that cover all of the surfaces of the organs (intraperitoneal), or just on one surface of the organs (retroperitoneal). As the organs develop and become covered in peritoneum they will form reflections of the peritoneum, ligaments or mesentery which will suspend the organs. Mesentery passes from the abdominal wall to the intestinal tract and a ligament passes from the abdominal wall to an organ[55]. These reflections provide a path for nerves and vascular structures to reach an organ. As all the organs are enclosed in the peritoneum, the peritoneum is only a potential space with lubricating fluid to allow smooth gliding of the organs past each other. The ovarian bursa communicates with the peritoneal cavity. Thus the only true tissue in the peritoneal cavity is the egg after ovulation[55].

The greater omentum is one of the most noticeable and specialised peritoneal reflections. It is divided into the large bursal portion and a smaller splenic and veil portion. It develops from the dorsal mesogastrium in the embryo. The bursal portion is divided into a superficial ventral layer and a deep dorsal layer. The superficial layer attaches alone to most of the greater curvature of the stomach. This then courses caudally to just cranial to the urinary bladder, which it is usually in contact with but not attached to. The greater omentum then reflects on itself to form the deep branch. This courses cranially towards the greater curvature and then reflects dorsally to attach to the dorsal body wall. The potential space between the two layers of the omentum is called the omental bursa, into which there is only one consistent opening, the epiploic foramen[55]. The epiploic foramen is bordered ventrally by the portal vein, dorsally by the caudal vena cava and medially by the caudate lobe of the liver. The splenic portion of the greater omentum, known as the gastrosplenic ligament, is that portion of the greater omentum that extends from the diaphragm, fundus and greater curvature of the stomach to the hilus of the spleen. The gastrosplenic ligament, when taut, is about 5cm in diameter and contains the splenic vessels and nerves. The veil portion is the smallest portion of the greater omentum and does not form part of the omental bursa. It contains the left lobe of the pancreas. The right margin blends in with the left mesocolon opposite the attachment of the duodenal-colic ligament. The left margin is free[55].

The lesser omentum is the largest derivative of the ventral mesogastrium. It resembles the greater omentum in appearance but is not nearly as voluminous. It loosely spans the distance from the lesser gastric curvature and the initial part of the duodenum to the portal area of the liver. It is continuous with the mesoduodenum or the hepatoduodenal ligament on the right. The demarcation is the bile duct which runs in the lesser omentum. The portion to the left of the bile duct is known as the hepatogastric ligament. The lesser omentum loosely envelops the papillary process of the caudate lobe of the liver[55]. It joins the greater omentum at the cardia of the stomach and the medial surface of the cranial part of the duodenum on the right thus closing off the omental bursa. There are three minor folds associated with the omental bursa which follow the branches of the celiac artery. The right gastropancreatic fold contains the hepatic artery and extends obliquely across the medial face of the portal vein. The second fold, the largest of the folds is formed by an upward displacement of the bursa by the splenic artery and nerves. The final fold, the gastropancreatic fold contains the left gastric artery and nerve plexus. It extends from the celiac artery to the left extremity of the lesser curvature.

The liver is divided into six lobes and two processes by deep fissures. The left hepatic lobe is the portion of the liver to the left of the median plane. This is divided into the left lateral lobe and the left medial lobe. The left lateral lobe begins under the left crus of the diaphragm and extends caudally along the diaphragmatic surface, widening and then narrowing down to a point dorsal to the last sternebra. The left medial lobe is triangular to oval in shape and separated from the lateral lobe by a deep fissure from the most dorsal

surface to the hepatic porta. There can be a portion of liver tissue joining the two lobes at the hilus, but most are just attached by the hepatic vessels. The quadrate lobe is in the median plane. It is located ventrally in the fissure between the left and right medial lobes[55]. The gall bladder is located in a fossa on the right surface of the quadrate lobe and the left medial lobe. The gall bladder consists of an apex and a body. The apex is the tip of the gallbladder opposite to the opening of the cystic duct which is the start of the billary tract. The cystic duct runs from the gallbladder to the first hepatic ducts, at this point it becomes the bile duct. These hepatic ducts drain each of the separate liver lobes. The bile duct travels in the lesser omentum to enter the duodenum[55]. The right hepatic lobe is smaller than the left lobe and lies completely to the right of the median plane it is similarly divided into lateral and medial lobes. The right medial lobe is fused medially to the quadrate lobe. It is longer than the left lateral lobe and extends caudally to the costal arch. It too contains a fossa on its medial aspect for the gallbladder. The right lateral lobe is a compressed hemisphere, overlapped cranially by the right medial lobe and caudally it overlaps the caudate process of the caudate lobe. The caudate lobe is made up of the caudate process laterally and by the papillary process medially separated by an isthmus which is compressed dorsally by the caudal vena cava and ventrally by the portal vein. The papillary process sits in the lesser curvature of the stomach. The caudate process bears a depression of the right kidney and can be partially fused to the right lateral lobe. The liver is completely enveloped in peritoneum which is fused to an underlying fibrous capsule. This fibrous capsule thickens at the porta to form the attachments of the liver to the abdominal wall. The coronary ligament, which is not a true peritoneal ligament as it is not in the form of a fold, continues over the dorsal surface of the caudal vena cava. This gives rise to three or more triangular ligaments and is continuous with the falciform ligament. The left triangular ligament, like the comparable right triangular ligament, may be double or triple and contains the fibrous appendix of the liver. If the second ligament is present it runs from the left lobe of the liver to the diaphragm similar to the right side. The falciform ligament is the remnant of the mesentery containing the umbilical vein. The proximal portion extends from the umbilicus to the diaphragm and is fat filled. The distal portion usually remains as a thin avascular fold that extends from the dorsal end of the fissure between the right and the left lobes to the coronary ligament[55]. This will become incorporated into the left triangular ligament. It may however be absent. The hepatorenal ligament attaches the right kidney to the renal fossa of the caudate process of the caudate lobe.

The pancreas consists of the right lobe, body and the left lobe. The right lobe of the pancreas is located in the mesoduodenum in the right dorsal flank region. The caudal extremity is in the concavity of the caudal duodenal loop. The body of the pancreas unites the left and right lobe at an angle of 45˚. It lies in the mesoduodenum in the pyloric region. The portal vein crosses the dorsal portion of the body of the pancreas and the bile duct crosses on the right. The left lobe of the pancreas lies in the deep leaf of the greater omentum. It follows the greater curvature of the stomach towards the hilus of the spleen

but does not contact the spleen. It is ventral to the caudate lobe of the liver. A full stomach can alter the position of the pancreas[52, 55].

The stomach is shaped like the letter C rotated 90˚ counter-clockwise in relation to the vertebral column and varies greatly in size depending on degree of filling. It has a massive capacity to accept food[55]. The oesophagus enters at the cardia and the duodenum leaves at the pylorus. The fundus lies to the left of the midline and the pylorus slightly to the right of the midline. The position of the stomach is relatively fixed as described above with all the attachments of the greater and lesser omentum.

The small intestine as a whole is relatively mobile in the abdominal cavity. Exceptions to this are the duodenum and the colon whose positions are fixed by peritoneal ligaments. The duodenum is attached to the liver by the lesser omentum. The descending duodenum can be found along the right lateral flank of the body wall coursing caudally opposite to the ninth intercostal space ventral to the right kidney and pancreas. It has three flexures. They are the cranial flexure at the pylorus; the caudal flexure or transverse duodenum which is at the entrance to the pelvic canal associated with the ileum and caecum and the last flexure is the duodenojejunal flexure where the duodenum continues as the jejunum. At the area of the ascending duodenum, the mesoduodenum becomes continuous with the mesocolon of the descending colon, forming the duodenal colic ligament. The jejunum makes up the bulk of the small intestine and is suspended from the dorsal body wall by the mesentery. The mesentery is continuous with the deep leaf of the greater omentum. The mesentery resembles a giant fan hanging from the dorsal body wall. The root or parietal attachment has an area of about 1.5cm and contains the cranial mesenteric artery. It extends from the duodenojejunal flexure to the ileocolic junction distally. The ileocaecal fold attaches the ileum to the caecum on the anti-mesenteric surface and contains the antimesenteric ileal vessels[55].

The large intestine is relatively short and unspecialised compared to the small intestine. It starts at the ileal sphincter and ends at the anus. The caecum is a diverticulum of the proximal portion of the colon. The ileocaecal fold is described above but there is a smaller fold from the base of the caecum to the ascending colon, known as the accessory caeco-colic fold. The caecum is found in a consistent position to the right of the median plane in the duodenal loop. The colon is divided into ascending, transverse and descending parts. The shape of the colon is that of a question mark with the tip of the curve, being the ascending colon on the right and cranial to the root of the mesentery. The curved part of the question mark, the transverse colon crosses the midline cranial to the root of the mesentery. The long descending arm of the question mark is the descending colon running along the left body wall. The mesocolon has the same divisions as the colon and suspends the colon from the dorsal body wall. The ascending mesocolon is the shortest and often attached to the areolar tissue of the mesenteric lymph nodes. The ascending, transverse

and descending mesocolon are continuous with each other and the mesorectum. No part of the colon lies retroperitoneally[55].

The kidneys are situated in the retroperitoneal space and are usually surrounded by fat. The dorsal surface is in contact with the sublumbar muscles and is not covered with peritoneum. The ventral surface is covered with peritoneum. Both kidneys lie laterally to the aorta and caudal vena cava on their respective sides. The hilus of the kidney points medio-ventrally. The vessels, nerves and ureter enter and exit at the hilus. The right kidney is located farther cranial to the left kidney and its attachment to the body wall is firmer. The right kidney is in contact with the liver and may be attached to the caudate process. Both kidneys have a fibrous capsule that passes inwards to the hilus and then radiates into the parenchyma and around the neurovascular structures at the hilus. This capsule is held in place by loose subperitoneal connective tissue surrounded by adipose tissue. The position is consistent but they are not rigidly fixed and may move with respiration. The ureters carry urine from the kidneys to the bladder. They course caudo-ventrally from the kidneys to the bladder. The right ureter is slightly longer than the left due to the position of the kidneys. They are bounded dorsally by the psoas muscles and ventrally by the peritoneum making them retroperitoneal. They then pass ventral to the deep circumflex and external iliac arteries and enter the peritoneal space in the lateral ligaments of the bladder after being associated with the broad ligaments of the uterus and enter into the trigone of the bladder[56].

The bladder consists of the body which is connected to the neck which leads into the urethra. The cranio-ventral aspect often contacts the greater omentum's caudal aspect. The cranio-dorsal aspect will often be in contact with portions of the small intestine. The peritoneal reflections from the lateral and ventral aspects of the bladder to the body wall form the ligaments of the bladder. These ligaments are made up of double reflections of peritoneum. Contained in these ligaments are blood vessels, nerves, adipose tissue, ureters, ductus deferens in the male and vestigial embryonic structures. The largest of these folds, the median ligament, runs from the ventral surface of the bladder to the pelvic symphysis. This contains the urachus which normally disappears shortly after birth. The ligament extends caudally to the level of the vaginovestibular junction in the female and the middle of the prostate in the male. The lateral ligaments connect the lateral aspect of the bladder to the lateral body wall. These ligaments contain the round ligament of the bladder, a fibrous cord which is the remnant of the umbilical artery. In the female the lateral ligaments blend laterally with the broad ligament of the uterus. The ureter and the round ligament cross at right angles to each other in the lateral ligament in the female[56].

The main organs of concern for this project in terms of the female reproductive system are the ovaries, oviducts and the uterus. These structures are attached to the dorsolateral walls of the pelvic cavity by paired folds of peritoneum known as the left and right broad ligaments. These ligaments do not support or suspend the organs but unite the different components of the genital system. The broad ligament attaches dorsally to the body wall at

the junction of the psoas and transverse abdominal muscles. Cranially it attaches to the middle and distal thirds of the last rib by means of the suspensory ligament of the ovary. Caudally it is reflected dorsally to the vagina onto the rectum and ventrally to the urethra and the bladder and a curved line laterally onto the wall of the pelvic canal as far caudally as the inguinal ring. A peritoneal fold runs from the lateral aspect of the broad ligament and extends from the level of the ovary to the inguinal canal and through the inguinal canal. This contains the round ligament of the uterus in its lateral border. The pouch of peritoneum that extends through the inguinal canal is known as the vaginal process. The vaginal process can be obscured by fat and in the female extends as far caudally as the subcutaneous tissues of the labia. The broad ligament is further divided into the mesovarium, mesosalpinx and the mesometrium. The mesovarium is the cranial boundary of the broad ligament. It attaches the ovary to the dorsal body wall and ends just caudal to the ovary. The mesosalpinx curves dorsoventrally around the ovary to attach to the medial surface of the broad ligament just dorsal to the ovary. This encloses the ovary within a small peritoneal cavity, called the ovarian bursa. The mesometrium begins at the cranial edge of the uterine horn where it is continuous with the mesovarium. It extends caudally to the point where the peritoneum reflects onto the bladder and colon. It then leaves the uterine horns, uterine body and vagina and attaches to the abdominal and pelvic walls. Together with the mesovarium the ovary has two other ligamentous structures: the suspensory ligament of the ovary and the proper ligament of the ovary. The suspensory ligament attaches to the cranial and middle thirds of the last one or two ribs and runs to the ventral aspect of the ovary and the mesosalpinx. It forms the cranial border of the broad ligament. The round ligament of the uterus attaches to the cranial tip of the ipsilateral uterine horn. It is the caudal continuation of the proper ligament of the ovary. This ligament runs towards the inguinal ring as described above.

The testicles sit in the scrotum in most dogs. A retained testicle can be situated along the path of testicular descent. The ductus deferens run in a peritoneal fold with the testicular vessels and curve back caudally to enter the prostate in close proximity to each other[56]. In the male, the vaginal process extends into the scrotum to form the vaginal tunics of the testis[56].

The ligaments can potentially become infiltrated with adipose tissue, which can alter the possible effect that the ligaments can have on anatomy. Taking this into account, the animals in this study need to be of an average body condition. The subjective assessment of body condition score has shown to correlate well with body fat percentage. A nine point system that has been previously described will be used[57].

2.5 CT Laparoscopic Anatomy

To date there are no descriptive studies of CT laparoscopic anatomy PoI. Computed tomography is the diagnostic modality of choice in human medicine in detecting post-operative pneumoperitoneum as a complication of abdominal surgery. This is most often incidental and clinical significance needs to be determined by the clinical condition of the patient[58]. This can however indicate early viscus rupture or surgical dehiscence of gastro-intestinal anastamosis[58]. The air or carbon dioxide will act as a negative contrast medium enhancing abdominal imaging and thus making it useful in this study. Pneumoperitoneum may also increase the visibility of the pancreas[14].

Laparoscopy is a relatively new veterinary technique. It is hoped that this study will provide insight into the topography of the abdominal organs expected during laparoscopy with insufflation to serve as an aid for inexperienced surgeons to become familiar with the relevant anatomy.

An interesting use of VE in regards to laparoscopy is the construction of a virtual teaching model in a simulator function for training of laparoscopic surgeons[25, 59]. This is a complex procedure. The mapping of the abdominal cavity of the male and female and has recently been completed in human medicine. This is done with a slice thickness of 0.33mm. This then has to be correlated to anatomical dissections and loaded into a software program to give a virtual abdomen as a teaching tool for laparoscopic anatomy and surgery[25]. It has been shown to be clinically effective in teaching human medical students surgical anatomy. The 3-D images produced make teaching the normal surgical anatomy easier as the student can relate to the 3-D images better than teaching from a 2-D radiograph[59].

2.6 Conclusions Drawn from the Literature Review

Laparoscopy has been well described as a surgical technique, with the first use of the technique dating back to the physicians of ancient Greece. However, the global topography of the abdomen after insufflation with carbon dioxide and the changes this may induce in the anatomy has not been described.

Most of the positions used in laparoscopy have come to be as an adaption by surgeons in the operating theatre. With laparoscopy becoming available to veterinarians there is a shortage of experienced laparoscopic surgeons to teach the techniques. It is envisaged that this study may assist in addressing this potential shortfall. Computer teaching models for laparoscopy are being used more in human medicine and it is hoped that this trend will transfer into veterinary medicine using this study as a base.

CHAPTER 3: MATERIALS AND METHODS

3.1 Animal Selection

Seven clinically healthy and intact female Beagle dogs were selected for the study. These dogs were provided by the University of Pretoria Biomedical Research Centre (UPBRC). Six dogs were used in the study and the seventh dog acted as a reserve in case one of the other six had to be excluded. All dogs were housed in the OVAH for the duration of the study and were fed an adult maintenance diet for medium breeds. Health was determined by a routine clinical examination, blood smear, urine analysis and abdominal ultrasound as described below.

All dogs were subjected to a direct peripheral blood smear. This was taken from an ear prick and stained with Diff-Quick (Kyro-Quick stain fixative, solution 1 and 2, Kyron Laboratories, Johannesburg, South Africa). The morphology of the red blood cells, presence of inflammatory shift, platelet numbers and any visible blood parasites were evaluated. All animals were de-wormed with Praziquantel, Febantel and Pyrantel Embonate (Drontal medium dog, Bayer, Isando, South Africa). Their abdomens were then clipped and cleaned of any macroscopic debris.

A cystocentesis sample was taken for urine analysis. A urine dipstick (Combur^9 test® Roche Basel, Switzerland) was examined for the pH, proteinuria and haematuria. The urine specific gravity was measured with a refractometer and the urine sediment was examined by the author under light microscopy after being stained with Sternheimer Malbin stain (Kyron Laboratories, Johannesburg, South Africa).

An abdominal ultrasound was performed by a specialist radiologist using a Sonoline Omnia ultrasound scanner (Siemens AG, Erlangen, Germany) using a 5-7.5 mHz curvilinear array transducer.

All animals were starved for at least 12 hours prior to having a CT scan performed. They were offered water up until 2 hours prior to the scans. All the data collected above was recorded in Appendix 1.

3.2 Experimental Procedure

3.2.1 Anaesthesia

An intra-venous 20 G cephalic catheter (Jelco ® Radiopaque, Smiths Medical, Croyden, South Africa) was placed in each animal. All animals were premedicated with Acetylpromazine (Aceprom 2 injection, 2mg/ml, Bayer, Isando, South Africa), 0.05ml/kg, and Buprenorphine

(Temgesic® 0.3mg/ml, Schering-Plough, Woodmead, South Africa), 0.02mg/kg, given for pain control as described in the ethics section and was given intravenously. General anaesthesia was induced with intravenous Propofol (Propofol 1% 10mg/ml, Fresenius Kabi, Midrand, South Africa) at an induction dose of 6.6mg/kg over a period of two to three minutes. All animals were intubated and anaesthesia was maintained with Isoflorane (Isofor 250ml, Safeline, Pharmaceuticals, Johannesburg, South Africa) for the duration of the CT scan. All animals were placed on a Ringers lactate (Sabax Ringers-lactate, Hartmanns solution, Adcock Ingram Critical Care, Krugersdorp, South Africa) drip at the time of premedication running at 10ml/kg/hour for the duration of the scans.

A 22 G arterial catheter was placed in the dorsal pedal artery just distal to the tarsus, between metatarsal bones II and III. This was connected to a blood pressure manometer for the direct measurement of arterial blood pressure. This was connected to the pressure transducer DTX BD (Manta Medical, Bryanston, South Africa) and a non-diverting capnography monitor was placed at the connection between the endotracheal tube and the anaesthetic circuit. This allowed measurement of the end tidal carbon dioxide. An oesophageal temperature probe was placed to measure body temperature. A pulse oximeter probe was placed on the tongue to measure the partial pressure of oxygen and hence the saturation. All of these were connected to a Dash 4000 GE (Medhold Medical, Midrand, South Africa). This information was recorded as a separate study and does not form part of this study.

A 10 G Foleys urinary catheter was placed and the bulb of the Foleys catheter inflated with 3ml of water. The distal end of the catheter was connected to a closed urine collection system. This was to prevent a distended bladder from affecting the position of the organs in the later scans.

Animals were kept warm with blankets over exposed parts of the body and a linen saver on the CT machine table.

3.2.2 CT Scan Technique

The CT scans were performed with a helical dual slice sliding gantry Somatom Emotion (Siemens AG, Erlangen, Germany). The machine was situated at the OVAH in Pretoria.

Respiratory movement was eliminated by administering a bolus of propofol 1% IV at 1mg/kg together with manual hyperventilation with closing the pop-off valve on the anaesthetic machine. Hypocarbia to a level of 40mm Hg was induced. This led to a temporary apnoea for the duration of the scans. The scans were performed in a cranial to caudal direction to minimise the potential effect of respiratory movement in the cranial thorax.

Each series of scans took an average of an hour to complete for each dog. Once all of the monitors were connected and the anaesthetist was sure the patient was stable, the series of

scans were started. The animals were placed in dorsal recumbency from being prepared prior to scanning. A lateral topogram was performed prior to all CT scans and the field of view adjusted to include the caudal part of the thorax to ensure the diaphragm and the cranial abdominal contents were in the scan. The topogram was extended caudal to the ischial tuberosities to ensure the entire pelvic canal was included, to evaluate the effects of insufflation on the pelvic cavity.

Slice collimation of 2.5 mm, slice thickness of 3mm, a pitch of 2 and a Kernel of B41s medium was used in all the animals. A 110 kV and a tube rotation speed of 0.8s were maintained in all the scans. The times and dates of the scans were recorded. The mAs and the computed tomography dose index (CTDI) received by each animal and were recorded to quantify the amount of radiation each subject received. For all scans the table was maintained at 90˚ to the gantry. For the Trendelenburg position the gantry was tilted at 30˚.

The first scan was performed with the animal in dorsal recumbency pre-insufflation (PrI). This was to simulate the most commonly used position in general surgery and laparoscopy. The animal was then positioned in the Trendelenburg position[27, 28]. This was achieved by placing the animal on a custom built high density triangular foam wedge with the acute angles being 30˚ and 60˚. The hindquarters were secured by crepe ties placed proximal to the hock joint. These ties were tied down with sandbags to ensure the animal did not slip off the foam wedge (Fig. 1). The gantry was then tilted to a fixed angle of 30˚ prior to scanning (Figs.2-3). This was only done for the Trendelenburg position. This was to ensure that the x-rays penetrated the patient as close as possible to 90˚ to the long axis of the body. This was to maintain a consistent transverse image plane for all the scans performed. The third scan was performed in standard left lateral recumbency (Fig. 4) and the gantry was returned to its normal position prior to starting this scan. The fourth scan was performed in standard right lateral recumbency. In all views the symmetry of the patient was confirmed to ensure that differences in each of the positions did not have an effect on the measurement performed.

Figure 1 – An image showing the VDT position during insufflation

Animal secured in the VDT position prior to tilting of the gantry. Point A shows the custom made high density foam wedge. Point B shows the cannula inserted into the umbilical scar.
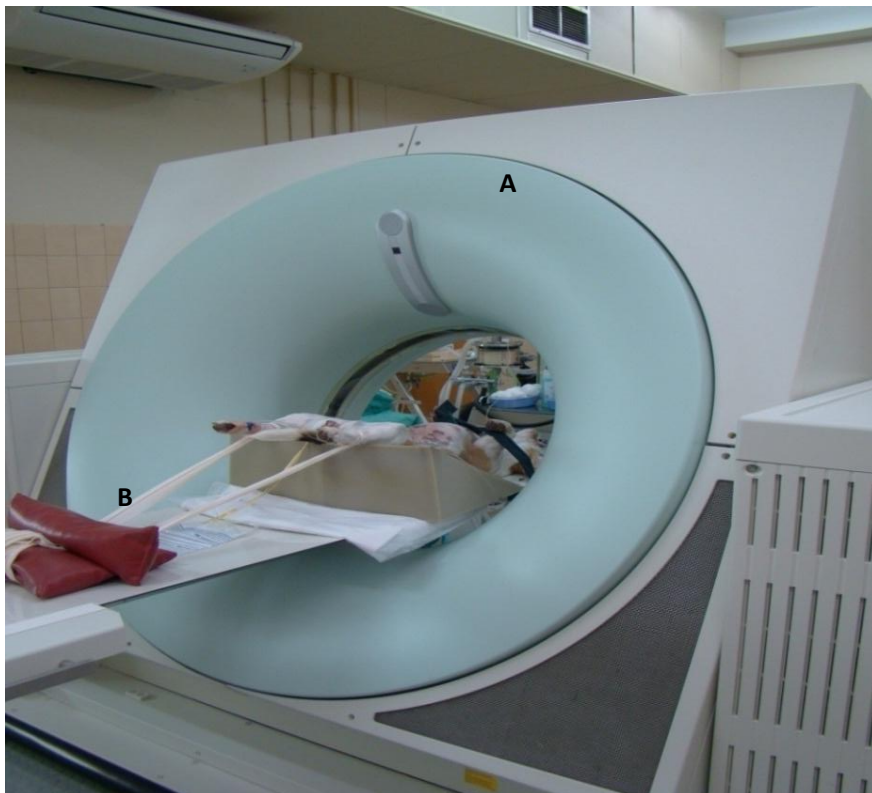
Figure 2 – An image showing the securing of the legs of the patient for the VDT position

The gantry (A) can be seen tilting 30˚ for the dog in the VDT position. The sand bags and ties (B) help maintain this position
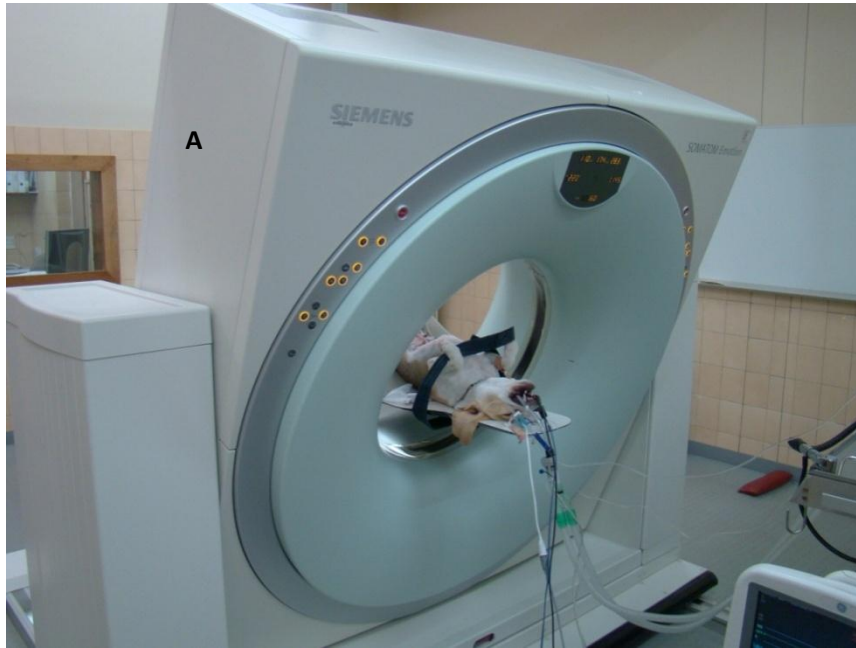
Figure 3 – An image showing the gantry position for the VDT position

The 30˚ tilt of the gantry (A) viewed from the cranial aspect of the dog.

Figure 4 – An image showing the RL position in the CT gantry

The dog is positioned in RL with the gantry (A) returned to 90˚ to the table. The closed urine collection (B) system is shown.

After the fourth scan the dog was repositioned in dorsal recumbency. Standard aseptic surgical technique was used in preparing the site for cannula placement. A 1.5 cm incision was made over the umbilicus, the linea alba was identified and grasped and a stab incision was made into the linea alba and the cannula was placed via the Hasson technique. A screw-in disposable laparoscopy 10mm cannula (Karl Stortz, Tuttlingen, Germany) was screwed into the incision (Fig. 5). The integrity of the seal and the security of the cannula in the incision were tested. If the seal or cannula was not secure, a 2-0 nylon (Scimitar surgical sutures, Gabler Medical, Selby, United Kingdom) suture was placed into the linea alba to secure and tighten the seal. The insufflation tube was connected to the cannula and insufflation was performed with a CO_2-PNEU Insufflator (WISAP, Munich, Germany) (Fig. 6).

Figure 5 – An image showing a VDR with the cannula in place in the abdomen

The cannula (A) can be seen in the umbilical scar connected to the insufflation tube (B) while the surgical site is draped with a standard window drape (C).
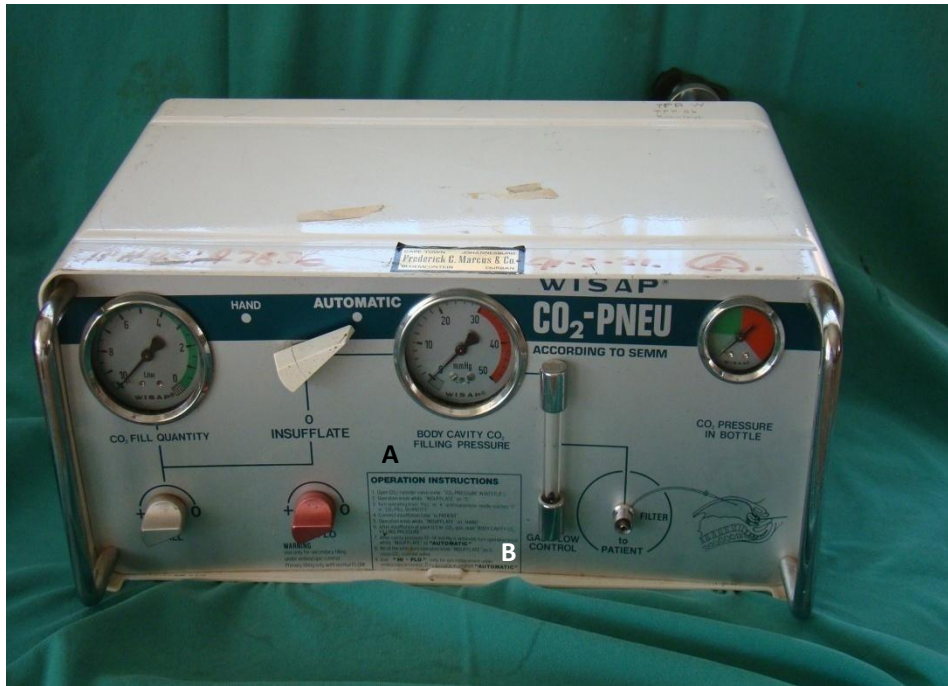
Figure 6 –An image showing the abdominal insufflator

The abdominal insufflator used with the intra-abdominal pressure gauge (A) and the connection port to the patient (B) clearly visible.

Insufflation was achieved using medical grade carbon dioxide (Afrox, Midrand, South Africa).The pressure gauge of the insufflator was set at high flow to achieve an insufflation pressure of 14mm Hg. Once achieved, the pressure was maintained at normal flow rates to a level of 10-14mm Hg to simulate surgical conditions under routine laparoscopy. All the scans were then repeated in the same order as above. The animal was disconnected from the insufflation tube during the changes in position. Prior to each scan the topogram was repeated.

Once the four PoI scans were completed, the cannula was removed and the linea alba was sutured with 2-0 nylon and the skin with 4-0 nylon. All catheters were removed and the dog was disconnected from the anaesthetic machine. The animal was moved off the CT table onto a Bair hugger (Arizant Medical, Eden Prairie, USA) and covered in blankets and monitored until awake, after which it was returned to the hospital ward. During this time the next animal was collected and was induced following the described protocol for all the dogs. The technical aspects of the CT scans for each dog were recorded (Appendix 2).

All scans were reconstructed with a slice thickness of 1.5mm. All images were examined in a soft tissue window width of 300 and level 40 in transverse and in dorsal, sagittal and parasagittal planes after multiplanar reconstruction. These scans were then analysed on the basis of a statistical and a subjective descriptive method described later.

3.2.3 Statistical analysis

A portion of the data was subjective and by using a descriptive analysis to evaluate the effects of position and insufflations was helpful in performing the analysis.

All data was entered into a spreadsheet (Microsoft Excel, Microsoft Corporation, Get City, USA). This data was then transferred into a statistical analysis program, Stata 10.0 (StatCorp, College Station, Texas, USA). The medians and ranges were determined.

The Kruskal-Wallis One Way of Variance (ANOVA) and the Tukey-Kramer Multiple Comparison Test were used to compare the different positions in each animal and the statistical significance of any changes between them. Statistical significance was set at $p< 0.05$.

3.2.4 Data measurements

3.2.4.1   EXTRA ABDOMINAL MEASUREMENTS AND GENERAL ABDOMINAL MEASUREMENTS

Oesophageal lumen short axis diameter - This value was measured at the level of T8 on a transverse image from the inner mucosal surface to the opposing mucosal surface of the oesophagus perpendicular to the direction of the lumen of the oesophagus (Fig. 7)

Oesophageal lumen long axis diameter - This was measured at the level of T8. This was measured in a transverse plane. It is measured from the inner wall of the floor of the oesophagus to the inner wall of the roof of the oesophagus, perpendicular to the direction of the lumen of the oesophagus (Fig. 7).

Oesophageal content - The content was examined and determined to be fluid or gas opacity to help elucidate the effects of increasing intra-abdominal pressure on reflux of gastric content. This was evaluated at the same level as above (Fig. 7).

Figure 7 – A VDR PoI transverse image showing the oesophageal measurements

The measurement of the oesophagus is shown by the arrow heads. The long axis diameter is shown by the double headed arrow and the short is diameter is shown by the 2 arrow heads.

Cranial extent of the diaphragmatic cupula in relation to the body of the thoracic vertebrae- The vertebral bodies were divided into thirds and the most cranial extent of the diaphragm in a parasagittal view was noted. The contact between the heart and the diaphragm was evaluated and measured if applicable (Fig. 8)
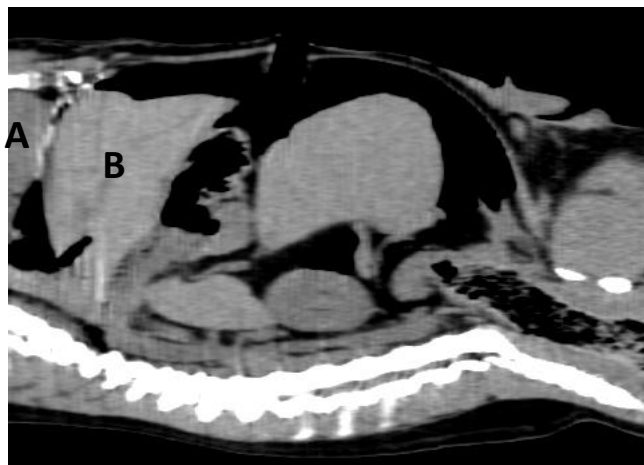
Figure 8 – A RL PoI sagittal image showing the diaphragmatic cupula position

The cardiac silhouette (A) can be seen in contact with the shadow of the liver (B) which represents the liver and the diaphragm.

Gas in the pelvic canal - The HU were measured in the pelvic cavity to determine if carbon dioxide dissected into the pelvic cavity. This was given a yes or no answer (Fig. 9).

Peritoneal reflections visible - Visibility of the peritoneal reflections in the pelvic canal was recorded as a yes or no answer (Fig. 9).
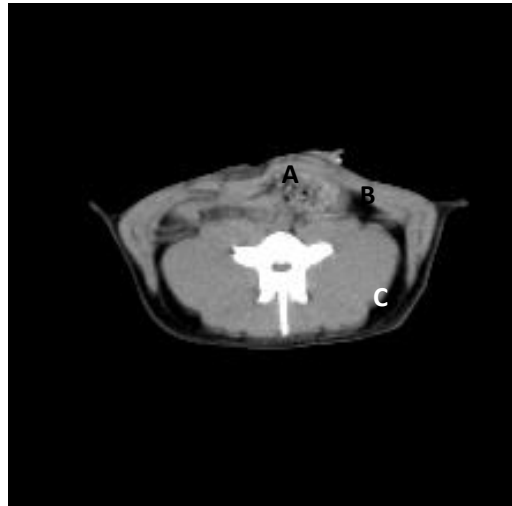
Figure 9 – A VDT PoI transverse image showing the contents of the pelvic cavity

The rectum (A) is visible in the pelvic canal. Lateral to the rectum the hypo-attenuated area (B) has a HU close to that of fat when compared to the sublumbar fat (C).

Abdominal parenchymatous organ height % of abdominal height at umbilicus- In the PrI abdomen the abdominal height measurement was taken from the cranial ventral surface of L3 to the ventral abdominal wall in the sagittal plane. The parenchymatous height was taken from the highest area of the parenchymatous organs to the ventral surface of L3. In the inflated abdomen the measurement was taken from the same described markers. In the lateral positions the measurement was taken at the same transverse slice but was from the parenchymatous organ mass to the lateral body wall (Fig. 10).

Figure 10 – A RL PoI transverse image showing the extra-abdominal measurements

A right lateral showing the abdominal height measurement from point (A) to (C) and the parenchymatous height measurement from point (B) to (C). Vertebra L3 (D) can clearly be seen

3.2.4.2 LIVER MEASUREMENTS

Distance from the caudal xiphoid to the liver- Measured from the most caudal transverse slice through the xiphoid process to the nearest ventral surface of the liver in a sagittal image (Fig. 11).

Figure 11 – A VDR PrI parasagittal image showing the distance from the liver to the xiphoid

The ventral surface of the liver (A) to the dorsal surface of the xiphoid of the sternum (B), showing where the measurement points are.

The percentage of contact between the liver and the body wall at T11 **-** The circumference of the liver in contact with the surface of the entire body wall was measured as a percentage of the entire circumference of the body wall in a transverse image (Fig. 12). This was made up of individual measurements of the *liver contact with the body wall* and the entire *abdominal circumference* in the same transverse image.
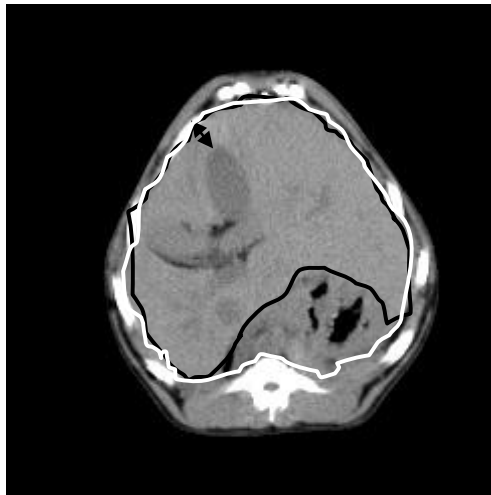
Figure 12 – A VDR PrI transverse image showing the circumference of the liver

The black drawn line represents the circumference of the liver in contact. The black arrowheads show the distance from the apex of the gallbladder to the body wall. The white line shows abdominal circumference.

Distance of the apex of the gallbladder to the right abdominal wall **-** Measured by a straight line from the apex of the gallbladder at the level of the widest cross sectional diameter of the gallbladder to the lateral abdominal wall on a transverse image (Fig. 12).

The % contact of hepatic parenchyma to the gallbladder- Circumference of the serosal surface of the gallbladder in contact with hepatic parenchyma measured as a percentage of the entire circumference of the gallbladder on a transverse image (Fig. 13). This consists of 2 measurements, being the gallbladder circumference and the contact of the hepatic parenchyma with the gallbladder circumference.

The % of gallbladder exposed- The percentage of the gallbladder exposed above the hepatic parenchyma as a *percentage* of the entire gallbladder circumference on a transverse image (Fig. 13).

Separation of the liver lobes **-** This was graded as 1 = 1 interlobar fissure open, 2 = 2 open, 3 = 3 open and 4 = 4 or more interlobar fissures open (Fig. 13). A sub-classification to evaluate the degree of separation of the fissures was A = <25% of the length of the fissure open, B = 25 -50% of the fissure open and C = >50% of the length of the fissure open. This was measured on a transverse image at the level of T11.
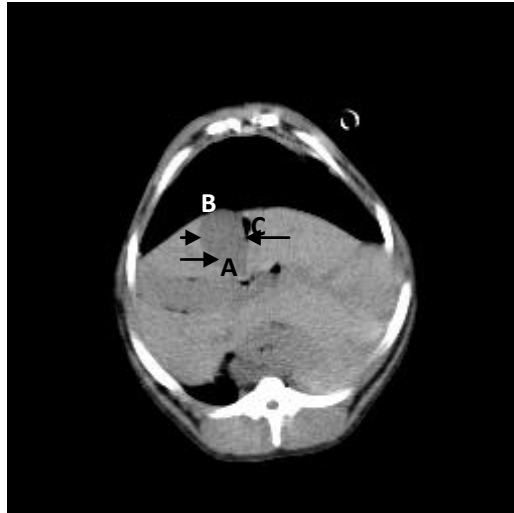
Figure 13 – A VDR PoI transverse image showing the gallbladder measurements and opening of the hepatic fissures

The gallbladder (A) can be seen and the exposed surface (B) is visible. The remaining contact with the hepatic tissue is shown by the arrows on either side. The opening up of a fissure can be seen (C). The arrowheads show the liver-gallbladder contact.

Distance of lesser curvature of the stomach to the caudal part of the caudate lobe of the liver - this was measured as the shortest distance in a straight line from the middle of the caudal surface of the caudate lobe to the nearest portion of the lesser curvature on a sagittal / parasagittal image (Fig. 14).
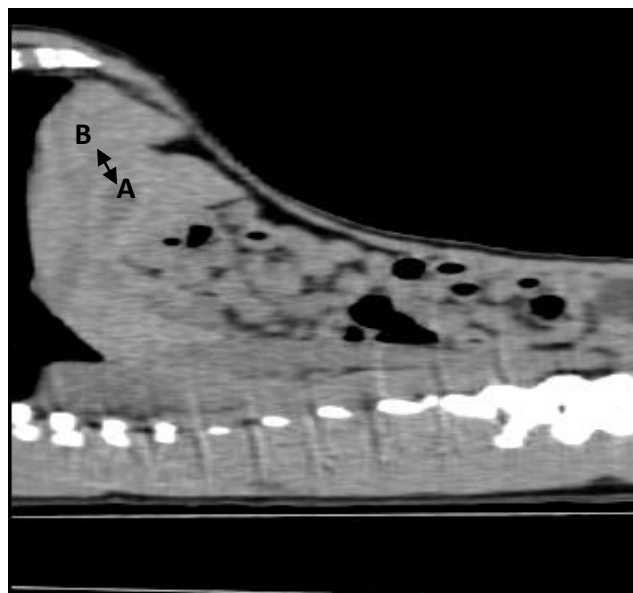
Figure 14 – A VDR PrI on a parasagittal image showing the stomach to liver distance

The gas bubble in the stomach (A) and the caudate lobe of the liver (B) showing the points for measurement described above, represented by the arrows.

Distance from the head of the spleen to the left lateral liver lobe **-** A straight line from the most dorsal part of the spleen on a sagittal image to the nearest part of the left lateral liver lobe (Fig. 15).
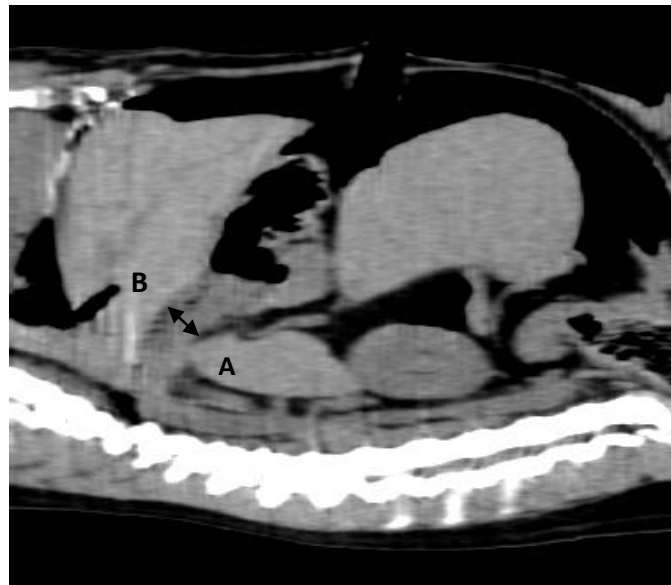
Figure 15 – A LL PoI parasagittal image showing the relationship between the liver and spleen

The spleen (A) and the left lateral liver lobe (B) can be seen and the arrow indicates the measured distance.

Cystic duct visibility - A yes or no answer, the duct should not be confused with the hepatic veins in the area.

Distance between the vena porta and the vena cava **-** This was measured as a straight line perpendicular to the V. Cava and to the V. Porta at the level of the T13-L1 intervertebral disc on a transverse image.

3.2.4.3   SPLENIC MEASUREMENTS
Percentage of spleen in contact with the body wall **-** Measured as a percentage of the total length of the parietal surface of the spleen compared to the portion of the parietal surface of the spleen in contact with the peritoneal surface of the body wall at the level of the transverse process of L1 measured on a transverse image (Fig. 16). Made up of two measurements, firstly the *parietal splenic length* and the *parietal length in contact with the body wall.*
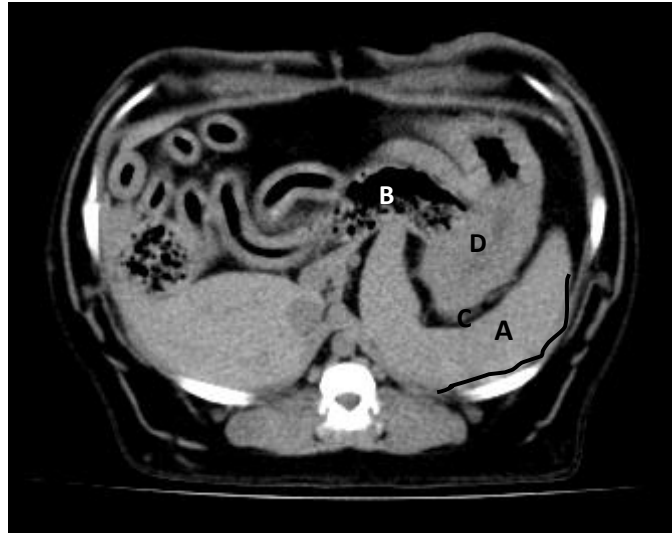
Figure 16 – A VDR PrI transverse image showing the relationship of the spleen to surrounding organs

The spleen (A) and the transverse colon (B) can be seen. The hilar area of the spleen can be seen (C) in close association with the stomach (D). The black line represents splenic contact with the body wall.

Hilar access **-** Is the vasculature of the hilus of the spleen exposed? Yes or no answer (Fig. 16).

Distance from the pelvis of the left kidney to the caudal portion of the head of the spleen **-** measured from the middle of the pelvis of the left kidney to the caudal portion of the spleen on a transverse image (Fig. 17).
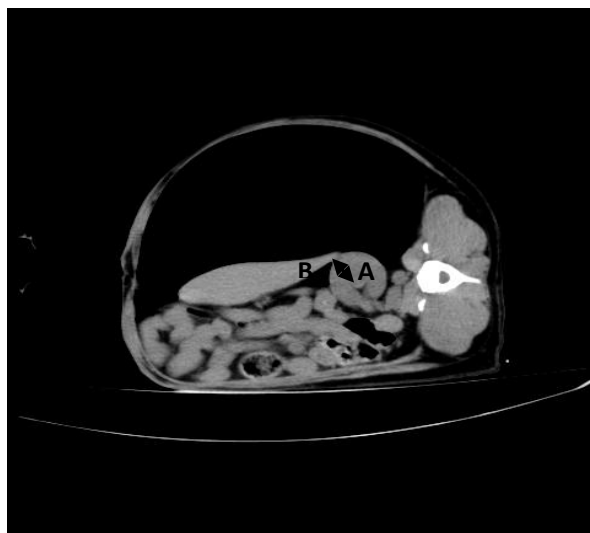
Figure 17– A RL PoI transverse image showing the relationship between the spleen and the kidney

The distance from the pelvis of the kidney (A) to the head of the spleen (B) can be seen as the arrows.

Contact distance between spleen and the stomach **-** The length of the visceral surface of the spleen in contact with the stomach. This was measured on a transverse image (Fig. 18).
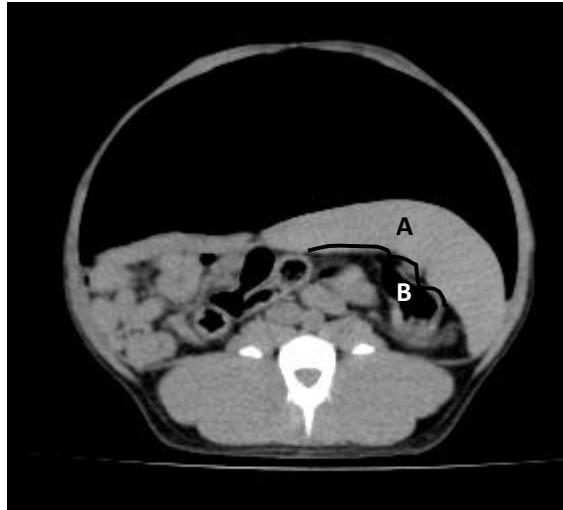
Figure 18 – A VDR PoI transverse image showing spleen to stomach contact

The spleen (A) is seen to lie on the gastric gas bubble (B). The contact distance is shown by the solid black line.

3.2.4.4 GASTRO-INTESTINAL MEASUREMENTS

Position of the pylorus in relation to the vertebral column - the position of the pylorus and its movement is noted in regards to the vertebra. A line drawn perpendicular to the vertebral column through the middle of the pylorus intersecting the vertebral column measured in a sagittal /parasagittal image (Fig. 19). The vertebrae were then divided into thirds and the point of intersection recorded.
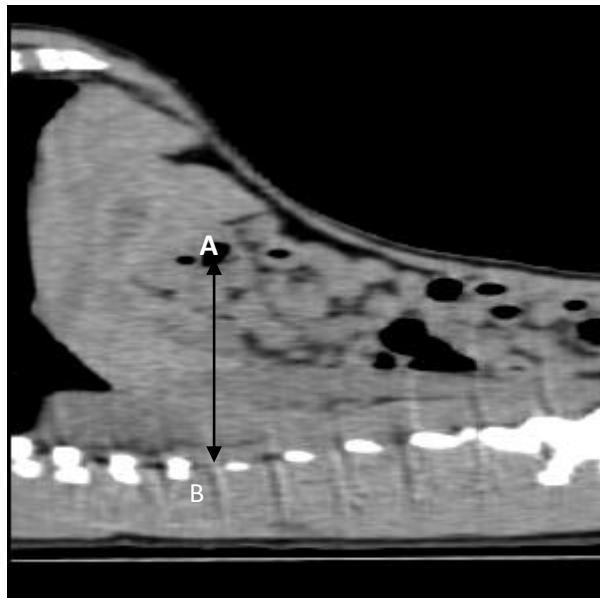
Figure 19 –A VDR PrI parasagittal image showing the position of the pylorus in relation to the vertebral column

The gas bubble in the pylorus (A) is measured from the middle to the vertebral column (B) shown by the arrows.

Stomach cross section long axis and short axis - on a transverse image at the widest visible part of the stomach, the short axis diameter was the distance from mucosal surface to mucosal surface. On the same transverse image the long axis diameter was measured from mucosal surface to mucosal surface roughly perpendicular to the short axis diameter (Fig. 20).
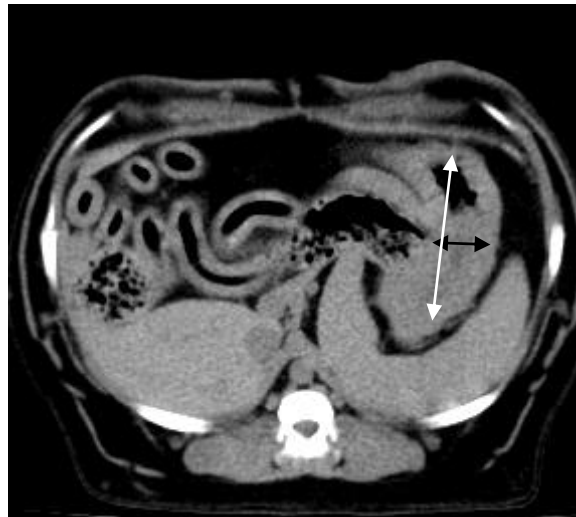
Figure 20 – A VDR PrI transverse image showing the cross sectional size of the stomach

The white arrows show the length and the black arrows show the width of the stomach in the described measurements.

Distance of the mid descending duodenum from the body wall **-** straight line from peritoneal surface of the right lateral body wall to the mid straight portion of the lateral surface of the descending duodenum measured on a transverse image at the level of the pelvis of the right kidney (Fig. 21).

Figure 21 – A LL PoI transverse image showing the distance of the mid descending duodenum from the body wall

The descending duodenum (A) can be clearly identified by the thickened wall. The distance from the peritoneal surface of the lateral surface body wall to the duodenum wall is measured which is represented by the white arrow.

Distance of the cranial duodenal flexure to the gallbladder - straight measurement from the cranial edge of the duodenal flexure to the junction of the cystic duct and the gallbladder measured on a parasagittal image (Fig. 22).

Figure 22 – A RL PoI parasagittal image showing the distance of the cranial duodenal flexure from the gallbladder

The pyloric antrum leading into the cranial duodenal flexure (A) is seen and the gallbladder (B) cystic duct junction. The measurement is shown by the black arrow.

Distance of the pelvis of the right kidney to the descending duodenum - measured on a transverse image at the level of the pelvis of the right kidney to the nearest portion of the serosal surface of the wall of the descending duodenum (Fig. 23).
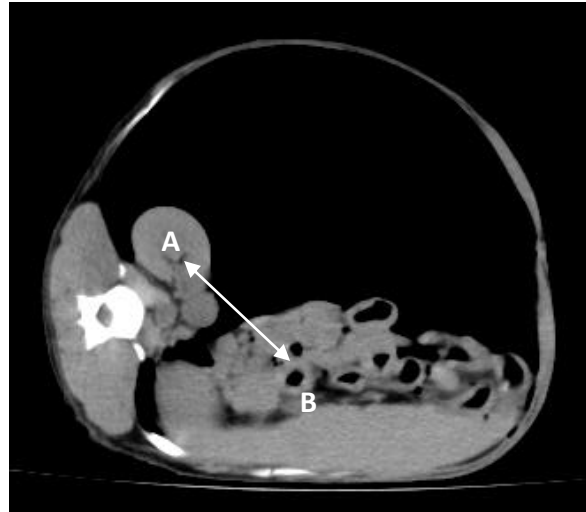
Figure 23 – A LL PoI transverse image showing the distance from the pelvis of the right kidney to the descending duodenum

The right kidney (A) and the descending duodenum (B), the measurement from the descending duodenum to the right kidney is shown by the white arrow.

3.2.4.5 PANCREAS MEASUREMENTS

The views where the right limb, the body and the left limb of pancreas could be seen were recorded. This made it possible to determine which view provides the best visibility on CT, however this may not represent visibility during laparoscopy.

3.2.4.6 KIDNEY MEASUREMENTS

Cross sectional diameter of the kidneys - measured at the widest point of the left and right kidney on a transverse image (Fig. 24).
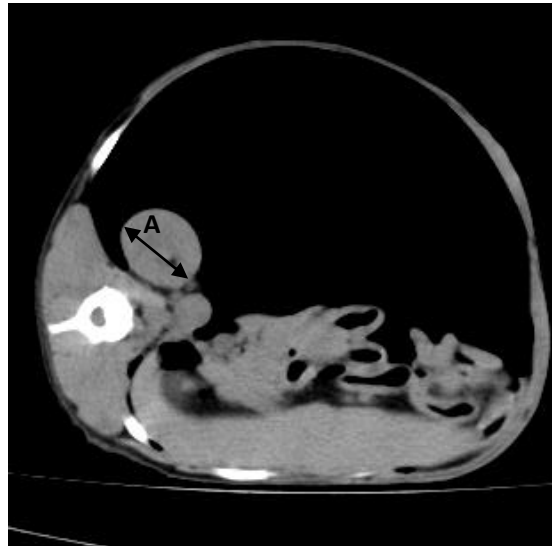
Figure 24 – A LL PoI transverse image showing the diameter of the kidney

The right kidney (A) with a black arrow representing kidney diameter measurement.

Distance of the cranial pole of the right kidney to the renal fossa of the liver **-** measured as a straight line on a parasagittal image at the level through the renal pelvis from the cranial pole of the kidney to the fossa of the liver (Fig. 25).
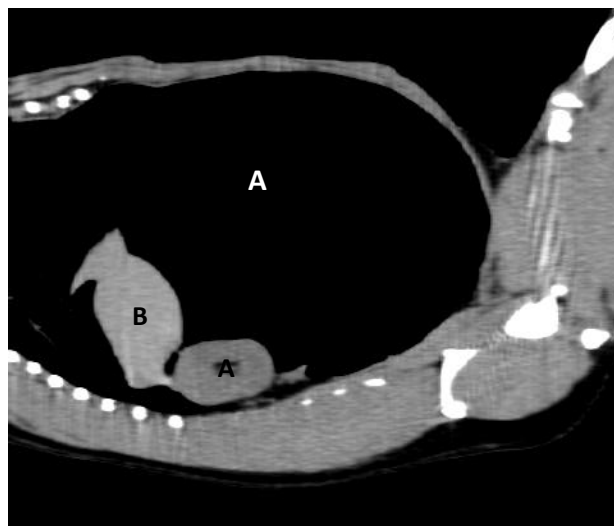
Figure 25 – A LL PoI parasagittal image showing the distance from the renal fossa to the right kidney

The renal pelvis (A) can be clearly seen. The measurement is from the cranial pole of the kidney to the caudal surface of the renal fossa (B).

Distance from the cranial and caudal halves of the kidneys to the aorta - measured by a line perpendicular to the aorta from the lateral surface of the aorta to the nearest medial surface of the cranial half of each kidney. The same was repeated at the caudal pole of the kidneys measured on a dorsal image (Fig. 26).
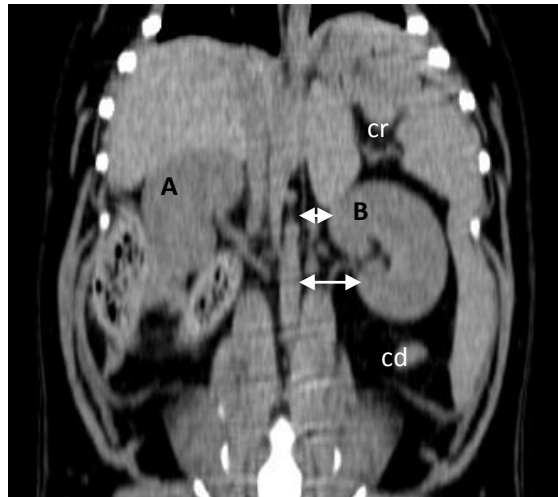
Figure 26 – A VDR PoI dorsal image showing the distance from the kidney to the aorta

The right kidney (A) and the left kidney (B) can be seen with the white arrows showing the measurements from the cranial (cr) and caudal (cd) half of the left kidney.

Distance from the tip of the transverse process of L2 to the nearest surface of each kidney - the distance from the tip of the transverse process of L2 to the dorso-lateral surface of the ipsilateral kidney was measured on a transverse image (Fig. 27).

Distance from the peritoneal surface of the nearest body wall to the mid lateral serosal surface of the kidney - measured by a perpendicular line to the outer lateral surface of the kidney to the ipsilateral body wall measured on a transverse image (Fig. 27).

Figure 27 – A LL PoI transverse image showing described kidney measurements

The right kidney (A) with measurements from the lateral peritoneal surface of the body wall represented by a white double arrow and from the tip of the transverse process of L2 shown by a white hourglass.

3.2.4.7   ADRENAL MEASUREMENTS

Distance from the closest aortic wall to the medial surface of the mid-body of the adrenal - measured on a dorsal image with a line perpendicular to the long axis of the aorta (Fig. 28).
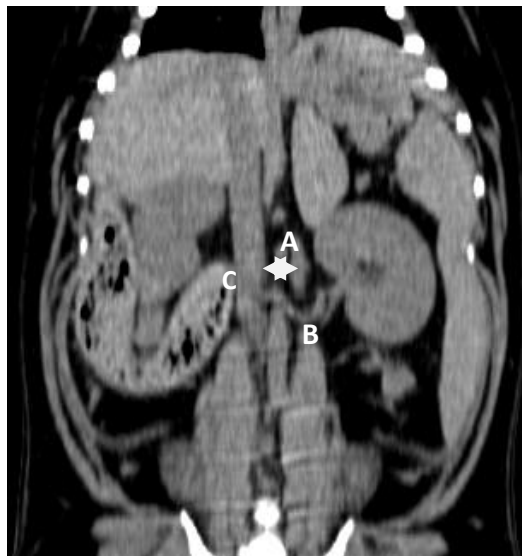
Figure 28 – A VDR PoI dorsal image showing the distance from the aorta to the adrenal

The left adrenal (A) and the Shepherd's crook of the left renal artery (B) are clearly visible. The aorta (C) and the distance to the aorta measured shown by the white arrowheads.

3.2.4.8   BLADDER MEASUREMENTS

Cross sectional diameter of the bladder - maximum diameter of the bladder on a sagittal image measured in a straight line from mucosal surface to mucosal surface (Fig 29).

Distance from the caudal aspect of the bladder to the rim of the pubis - a straight line from the cranio-dorsal aspect of the pubic symphysis to the junction of the bladder and urethra measured on a sagittal image (Fig. 29).

Distance from the apex of the bladder to the ventral body wall - measured by a line from the apex of the bladder drawn perpendicular to the long axis of the body, intersecting a point on the inner ventral body wall on a sagittal image (Fig. 29).
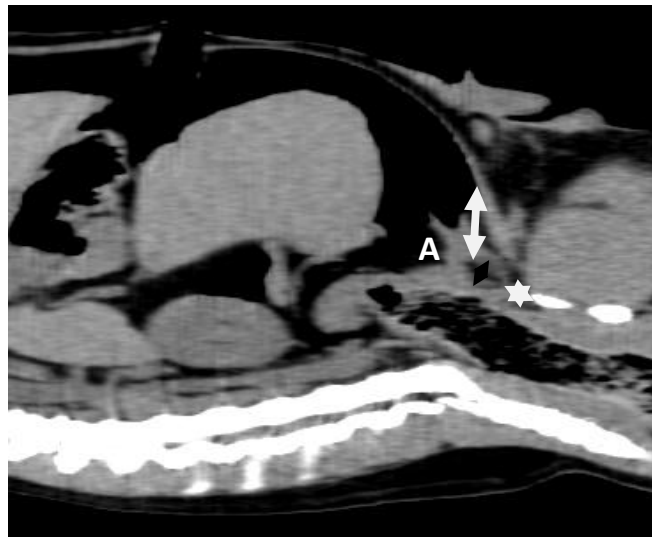
Figure 29 – A VDR PoI showing the measurements of the bladder

The bladder (A) with the measurements described above shown firstly from the cranial pubic symphysis to the ventral bladder shown by a white star. Secondly the body wall to the apex shown by a thick white arrow. The black arrow shows the diameter measurement of the bladder.

3.2.4.9   UTERUS AND OVARIAN MEASURMENTS

Cross sectional diameter of the uterus at the level of the pelvic inlet - cross sectional diameter of the uterus at the level of the pelvic inlet measured on a transverse image.

Cross sectional length and width of the ovaries - the long and short axis diameter of the ovaries measured on a parasagittal image (Fig. 30).
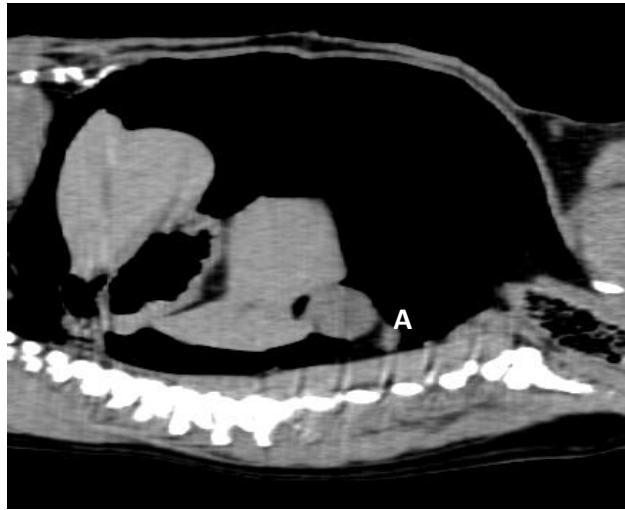
Figure 30 – A RL PoI parasagittal image showing the left ovary

The ovary (A) is measured in length and width.

Length of visible uterus from the mid-pubic symphysis and both uterine horns - length of visible uterus from the middle of the symphysis to the uterine bifurcation (Fig. 31). Then the visible length of each separate uterine horn up to the ovary was followed and measured on sequential parasagittal images.

Length / contact distance between the uterine body and colon - length of the uterus in contact with the colon from the middle of the pelvic symphysis taken from the middle of the obturator foramina until the uterine bifurcation. This was measured on a transverse image using sequential slices and slice thickness (Fig. 31).

Figure 31 – A VDT PoI transverse image showing the relationship between the uterus and colon

The uterine body (A) was seen ventral and lateral to the colon (B). This slice was taken cranial to the pubic symphysis. The uterine body is followed and the length measured. The uterine horns were followed and measured from this point. The contact between the uterine body and the colon was clearly seen.

Distance from the caudal pole of the kidney to the cranial pole of the ovary - measured by a straight line parallel to the long axis of the ovary from the cranial pole of the ovary to the nearest part of the caudal pole of the kidney. Both sides were measured on a parasagittal image (Fig. 32).
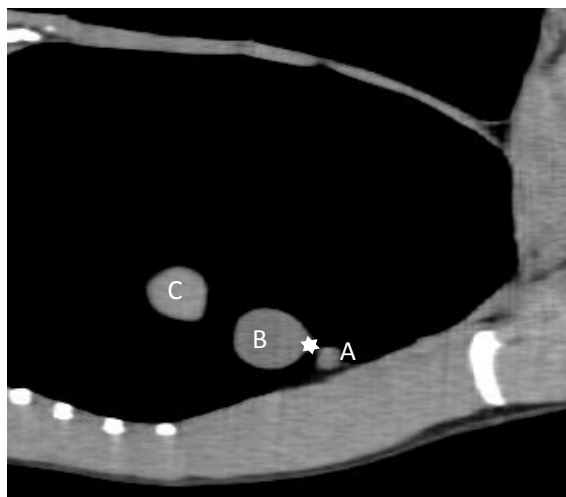
Figure 32 – A VDR PoI parasagittal image showing the distance from the caudal pole of the kidney to the cranial pole of the ovary

The left ovary (A) in relation to the left kidney (B) and the spleen (C) can be seen. The distance from caudal pole of the kidney to the cranial pole of the ovary is shown by the white star.

3.3 Ethical Considerations

All animals were provided by the UPBRC and were selected on the basis that they were bred for experimental work and were healthy. All animals were treated with respect. They were given a standard acceptable anaesthetic protocol, pain control prior to the induction of anaesthesia and woken up once the CT procedures were completed. All procedures were done in accordance with the regulations and standards of the Animal Use and Care Committee of the Faculty of Veterinary Science, University of Pretoria and with their approval of the protocol (V062-09).

The animals were exposed to radiation from the CT scan and there was potential for harm. To expose the animals to as little radiation as possible, only the essential scans representing the most commonly used positions in laparoscopy were performed. A CARE 4D dose was used as in human paediatrics. This only exposed the patient to the required amount of x-ray photons and hence radiation required to produce an image for that thickness of the body for the photons pass through. A slice thickness of 3mm and a 2.5mm collimator were used because it allowed for rapid scanning with the least amount of exposure to radiation to get useable images. The settings on the CT machine enabled the recording of the CTDI for each animal throughout the duration of the study.

No one was present in the scan room during the actual scan. All persons involved were situated in the control room behind lead impregnated glass during the scanning. The responsibility of maintaining the apnoea in the animals was shared between Dr. K. Joubert and Dr. R. Elliott which was done prior to the onset of scanning.

CHAPTER 4: RESULTS

4.1 Extra-abdominal Structures

Oesophagus

A higher number of dogs showed no content in the oesophagus than dogs showing content in the PrI scans in all positions. The left lateral (LL) position resulted in the most animals with oesophageal content present and the right lateral (RL) position the least (Table. 1).

In the PoI scans the majority of dogs had air in the oesophagus followed by fluid, with very few having no content in the oesophagus in all positions (Table. 1).

Table 1: Oesophageal lumen short axis diameter and content pre- and post-insufflation

	Pre-Insufflation		Post-Insufflation		
	Oesophageal content	Short axis Median (Range) in cm	Oesophageal content	Short axis Median (Range) in cm	P value
VDR	5E 1F	0.76 (0.49-1.48)	2A 2F 2FA	1.15 (0.66-1.68)	0.085
VDT	5E 1A	1.01 (0.77-1.3)	1E 3F 2A	1.34 (0.96-1.64)	0.086
LL	4E 1F 1A	0.75 (0.54-0.89)	5A 1FA	1.53 (0.89-2.07)	0.001
RL	6E	0.85 (0.53-1.1)	3A 1F 2FA	1.41 (1.15-2.08)	0.002

E= Empty, A= Air, F= Fluid and FA= Fluid and air

There was a statistically significant increase in oesophageal short axis diameter in the RL and the LL when comparing the PrI and PoI scans. In the VDR and the VDT there was no significant increase. However there was a trend towards an increase in the VDR and VDT when comparing the PrI and PoI scans (Fig. 34).

Table 2: Oesophageal lumen long axis diameter pre- and post-insufflation

	Pre-Insufflation Median (Range) in cm	Post-Insufflation Median (Range) in cm	P value
VDR	1.93 (1.78-2.44)	2.23 (1.7-2.48)	0.279
VDT	2.24 (1.93-2.71)	2.56 (2.04-3.26)	0.129
LL	2.21 (1.59-2.44)	2.6 (2.18-3.23)	0.001
RL	2.01 (1.8-2.2)	2.45 (2.05-2.83)	0.006

There was a statistically significant increase in the oesophageal long axis diameter in only the LL and RL when comparing the PrI and PoI scans. However, there was a trend in the VDR and the VDT towards an increase when comparing the PrI and PoI scans (Fig. 33).
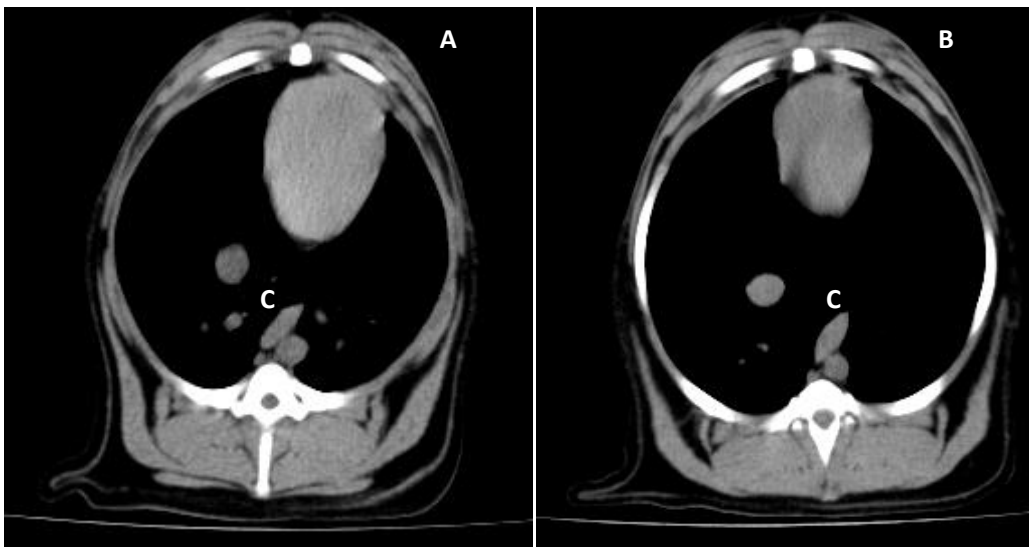
Figure 33 – A series of VDR PrI and PoI transverse images showing the oesophagus

The PrI (A) VDR shows an empty oesophagus (C) with a narrow diameter and the PoI (B) VDR shows the oesophagus (C) filled with a small amount of fluid.

Cranial extent of the diaphragmatic cupula in relation to the body of the thoracic vertebrae

In all of the images, PrI and PoI, there was contact between the heart and the diaphragm at some point in each series. All positions showed a trend towards cranial movement of the cupula when comparing the PrI and PoI scans. The most cranial movement was seen in the LL (Fig. 34).

In the VDR position the cupula moved cranially in all but one dog when the PrI and PoI scans were compared (Graph 1).

In the VDT, LL and RL positions the cupula moved cranially in all of the dogs when the PrI and PoI scans were compared (Graph 1).

Graph 1: Cranial movement in vertebral length of the diaphragmatic cupula in all positions
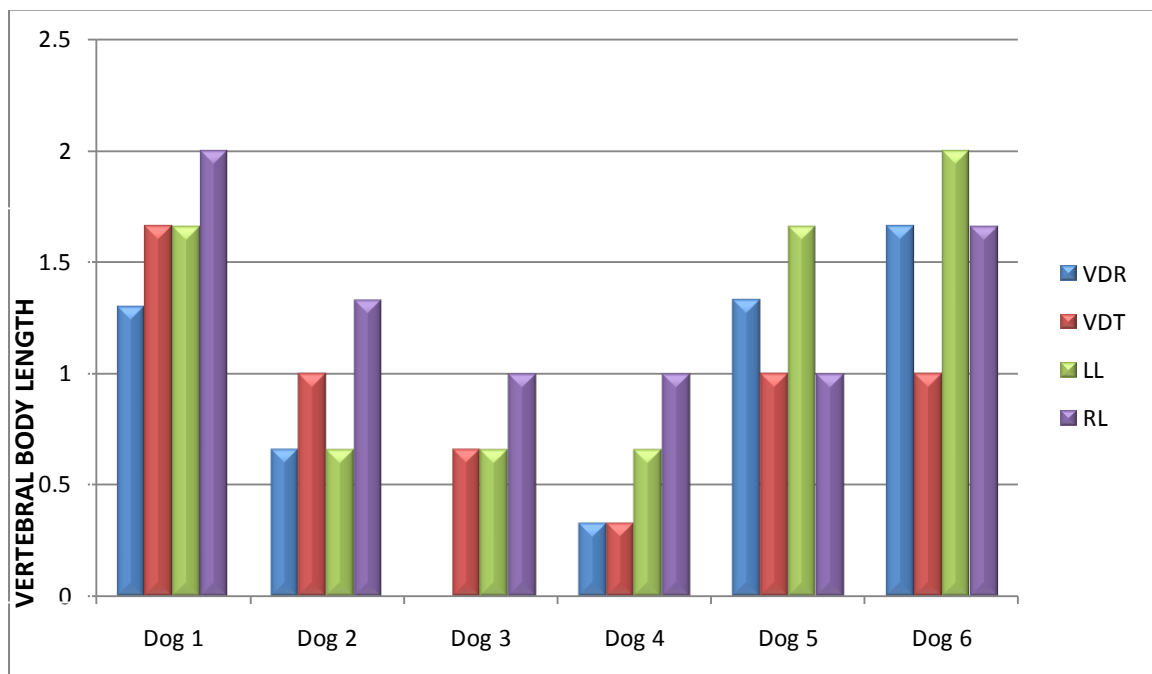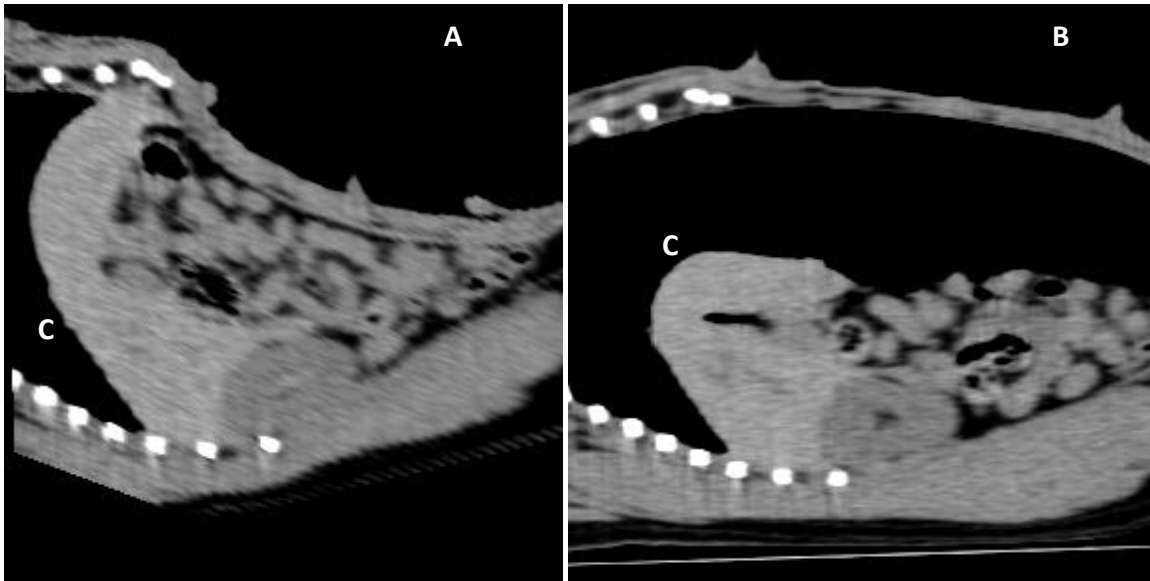
Figure 34 – A series of VDT PrI and PoI parasagittal images showing the cupula of the diaphragm

The PrI image (A) shows the most cranial point of the diaphragmatic cupula (C). This can be seen to move further cranial in the PoI image (B).

Gas in the pelvic cavity

In the VDR, VDT and the LL, there was no gas visible in the pelvic canal in the PrI and PoI scans.

Gas was only present in the pelvic canal of one dog in a RL PoI scan. This gas was sitting laterally to the colon and medial to the lateral wall of the pelvic canal.

Peritoneal reflections visible

Peritoneal reflections were not visible in any scans in any of the described positions.

Abdominal parenchymatous organ height % of abdominal height at umbilicus

Table 3: Abdominal parenchymatous organ height at umbilicus pre- and post-insufflation

	Pre-Insufflation Median (Range) in cm	Post-Insufflation Median (Range) in cm	P value
VDR	6.41 (5.34-6.75)	5.08 (4.1-6.1)	0.082
VDT	6.07 (5.23-6.95)	5.42 (4.77-5.98)	0.405
LL	12.05 (10.3-12.44)	5.3 (1.68-14.64)	0.001
RL	12.16 (10.33-14)	10.91 (5-15.14)	0.001

There was a statistically significant decrease in the parenchymatous organ height in LL and RL positions when comparing the PrI and PoI scans. In the VDR and the VDT there was a trend towards a decrease in the parenchymatous organ height when comparing the PrI and PoI scans.

The LL and RL show statistically significant increases in the parenchymatous organ height when compared to the VDR and the VDT in both PrI and PoI scans respectively.

Table 4: Abdominal wall height and parenchymatous organ % of abdominal height pre-and post-insufflation

	Pre-Insufflation		Post-Insufflation		
	Median (Range) in cm	% PrI	Median (Range) in cm	% PoI	P value
VDR	6.71 (5.47-6.8)	95	12.73 (10.65-12.78)	39	0.003
VDT	6.38 (5.44-7.04)	95	12.75 (10.06-14.67)	42	0.003
LL	12.95 (10.58-15.33)	93	14.9 (13.22-19.42)	35	0.703
RL	12.51 (10.46-15.72)	97	14.75 (8.29-17.54)	42	0.086

%= the abdominal organ height as a % of the abdominal height.

There was a statistically significant increase in the abdominal height in the VDR and the VDT when comparing the PrI and PoI scans. There was a trend in the LL and RL positions towards an increase in the abdominal height when comparing the PrI and PoI scans.

The LL and RL PrI scans showed a statistically significant higher value than the PrI scans in the VDR and VDT positions.

There was a trend in all positions showing a decrease in the parenchymatous organ height as a percentage of the abdominal height when comparing the PrI and PoI scans (Fig. 35).
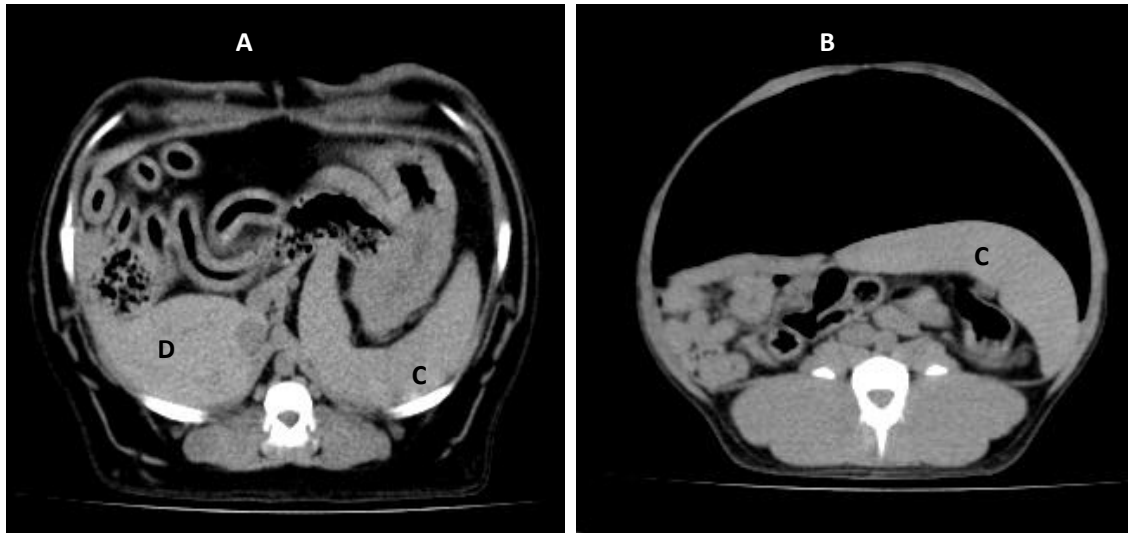
Fig 35 – A series of VDR PrI and PoI transverse images showing the change in abdominal organ height

PrI (A) transverse scan and PoI (B) transverse scan showing the compression of the parenchymatous organ mass. Different slice levels taken to illustrate the movement of the spleen (C) and associated organs. A liver lobe (D) can be seen in the PrI.

4.2 Liver

Distance from the caudal xiphoid to the liver

Table 5: Xiphoid to liver pre- and post-insufflation

	Pre-Insufflation Median (Range) in cm	Post-Insufflation Median (Range) in cm	P value
VDR	0.98 (0.7-2.05)	6.43 (5.3-7.13)	0.001
VDT	1.23 (0.38-2.54)	5.12 (4.24-5.59)	0.001
LL	0.83 (0-1.26)	4.55 (2.79-7.43)	0.002
RL	0.68 (0-1.08)	3.56 (1.56-4.53)	0.002

There was a statistically significant increase in the distance from the xiphoid to the ventral surface of the liver in all positions when the PrI and PoI scans are compared. The largest increase between PrI and PoI scans was seen in the VDR when compared to all the other positions (Fig. 36).
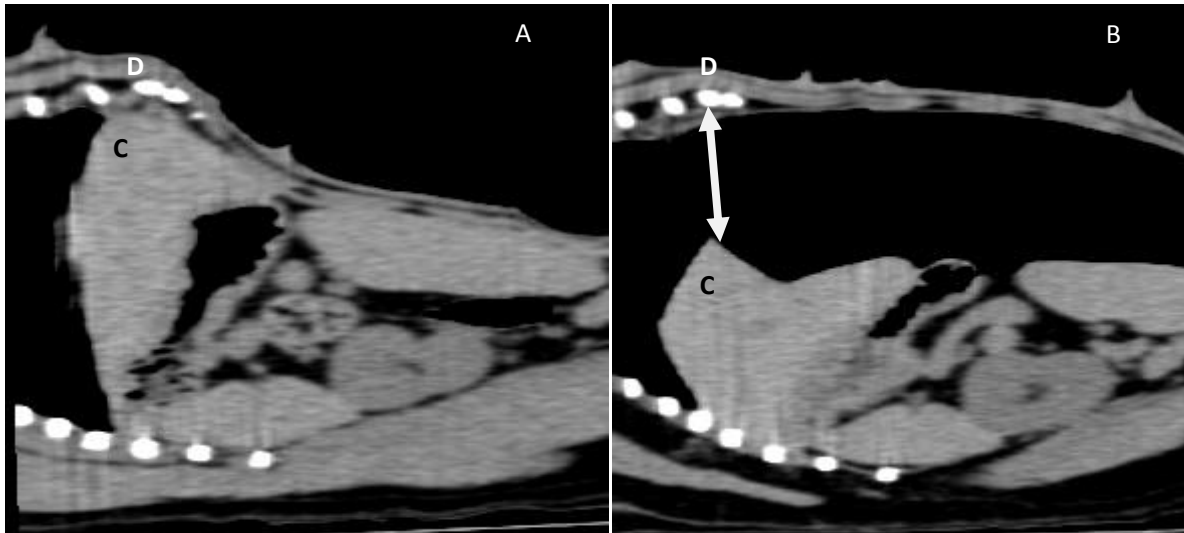
Figure 36 – A series of VDR PrI and PoI parasagittal images showing contact between the liver and xiphoid

The PrI (A) VDR shows the contact between the liver (C) and the xiphoid (D). In the PoI VDR (B) the increased distance is shown by the arrow.

Percentage contact between the liver and the body wall at T11

Table 6: Distance of liver contact with the body wall pre- and post-insufflation

	Pre-Insufflation Median (Range) in cm	Post-Insufflation Median (Range) in cm	P value
VDR	24.45 (17.2-29.3)	20.16 (11.72-21.1)	0.055
VDT	31.35 (10.4-39.9)	21.03 (9.98-28.92)	0.17
LL	26.28 (17.6-29.97)	14.65 (12-19.66)	0.011
RL	24.9 (16.22-33.2)	14.9 (8.16-19.46)	0.001

There was a statistically significant decrease in the distance of contact of the serosal surface of the liver in the RL and LL positions when comparing the PrI and PoI scans. In the VDR and

VDT there was a definite trend towards a decrease in the distance when comparing the PrI and PoI scans.

Table 7: Abdominal circumference and liver contact as a % of abdominal circumference pre- and post-insufflation

	Pre-Insufflation		Post-Insufflation		
	Median (Range) in cm	% PrI	Median (Range) in cm	% PoI	P value
VDR	42.59 (39.34-44.3)	52	47.18 (44.8-49.6)	42	0.055
VDT	43.95 (41.43-48.14)	71	46.68 (43.08-50.42)	45	0.085
LL	40.38 (39.39-42.54)	57	46.08 (43.56-50.96)	31	0.002
RL	40.12 (40.03-42.3)	64	46.99 (43.09-49.23)	31	0.001

%= contact of the liver circumference as a % of body wall circumference

There was a statistically significant increase in the abdominal circumference in the LL and RL positions when comparing the PrI and PoI scans. In the VDR and VDT there was a definite trend towards an increase in the abdominal circumference.

The percentages showed a definite trend towards a decrease in the amount of liver in contact with the body wall when comparing the PrI and PoI scans in all positions (Fig. 37).
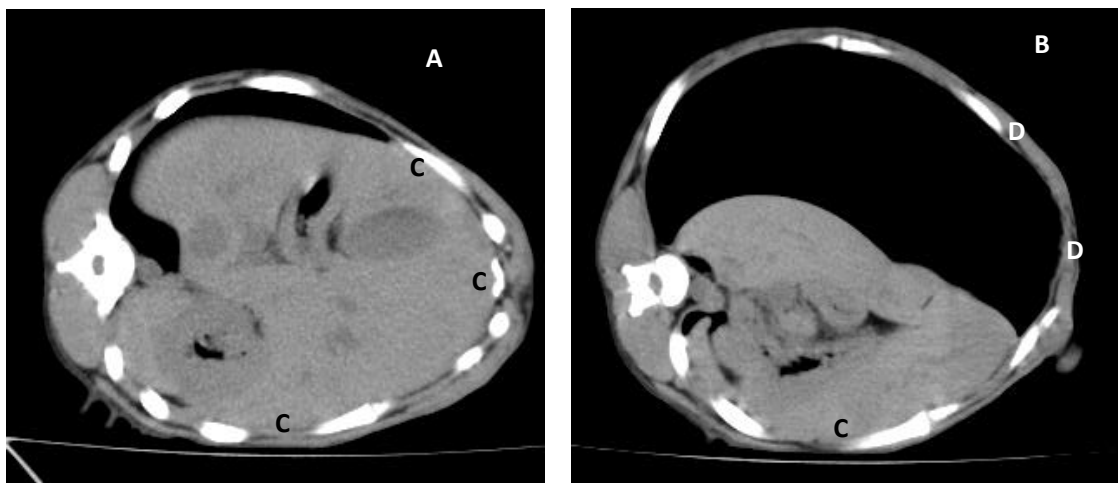
Figure 37 – A series of PrI and PoI LL transverse images showing liver contact with the body wall

The PrI (A) shows contact with the boy wall (C). The PoI scan (B) shows decreased contact with the body wall (D).

Distance from the apex of the gallbladder to the right abdominal wall

Table 8: Distance from the apex of the gallbladder to the right body wall pre- and post-insufflation

	Pre-Insufflation Median (Range) in cm	Post-Insufflation Median (Range) in cm	P value
VDR	1 (0.3-2.6)	4.41 (3.6-5.84)	0.001
VDT	1.17 (0.7-2.15)	3.32 (2.7-3.74)	0.001
LL	0.93 (0.29-1.91)	2.71 (1.28-3.96)	0.012
RL	0.62 (0.23-1.4)	0 (0-0.41)	0.011

There was a statistically significant increase in the distance from the lateral body wall to the apex of the gallbladder in all views except the RL when the PrI and PoI scans are compared (Fig. 38). The RL position showed a statistically significant decrease.
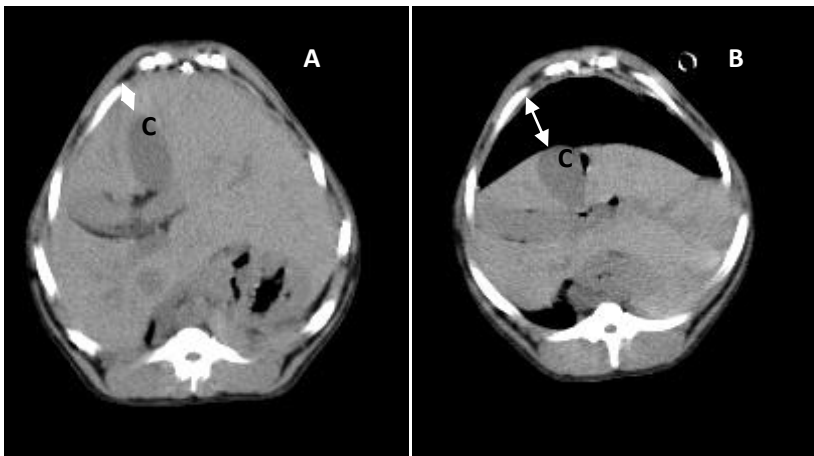
Figure 38 – A series of VDR PrI and PoI transverse images showing the distance from the apex of the gall bladder to the body wall

The distance from the apex of the gall bladder (C) to the body wall was increased between PrI (A) and PoI (B) scans. This distance is shown by the white arrows. The exposure of the gallbladder and decrease in hepatic contact can be seen.

The % contact of hepatic parenchyma to the gallbladder

Table 9: Gallbladder circumference pre- and post-insufflation

	Pre-Insufflation Median (Range) in cm	Post-Insufflation Median (Range) in cm	P value
VDR	10.04 (7.15-12.07)	9.84 (7.15-11.01)	0.923
VDT	9.89 (8.47-11.9)	10.23 (8.45-11.9)	0.833
LL	9.29 (8.32-11.01)	9.4 (8.73-11.94)	0.602
RL	9.93 (8.75-10.78)	9.59 (8.03-11.12)	0.661

There was no statistically significant change in the gallbladder circumference when comparing the PrI and PoI scans in all positions.

Table 10: Gallbladder contact with hepatic parenchyma pre- and post-insufflation

	Pre-Insufflation		Post-Insufflation		
	Median (Range) in cm	% PrI	Median (Range) in cm	% PoI	P value
VDR	9.92 (7.15-11.49)	98	7.03 (2.87-9.98)	70	0.019
VDT	9.49 (8.47-11.01)	95	5.66 (4.2-10.16)	55	0.039
LL	9.29 (8.32-11.01)	100	6.04 (5.26-9.92)	64	0.06
RL	9.93 (8.75-10.78)	100	8.63 (6.65-10.04)	89	0.068

%= the change in hepatic contact with the serosal surface of the gallbladder as a % of the entire gallbladder circumference

The two positions that showed a statistically significant decrease in the hepatic contact around the gallbladder were the VDR and the VDT when comparing PrI and PoI. In the LL and the RL there was no statistically significant increase, however there was a trend of decreasing hepatic parenchyma contact with the serosal surface of the gallbladder.

There was a definite trend towards a decrease in the percentage contact of the liver tissue around the gallbladder when the PrI and PoI scans were compared (Figs. 38 & 39).

The % of the gallbladder exposed

Table 11: Gallbladder exposed pre- and post-insufflation

	Pre-Insufflation Median (Range) in cm	Post-Insufflation Median (Range) in cm	P value
VDR	0 (0-0.58)	2.37 (1.03-3.02)	0.007
VDT	0.15 (0-0.91)	2.99 (1.51-5.94)	0.007
LL	0 (0)	2.32 (2.02-3.55)	0.001
RL	0 (0)	0 (0)	-

There was a statistically significant increase in the amount of the gallbladder exposed in all positions except the RL position when comparing PrI and PoI scans (Figs. 38 & 39).

Separation of the liver lobes

When comparing the PrI and PoI scans in all positions there was a consistent increase in the separation of the number of liver fissures and the length they opened. Only two dogs showed no change in the separation and length of fissure opening when comparing the PrI and PoI scans. No position led to a dramatic increase in the number and length of fissure opening (Fig. 39).

In the VDR two of the dogs had separation of one hepatic fissure with less than 25% of that fissure open during PrI. In the PoI one of these two dogs showed opening of three hepatic fissures to less than 25%, while the other dog showed opening of two hepatic fissures to more than 50% of their length. One dog showed a PrI opening of one fissure to 25-50% and a PoI opening of three hepatic fissures to more than 50%. One dog showed opening of two hepatic fissures to 25-50% in the PrI scans and opening of three fissures to 25-50% in the PoI scan. One showed opening of three hepatic fissures to less than 25% in the PrI and the opening of three hepatic fissures to more than 50% in the PoI. One dog showed opening of two fissures to less than 25% in the PrI and opening of three hepatic fissures to more than 50% in the PoI scan.

In the VDT two dogs showed one hepatic fissure open to less than 25% in the PrI scan. Both of these dogs showed opening of three hepatic fissures to 25-50% in the PoI. Two dogs showed opening of one hepatic fissure to 25-50% in the PrI scan and of these two dogs one showed opening of two hepatic fissures to 25-50% and the other showed opening of two

hepatic fissures to more than 50%. Two dogs showed opening of one hepatic fissure to more than 50% in the PrI and opening of three hepatic fissures to less than 25% in the PoI scan. One dog showed opening of two hepatic fissures to less than 25% in both the PrI and PoI scans.

In the LL scans four dogs showed opening of one hepatic fissure to less than 25% in the PrI scans. Of these four dogs, three showed opening of two hepatic fissures to more than 50% in the PoI scans. One dog of these four showed opening of three hepatic fissures to 25-50% in the PoI scan. One dogs showed opening of one hepatic fissure to 25-50% in the PrI scan and opening of three hepatic fissures to 25-50% in the PrI. One dog showed opening of two hepatic fissures to 25-50% in the PrI scan and opening of three hepatic fissures to less than 25% in the PoI scan.

In the RL scans all dogs showed opening of one hepatic fissure less than 25% in the PrI scan. Two dogs showed opening of two hepatic fissures to 25-50% in the PoI. One dog showed opening of one hepatic fissure to more than 50%, one dog showed opening of two hepatic fissures to less than 25% and one dog showed opening of three hepatic fissures to less than 25% in the PoI scans. One dog showed no change in the opening of hepatic fissures between the PrI and PoI and remained with one hepatic fissure open to less than 25%.

Figure 39 – A series of VDR PrI and PoI transverse images showing the relationship between the liver and the gallbladder

The PrI scan (A) clearly shows on open fissure (C) and the gallbladder (D) can be clearly seen surrounded by hepatic tissue. In the PoI scan (B) three fissures (E) can be seen to open and the apex of the gallbladder (D) is now exposed.

Distance of the lesser curvature of the stomach to the caudal part of the caudate lobe of the liver

Table 12: Distance of the lesser curvature of the stomach to the caudate liver lobe pre- and post-insufflation

	Pre-Insufflation Median (Range) in cm	Post-Insufflation Median (Range) in cm	P value
VDR	2.24 (1.3-4.25)	2.1 (0-3.68)	0.328
VDT	3.55 (0-6.68)	2.25 (0-5.03)	0.595
LL	2.83 (0-5)	2.3 (0-4.78)	0.662
RL	2.44 (0-5.3)	2.4 (0-4.19)	0.754

There was no statistically significant change in the distance between the lesser curvature of the stomach and the caudate lobe in any of the positions when comparing the PrI and PoI scans. There was a trend in the VDT, VDR and the LL towards a decrease in this distance and the RL showed no change when the PrI and PoI scans were compared.

Distance from the head of the spleen to the left lateral liver lobe

Table 13: Distance from the head of the spleen to the left lateral liver lobe pre- and post-insufflation

	Pre-Insufflation Median (Range) in cm	Post-Insufflation Median (Range) in cm	P value
VDR	0.85 (0.15-1.61)	0.54 (0-1.1)	0.261
VDT	0.31 (0-1.16)	0.18 (0-1.4)	0.9
LL	0.76 (0-2.41)	0.48 (0-1.1)	0.259
RL	0.98 (0-3.29)	1.36 (0.2-2.37)	0.789

There was no statistically significant change in the distance from the head of the spleen to the left lateral liver lobe when comparing the PrI and PoI scans in all positions. However

there was a definite trend in the VDR, VDT and the LL towards a decrease and in the RL there was a trend towards an increase when comparing the PrI and PoI scans (Fig. 40).
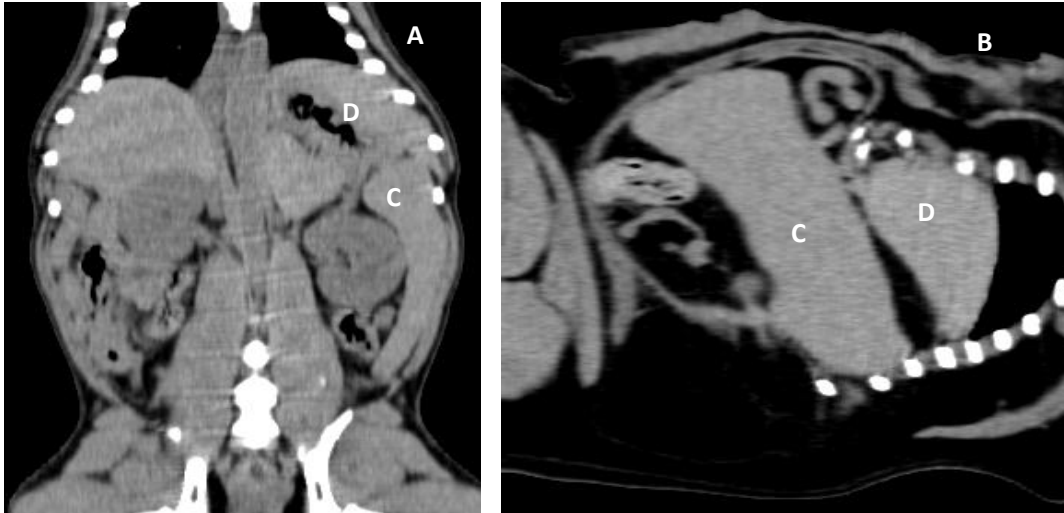
Figure 40 – A series of PoI dorsal and parasagittal images showing the relationship between the spleen and liver

A dorsal PoI image (A) shows the close relationship between the spleen (C) and the liver (D). The same close relationship can be seen in the parasagittal PoI image (B).

Cystic duct visibility

When comparing the PrI and PoI scans there was no position that provided better accessibility of the cystic duct or visualisation on CT.

In the VDR, the cystic duct was visible in three dogs in the PrI scans. In the PoI scans the cystic duct was visible in two of these three dogs. These were the only two dogs in which the cystic duct was visible in PoI.

In the VDT, the cystic duct was visible in one dog in the PrI scans. In the PoI scans it was visible in two of the dogs, but it was not visible in the dog in which it had been in the PrI scans.

In the LL, the cystic duct was visible on in four of the dogs in the PrI scans. In the PoI scans it was visible in these same four dogs.

In the RL the cystic duct was visible on in five of the dogs in the PrI scans. In the PoI scans it was visible in only three of these five dogs. The cystic duct was not visible in one dog PrI or PoI (Fig. 41).
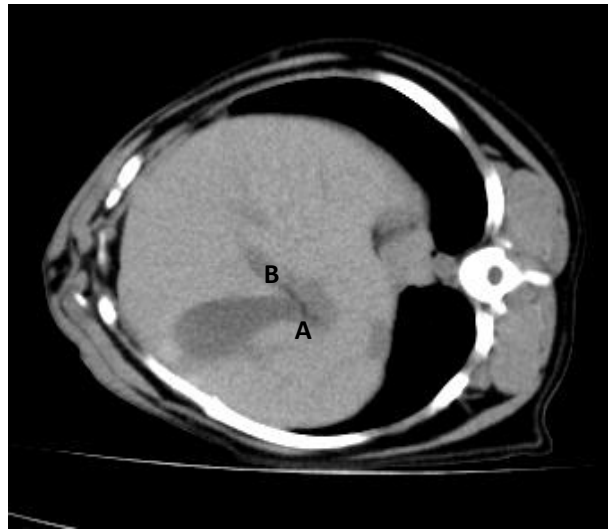
Figure 41 – A RL PrI transverse image showing the cystic duct

The cystic duct (A) could be seen on CT within the liver tissue. The hepatic veins (B) can be seen.

Distance between the vena porta and the vena cava

Table 14: Distance of the portal vein to the caudal vena cava pre- and post-insufflation

	Pre-Insufflation Median (Range) in cm	Post-Insufflation Median (Range) in cm	P value
VDR	0.65 (0.15-2.5)	0.41 (0-1.1)	0.108
VDT	0.66 (0.5-0.97)	0.67 (0.27-1.37)	0.803
LL	0.92 (0.57-1.69)	1.19 (0-2.27)	0.672
RL	0.74 (0.3-1.73)	0.63 (0.37-2.3)	0.870

There was no statistically significant change in the distance from the portal vein to the caudal vena cava in any of the positions when comparing the PrI and PoI scans. The VDR and the RL showed a trend towards a decrease in the distance and the LL showed a trend towards an increase when the PrI and PoI scans were compared. The VDT showed no change (Fig. 42).
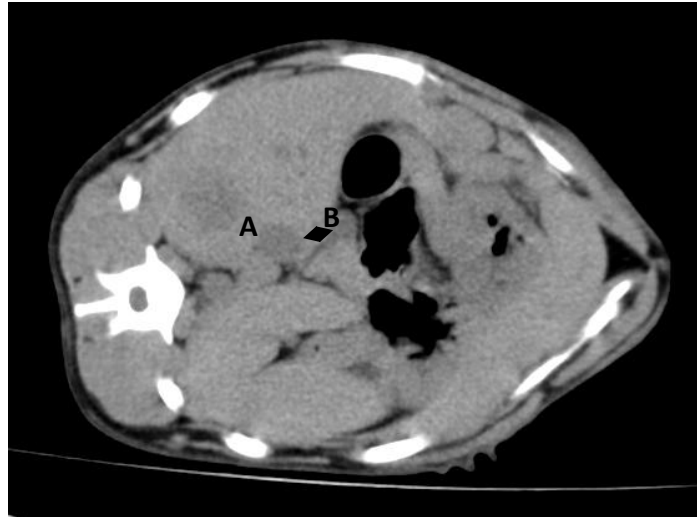
Figure 42 – A LL PrI transverse image showing the distance from the vena cava to the portal vein

The relationship between the caudal vena cava (A) and the portal vein (B) which does not show significant change between the PrI and PoI scan. The distance is shown by the black arrowheads.

4.3 Spleen

Percentage of spleen in contact with the body wall

Table 15: Parietal splenic length pre- and post-insufflation

	Pre-Insufflation Median (Range) in cm	Post-Insufflation Median (Range) in cm	P value
VDR	14.02 (12.63-18.25)	12.33 (8.92-17.8)	0.217
VDT	19.7 (15.44-23.45)	19.03 (15.89-22.14)	0.657
LL	15.82 (13.66-16.85)	15.63 (12.78-18.92)	0.641
RL	17.96 (13.3-19.42)	14.02 (12.4-17.32)	0.023

There was no statistically significant change in the visible length of the parietal surface of the spleen in any of the positions when comparing PrI and PoI scans except the RL. The RL showed a statistically significant decrease in the visible length when comparing PrI and PoI scans

Table 16: Splenic parietal surface contact distance with lateral peritoneal surface of the body wall pre- and post-insufflation

	Pre-Insufflation		Post-Insufflation		
	Median (Range) in cm	% PrI	Median (Range) in cm	% PoI	P value
VDR	8.87 (7.56-13.9)	63	7.01 (5.52-10.05)	57	0.101
VDT	12. 05 (9.6-19.81)	61	10.42 (5.82-11.62)	54	0.077
LL	9.23 (6.37-14.27)	58	12.17 (6.94-14.08)	77	0.251
RL	12.21 (6.99-14.86)	67	1.46 (0-4.66)	10	0.001

%= the parietal surface of the spleen in contact with the body wall as a % of the entire parietal splenic surface

There was a statistically significant decrease in the contact of the parietal surface of the spleen with the peritoneal surface of the lateral body wall in the RL position when comparing the PrI and PoI scans. All other positions showed no significant change in the contact when comparing PrI and PoI scans. However there was a trend in both the VDR and VDT positions towards a decrease and in the LL there was a trend towards an increase in the contact distance when comparing the PrI and PoI scans.

The percentage of contact of the spleen to the body wall showed a trend towards a decrease in all of the positions except the LL when the PrI and PoI scans were compared. The LL percentage showed an increase in splenic parietal surface contact when PrI and PoI scans were compared (Fig. 43).
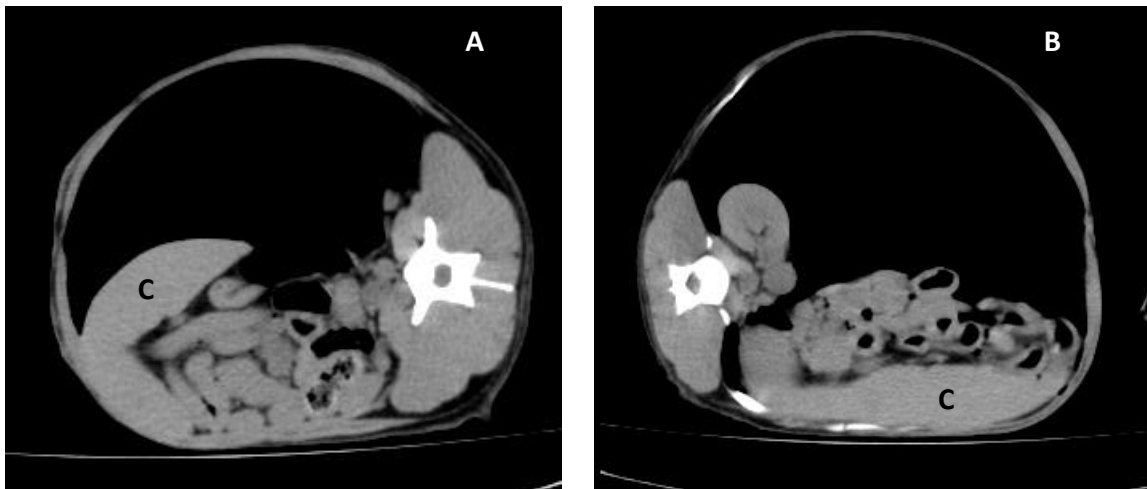
Figure 43 – A series of PoI RL and LL images showing the position of the spleen

A RL PoI (A) compared to a LL PoI (B). The movements of the spleen (C) can be seen and its relation to the body wall. The scans are taken from different slices to illustrate the splenic movement.

Hilar access

The hilar area was not accessible in any of the scans in any of the positions described.

Distance from the pelvis of the left kidney to the caudal portion of the head of the spleen

Table 17: Distance from the pelvis of the left kidney to the head of the spleen pre- and post-insufflation

	Pre-Insufflation Median (Range) in cm	Post-Insufflation Median (Range) in cm	P value
VDR	2.35 (1.61-2.88)	2.66 (2.2-3.45)	0.156
VDT	2.99 (1.79-6.1)	3.35 (2.3-7.31)	0.722
LL	1.93 (1.64-2.3)	3.31 (1.81-5.06)	0.18
RL	2.07 (1.35-3.62)	2.23 (1.83-4.28)	0.722

There was no statistically significant change in the distance from the pelvis of the left kidney to the head of the spleen in any of the positions, when comparing the PrI and PoI scans.

However all positions showed a definite trend towards an increase in this distance when comparing the PrI and PoI scans (Fig. 44).
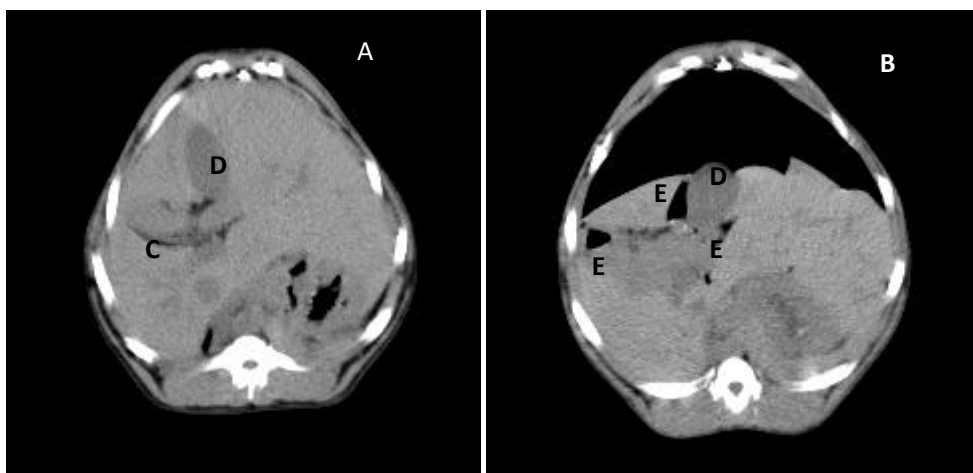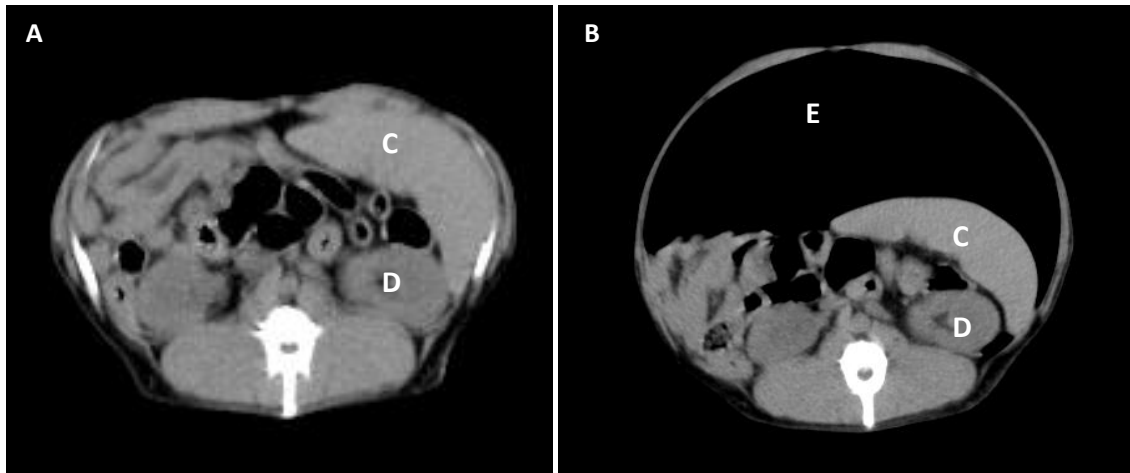

Figure 44 – A series of VDR PrI and PoI transverse images showing the relationship between the spleen and the left kidney

The PrI VDR (A) shows the relationship between the spleen (C) and the left kidney (D) with the gas cap (E) in the PoI VDR (B).

Contact distance between the spleen and the stomach

Table 18: Splenic contact length with the stomach in pre- and post-insufflation

	Pre-Insufflation Median (Range) in cm	Post-Insufflation Median (Range) in cm	P value
VDR	7.3 (3.23-8.08)	6.16 (3.74-7.56)	0.501
VDT	9.26 (8.72-11.91)	9.04 (6.07-12.31)	0.708
LL	6.52 (5.65-7.48)	6.57 (5.89-10.78)	0.320
RL	6.46 (5.27-8.27)	6.03 (2.07-6.34)	0.086

There was no statistically significant change of the splenic contact with the stomach in any of the positions when comparing the PrI and PoI scans. There was however a trend in the VDR, VDT and the RL towards a decrease in the contact distance and the LL showed no change when comparing PrI and PoI scans (Fig. 45).
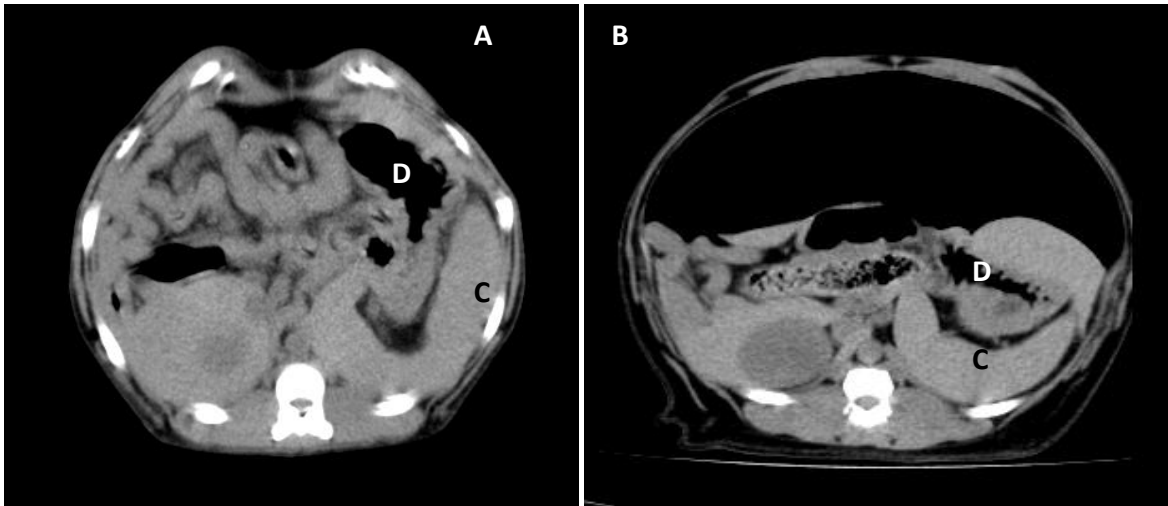
Figure 45 – A series of VDR PrI and PoI transverse images showing the relationship between the spleen and stomach

The PrI VDR (A) scan shows the spleen (C) in contact with the stomach (D). The PoI VDR (B) scan shows the relationship after insufflation.

4.4   Gastro-intestinal Tract

Position of the pylorus in relation to the vertebral column

Graph 2: Movement of the pylorus in vertebral body length in all positions
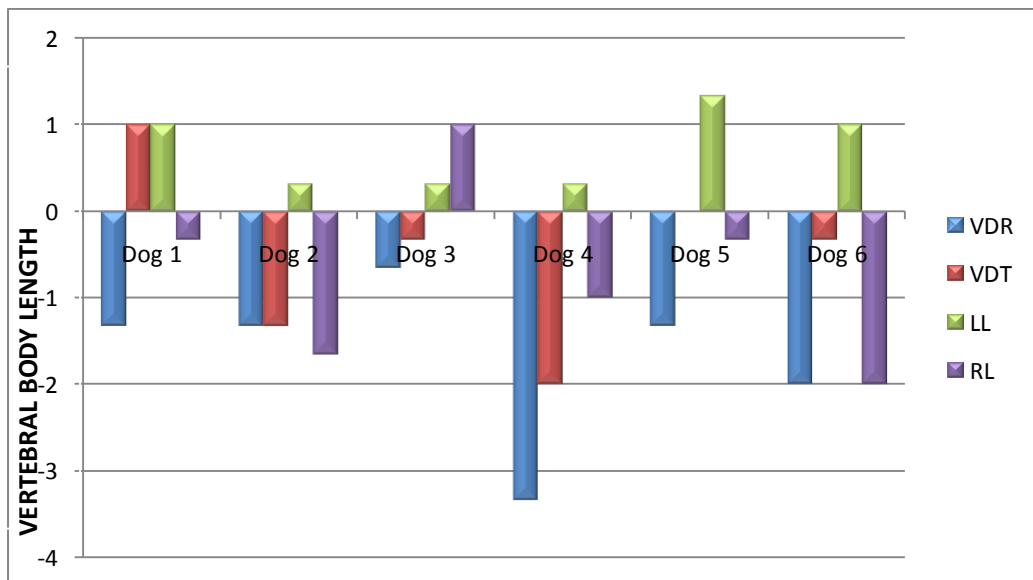
A negative value indicates caudal movement of the pylorus and a positive value indicates cranial movement. The PrI value is compared to the PoI value to quantify the movement.

The position of the pylorus moved caudally in all dogs in the VDR position (Graph 2).
In the VDT position there was cranial movement in one dog, no movement in one dog and caudal movement in all the other dogs (Graph 2).

In the LL position there was cranial movement in all the dogs (Graph 2).

In the RL position there was cranial movement in one dog and caudal movement in all the others (Graph 2).

Stomach cross section long axis and short axis

Table 19: Stomach cross section long axis and short axis pre- and post-insufflation

	Pre-Insufflation		Post-Insufflation			
	Long axis Median (Range) in cm	Short axis Median (Range) in cm	Long axis Median (Range) in cm	Short axis Median (Range) in cm	P value long axis	P value short axis
VDR	9.04 (7.59-11.02)	2.44 (1.86-3.2)	9.21 (8.83-9.71)	1.81 (1.73-2.61)	0.850	0.085
VDT	10.4 (9.95-11.24)	2.6 (1.94-2.79)	8.4 (6.94-10.6)	2.49 (1.88-2.69)	0.14	0.679
LL	10.03 (8.6-11.55)	2.64 (1.17-4.75)	11.92 (10.23-13.04)	2.57 (2.13-3.34)	0.16	0.799
RL	9.72 (9.2-11.38)	2.28 (1.8-4.65)	10.28 (9.71-11.54)	2.5 (1.8-3.1)	0.286	0.868

In the VDT there was a statistically significant decrease in the cross sectional long axis diameter of the stomach when the PrI and PoI scans were compared. However in the other 3 positions there was a trend towards an increase in the long axis diameter of the stomach when comparing the PrI and PoI scans (Fig. 46).

There was no statistically significant change in the short axis diameter of the stomach when comparing PrI and PoI scans in all the described positions (Fig. 46).
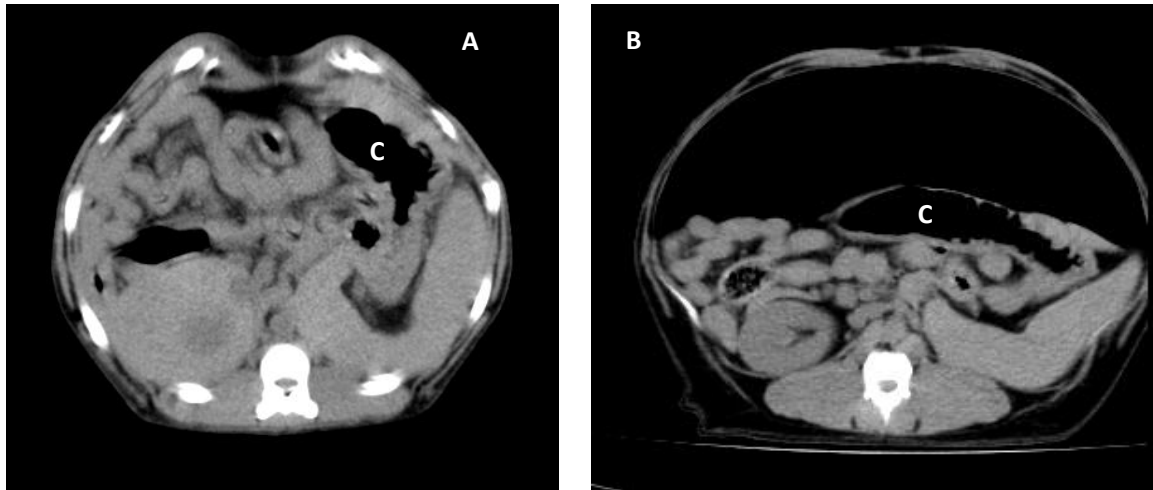
Figure 46 – A series of VDR PrI and PoI transverse images showing the stomach size

The size of the stomach (C) seen in the PrI VDR (A) and the PoI VDR (B).

Distance of the mid descending duodenum from the body wall

Table 20: Distance from the body wall to the descending duodenum pre- and post-insufflation

	Pre-Insufflation Median (Range) in cm	Post-Insufflation Median (Range) in cm	P value
VDR	0.05 (0-0.64)	0 (0-0.1)	0.235
VDT	0 (0-0.73)	0 (0)	0.363
LL	0 (0-0.63)	8.48 (7.11-9.4)	0.001
RL	0 (0-0.99)	0 (0)	0.341

There was no statistically significant change in the distance from the body wall to the descending duodenum in the VDR, VDT and the RL when comparing PrI and PoI scans. In the LL there was a statistically significant increase in the distance described when comparing the PrI and PoI scans (Fig. 47).
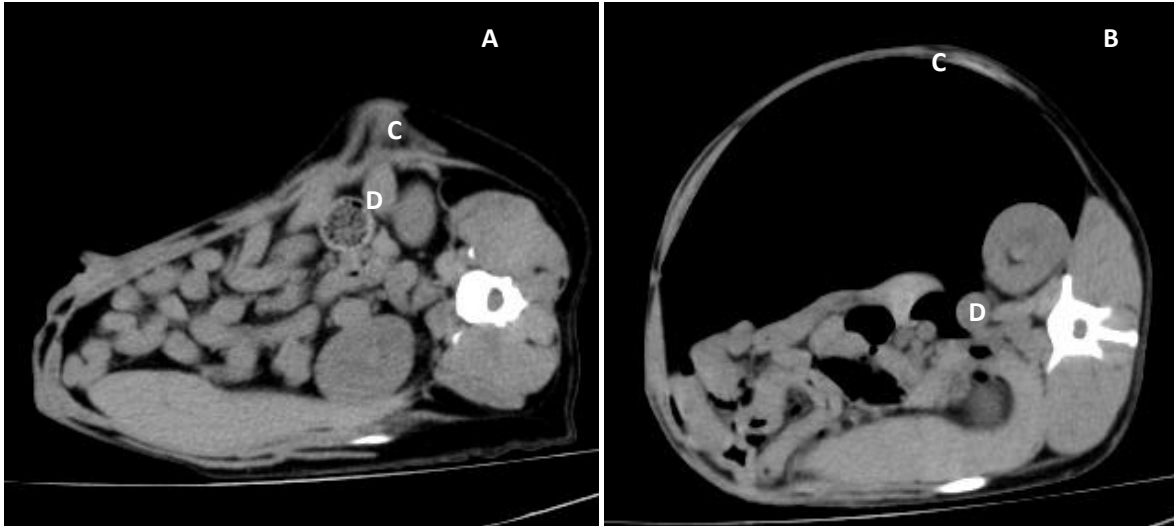
Figure 47 – A series of LL PrI and PoI transverse images showing the relationship between the body wall and the descending duodenum

The PrI (A) showing the relationship between the body wall (C) and the descending duodenum (D). An increase in distance is seen in the PoI (B). A slice taken caudal to the PrI is shown to give the best image of the duodenum.

Distance of the cranial duodenal flexure to the gallbladder

Table 21: Distance from the cranial duodenal flexure to the gallbladder pre- and post-insufflation

	Pre-Insufflation Median (Range) in cm	Post-Insufflation Median (Range) in cm	P value
VDR	1.95 (0.71-2.29)	1.78 (1.1-1.88)	0.714
VDT	1.63 (0.15-2.86)	1.88 (0.6-2.77)	0.793
LL	2.17 (1.3-2.76)	1.77 (0.45-2.33)	0.147
RL	1.79 (0.87-2.32)	1.83 (0.7-4.03)	0.504

There was no statistically significant change in the distance from the cranial duodenal flexure to the gallbladder when comparing the PrI and PoI scan in all positions. However, in the LL and the VDR there was a trend towards a decrease in the described distance when comparing the PrI and PoI scans. The VDT and RL showed a trend towards increasing this distance when comparing PrI and PoI scans.

Distance from the pelvis of the right kidney to the descending duodenum

Table 22: Pelvis of the right kidney to the descending duodenum pre- and post-insufflation

	Pre-Insufflation Median (Range) in cm	Post-Insufflation Median (Range) in cm	P value
VDR	4.39 (3.09-4.59)	3.62 (2.39-4.14)	0.122
VDT	6.04 (4.23-6.49)	4.46 (3.23-7.17)	0.315
LL	5.11 (4.81-7.98)	6.12 (4.17-8.95)	0.776
RL	5.87 (4.62-7.19)	5.71 (4.1-9.82)	0.387

There was no statistically significant change in the distance from the pelvis of the right kidney to the descending duodenum when comparing PrI and PoI scans in all the positions. However there was a trend towards a decrease in the distance in the VDR, VDT and the RL when comparing PrI and PoI scans. The LL showed a trend towards an increase when comparing the PrI and PoI scans. (Fig. 48).
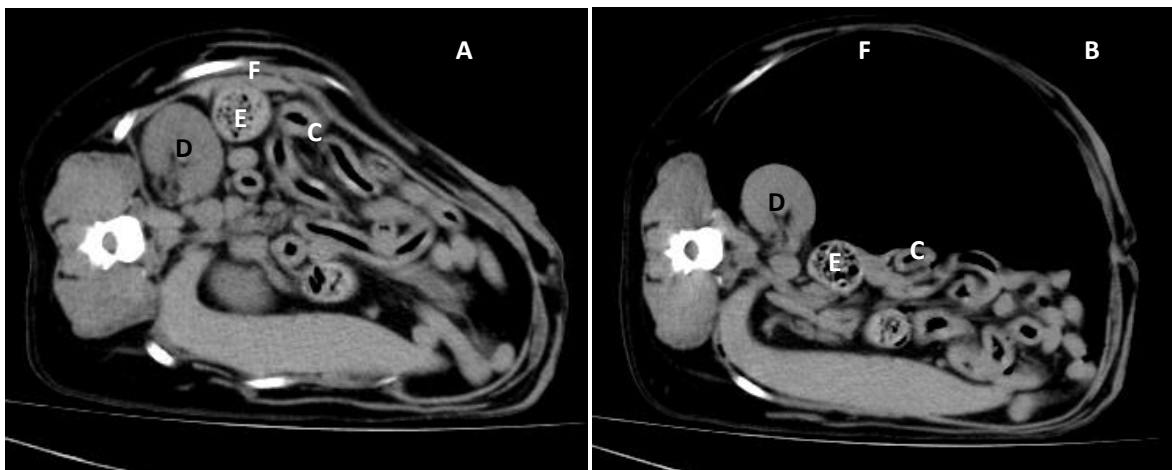
Figure 48 – A series of LL PrI and PoI transverse images showing the relationship between the duodenum, right kidney and colon

The PrI (A) shows the close association between the duodenum (C), the right kidney (D) and the colon (E). In the PoI (B) one can still see the close association, however all the described organs have moved away from the right body wall (F).

4.5 Pancreas

The pancreas was difficult to visualise in all positions PrI and PoI. There was no position that allowed one to visualise the pancreas best on CT imaging.

Right limb of the pancreas

The right limb of the pancreas (Fig. 49) was easily identified in the highest number of dogs. The VDR and the VDT showed better identification but this was marginal (Graph 3).

Body of the pancreas

The body of the pancreas was the second easiest to identify in most dogs. It was better seen in the PrI scans of the VDT, LL and RL (Graph 3).

Left limb of the pancreas

The left limb was the most difficult to identify in all scans and positions. The RL PoI scan showed no visibility in any of the dogs (Graph 3).

Graph 3: Visibility of the different parts of the pancreas in all positions
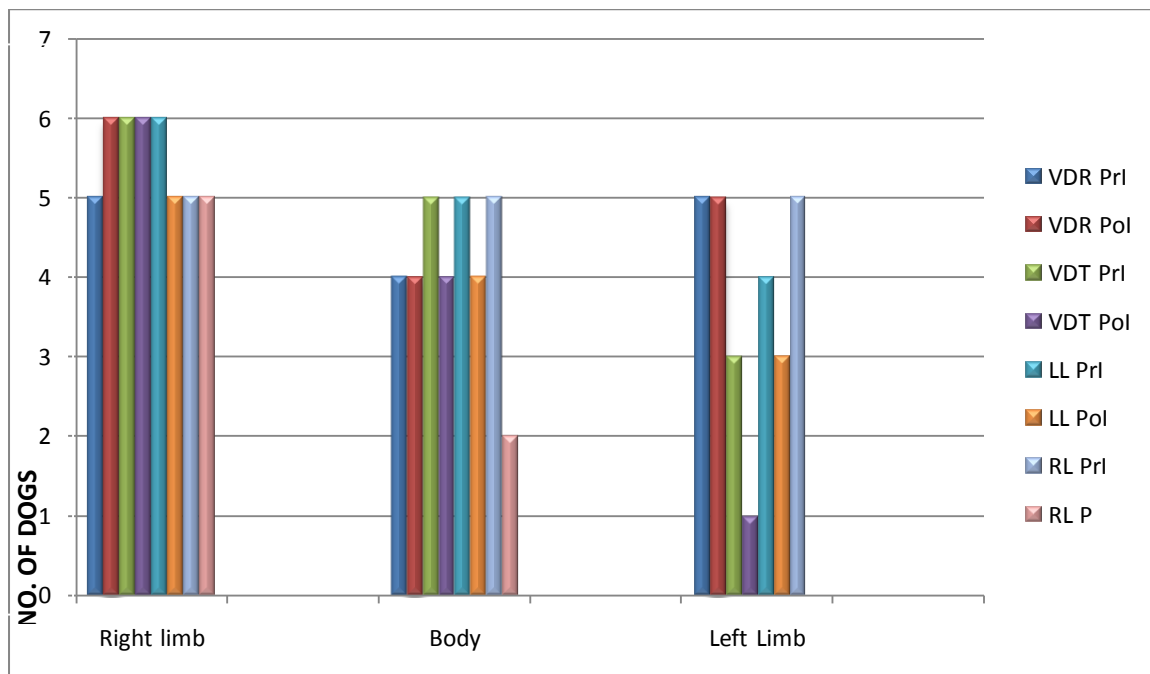
Figure 49 - A VDR PoI transverse image showing the relationship between the pancreas and duodenum
The duodenum (A) is seen in relation to the right kidney (B). The right limb of the pancreas can be seen (C)

4.6 Kidneys

Cross sectional diameter of the kidneys

Table 23: Cross sectional diameter of the left and right kidney pre- and post-insufflation

	Pre-Insufflation		Post- Insufflation			
	Left Median (Range) in cm	Right Median (Range) in cm	Left Median (Range) in cm	Right Median (Range) in cm	P value left	P value right
VDR	2.84 (2.37-3.34)	2.88 (2.73-3.1)	2.71 (2.65-2.84)	2.82 (2.66-3.2)	0.465	0.652
VDT	2.96 (2.51-3.13)	3.1 (2.39-3.48)	2.65 (2.37-2.95)	3.04 (2.61-3.66)	0.185	0.646
LL	2.93 (2.74-3.36)	2.86 (2.6-3.12)	3.15 (3.2-3.3)	2.97 (2.63-3.2)	0.382	0.788
RL	2.86 (2.41-2.92)	2.84 (2.71-3.11)	2.93 (2.61-2.94)	2.96 (2.69-3.23)	0.507	0.881

In all positions there was no significant change in the diameter of the left kidney when comparing the PrI and PoI scans.
In all positions there was no significant change in the diameter of the right kidney when comparing PrI and PoI scans.

Distance from the cranial pole of the right kidney to the renal fossa of the liver

Table 24: Distance from the cranial pole of the right kidney to the renal fossa, pre- and post-insufflation

	Pre-Insufflation Median (Range) in cm	Post-Insufflation Median (Range) in cm	P value
VDR	0 (0)	0 (0-0.32)	0.363
VDT	0 (0)	0 (0)	-
LL	0 (0)	0.76 (0.34-1.65)	0.001
RL	0 (0-0.15)	0 (0-0.2)	0.845

There was no statistically significant change in the distance from the renal fossa to the cranial pole of the right kidney in any of the positions except the LL position. In the LL there was a statistically significant increase in the distance from the PrI to the PoI (Fig. 50).
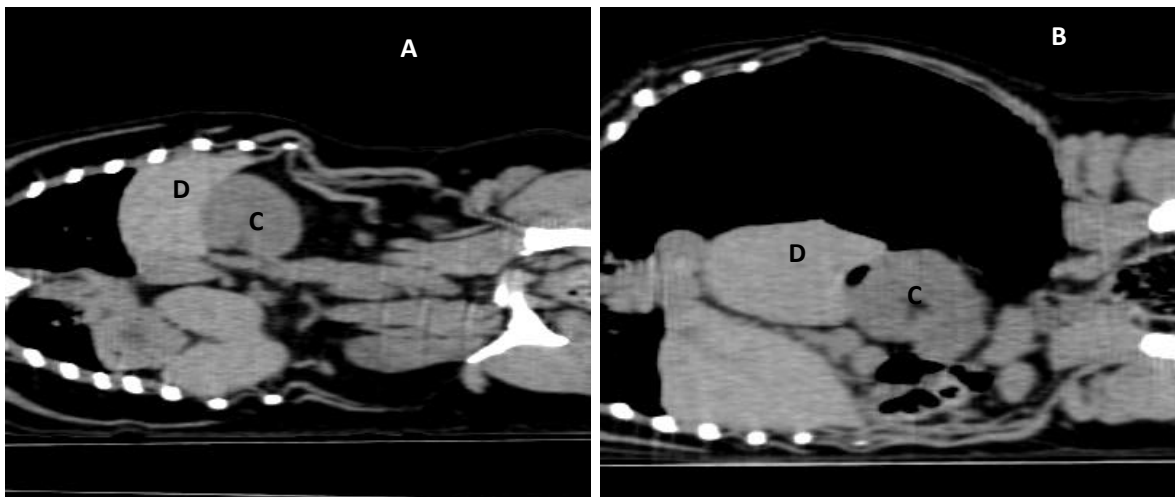
Figure 50 – A series of LL PrI and PoI parasagittal images showing the relationship between the liver and the right kidney

The PrI (A) shows the contact between the right kidney (C) and the renal fossa (D). In the PoI (B) the slight increase in distance between the right kidney (C) and the renal fossa (D) can be seen.

Distance from the cranial and caudal halves of the kidneys to the aorta

Table 25: Distance of the cranial and caudal halves of the left kidney to the aorta pre- and post-insufflation

	Pre-Insufflation		Post-Insufflation			
	Cranial Median (Range) in cm	Caudal Median (Range) in cm	Cranial Median (Range) in cm	Caudal Median (Range) in cm	P value cranial	P value caudal
VDR	2.41 (0.76-3.04)	3.4 (1.9-4.75)	2.59 (2.1-3.31)	3.51 (2.71-5.61)	0.273	0.391
VDT	2.52 (1.42-3.31)	3.72 (3.41-4.69)	1.97 (1.64-3.97)	3.59 (2.67-4.09)	0.863	0.268
LL	1.4 (0.69-2.15)	2.26 (0.95-3.01)	1.79 (1.74-2.58)	2.96 (1.02-4.61)	0.051	0.193
RL	1.53 (1-2.19)	1.28 (0.68-2.52)	1.16 (0.47-2.89)	1.07 (0.12-3.01)	0.612	0.922

There was no statistically significant change in the distance from the cranial half of the left kidney to the aorta in any of the positions when comparing the PrI and PoI scans. However, in the VDT and the RL there was a trend towards a decrease in the distance and in the VDR and the LL there was a trend towards an increase when PrI and PoI scans were compared. (Fig. 51).

There was no significant change in the distance from the caudal half of the left kidney to the aorta in any of the positions when comparing the PrI and PoI scans. The VDR and LL showed a trend towards increasing the described distance. The VDT and the RL showed a trend towards a decrease of the distance when comparing the PrI and PoI scans in both positions (Fig. 51).

*Table 26: Distance from the cranial and caudal halves of the right kidney to the aorta pre-
and post-insufflation*

	Pre-Insufflation		Post-Insufflation			
	Cranial Median (Range) in cm	Caudal Median (Range) in cm	Cranial Median (Range) in cm	Caudal Median (Range) in cm	P value cranial	P value caudal
VDR	2.25 (1.31-3.11)	2.19 (1.59-3.11)	1.37 (0.43-1.43)	1.53 (0.49-1.78)	0.149	0.488
VDT	2.07 (1.88-2.58)	2.04 (0.79-3.06)	1.29 (0.41-2.21)	1.46 (0.55-3.6)	0.519	0.964
LL	2.76 (1.54-3.78)	4.08 (2.58-4.19)	1.83 (0.58-3.23)	3.56 (2.73-3.9)	0.019	0.023
RL	2.22 (0.53-3.13)	3.36 (1.96-4.6)	1.4 (1.08-2.73)	3.05 (2.24-4.22)	0.009	0.025

There was a statistically significant increase in the LL and the RL positions when comparing the PrI and PoI scans. There was no statistically significant difference in the VDT and VDR when comparing PrI and PoI scans of the cranial half of the right kidney to the aorta. However the VDR showed a trend towards a decrease and the VDT showed no change when the PrI and PoI scans were compared. (Fig. 51).

The LL and RL showed a statistically significant increase when comparing the PrI and PoI scans. There was no statistically significant change in the distance of the right caudal half of the kidney from the aorta in the VDR and the VDT when comparing PrI and PoI scans. The VDR and VDT positions showed a trend of an increase in the distance when PrI and PoI scans are compared (Fig. 51).
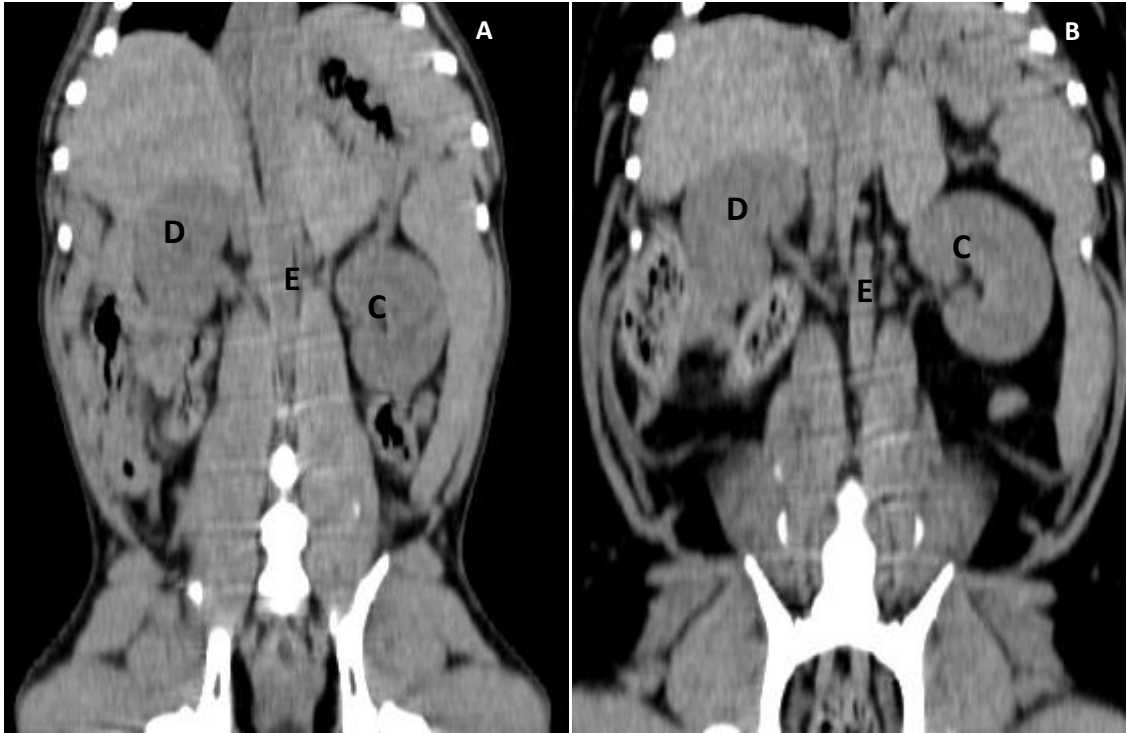
Figure 51 – A series of VDR PrI and PoI dorsal images showing the relationship between the kidneys and the aorta

The PrI (A) dorsal scan taken through the pelvis of the left kidney (C) showed a close relationship between the left and right (D) kidney and the aorta (E). In the PoI (B) at the same level this distance was seen to increase.

Distance from the tip of the transverse process of L2 to the nearest surface of each kidney

Table 27: Distance from the left and right kidney to the tip of the respective transverse process of L2 pre- and post-insufflation

	Pre-Insufflation		Post-Insufflation			
	Left Median (Range) in cm	Right Median (Range) in cm	Left Median (Range) in cm	Right Median (Range) in cm	P value left	P value right
VDR	1.07 (0.88-1.37)	0.95 (0.65-1.63)	0.79 (0.44-1.37)	0.88 (0.43-1.76)	0.137	0.643
VDT	1 (0.64-1.52)	0.82 (0.4-1.81)	0.69 (0.34-1.18)	0.82 (0.3-1.12)	0.207	0.395
LL	1.46 (0.37-2.3)	1.04 (0.82-1.51)	1.17 (0.65-2.13)	0.75 (0.45-1.8)	0.748	0.348
RL	1.28 (0.7-1.79)	0.86 (0.52-1.67)	2.79 (1.45-3.67)	1.1 (0.31-1.28)	0.003	0.889

There was a statistically significant increase in the distance from the left kidney to the tip of the L2 transverse process in the RL position when comparing the PrI and PoI scans. In the

other 3 positions there was a trend towards a decrease in the described distance when comparing the PrI and PoI scans.

There was no statistically significant change in the distance from the right kidney to the tip of the transverse process of L2 in any of the positions when comparing PrI and PoI scans. However, the LL showed a trend towards a decrease in the distance when comparing PrI and PoI scans (Fig. 52). The RL showed a trend towards an increase when comparing the PrI and PoI scans.

Distance from the lateral peritoneal surface of the body wall to the mid lateral serosal surface of the kidney

Table 28: Distance from the left and right body wall to the nearest lateral surface of the left and right kidney respectively pre- and post-insufflation

	Pre-Insufflation		Post-Insufflation			
	Left Median (Range) in cm	Right Median (Range) in cm	Left Median (Range) in cm	Right Median (Range) in cm	P value left	P value right
VDR	0.88 (0-0.93)	0.89 (0-2.36)	1.92 (0.53-2.82)	0.9 (0.3-1.68)	0.92	0.94
VDT	0.39 (0.13-0.66)	0.92 (0.64-1.97)	1.07 (0-1.47)	1.92 (0.83-2.65)	0.06	0.129
LL	1.74 (0-2.24)	0.23 (0-1.48)	0 (0-1.88)	3.99 (2.91-4.86)	0.055	0.001
RL	1.65 (0-0.63)	0 (0-0.63)	6.9 (4.36-7.82)	0 (0-0.42)	0.001	0.797

There was a statistically significant increase in the distance from the body wall to the left kidney in the RL when comparing the PrI and PoI scans. There was a trend towards an increase in the distance in the VDR and the VDT when comparing PrI and PoI scans. The LL showed a trend towards a decrease in this distance when comparing the PrI and PoI scans.

There was a statistically significant increase in the distance of the right kidney to the body wall in the LL view when comparing PrI and PoI scans. There was a trend towards an increase in the distance in the VDR and the VDT positions when comparing PrI and PoI scans. The RL showed no real change. (Fig. 52)
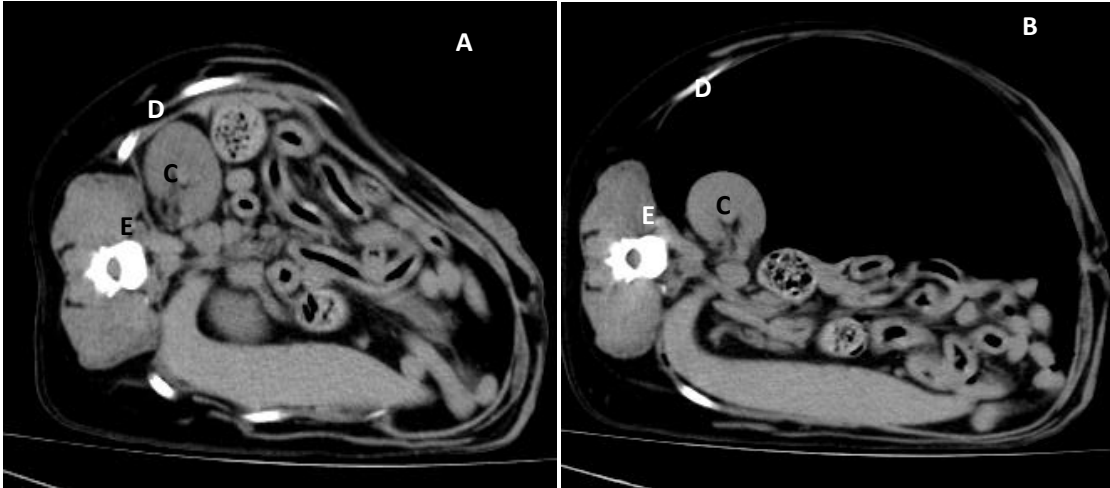
Figure 52– A series of PrI and PoI LL transverse images showing the relationship of the right kidney, body wall and vertebra

The PrI (A) shows the right kidney (C) in contact with the body wall (D). In the PoI (B) the right kidney (C) can be seen to fall away from the body wall (D). In both the relationship between the tip of the transverse process of L2 (E) and the right kidney is visible and seen to increase in the PoI image.

4.7   Adrenals

Distance from the closest aortic wall to the medial surface of the mid-body of the adrenal

Table 29: Distance from the medial surface of the left adrenal to the aorta pre- and post-insufflation

	Pre-Insufflation		Post-Insufflation			
	Left Median (Range) in cm	Right Median (Range) in cm	Left Median (Range) in cm	Right Median (Range) in cm	P value left	P value right
VDR	0.2 (0-0.3)	0.84 (0.76-1.31)	0.15 (0-0.39)	0.87 (0.15-1.02)	0.983	0.394
VDT	0 (0-0.28)	0.95 (0.58-1.32)	0 (0-0.29)	0.76 (0.56-1.23)	0.764	0.286
LL	0 (0-0.32)	0.59 (0.42-0.88)	0.19 (0-0.49)	0.49 (0.1-0.96)	0.376	0.427
RL	0.27 (0.1-0.35)	0.44 (0.1-0.35)	0.19 (0-1.22)	0.27 (0.1-1.69)	0.575	0.686

There was no statistically significant change in the distance from the medial wall of the adrenal to the nearest lateral wall of the aorta when comparing the PrI and PoI scans in all positions. However there was a trend towards an increase in the VDR, LL and RL when comparing the PrI and PoI scans. The RL showed no real change. (Fig. 53).

There were no statistically significant changes in the distance from the medial surface of the right adrenal to the lateral wall of the aorta when comparing the PrI and PoI scans in all positions. In all the positions the distance to the aorta was significantly larger from the aorta to the right adrenal than the left adrenal (Fig. 53). However there was a trend towards a decrease in the VDT, LL and RL positions. The VDR showed no real change.
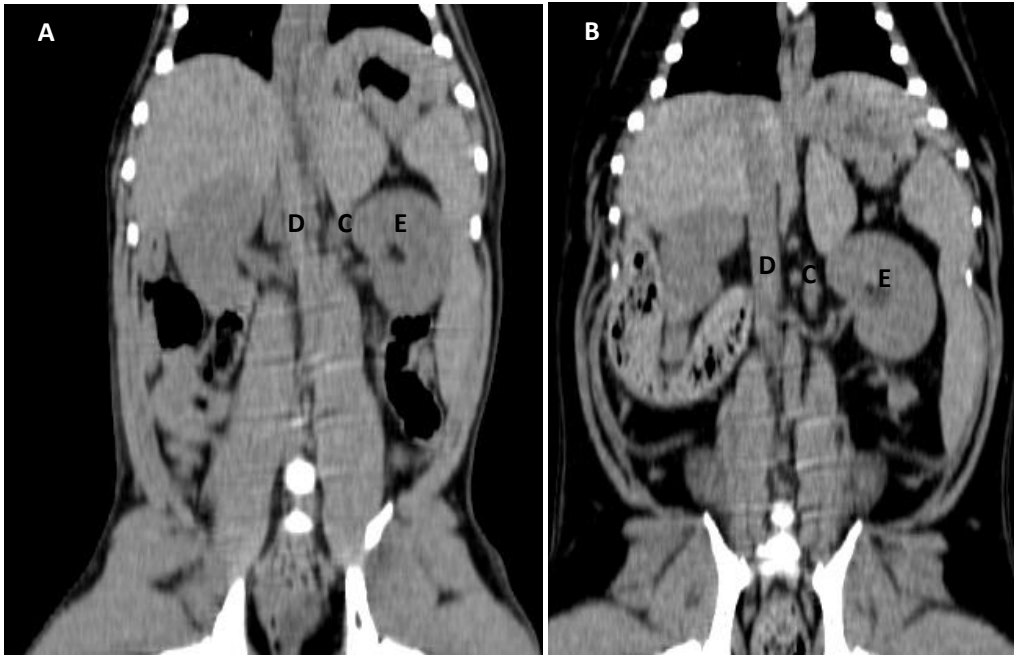
Figure 53 – A series of VDR PrI and PoI dorsal images showing the relationship between the kidney, aorta and adrenal

The PrI (A) showing the left adrenal (C) close to the aorta (D) and the left kidney (E). In the PoI (B) there is a clear separation between these organs visible. This was, however, not statistically significant.

4.8 Bladder

Cross sectional diameter of the bladder

Table 30: Cross sectional diameter of bladder pre- and post-insufflation

	Pre-Insufflation Median (Range) in cm	Post-Insufflation Median (Range) in cm	P value
VDR	2.31 (1.83-4.04)	1.97 (1.62-2.39)	0.127
VDT	1.92 (1.55-2.03)	1.8 (1.49-2.2)	0.665
LL	1.81 (1.62-2.25)	1.97 (1.42-2.07)	0.991
RL	1.73 (1.65-2.02)	1.87 (1.77-1.97)	0.177

There was no statistically significant difference in the cross sectional diameter of the bladder when comparing the PrI and PoI scans in all positions.

Distance from the caudal aspect of the bladder to the rim of the pubis

Table 31: Distance of the caudal aspect of the bladder to the rim of the pubis pre- and post-insufflation

	Pre-Insufflation Median (Range) in cm	Post-Insufflation Median (Range) in cm	P value
VDR	0.38 (0-0.91)	0.15 (0-0.93)	0.634
VDT	1.04 (0-2.48)	0.77 (0-1.63)	0.361
LL	0.33 (0-2.8)	0.17 (0.7-2.17)	0.727
RL	0.65 (0-2.16)	0.83 (0-1.32)	0.806

There was no statistically significant change in the distance from the dorsal aspect of the pubis to the caudal aspect of the bladder in all positions when the PrI and PoI scans were compared. However, there was a trend in the VDR, VDT and the LL towards a decrease in the distance described above when comparing the PrI and PoI scans. The RL showed a trend towards an increase when the PrI and PoI scans were compared. (Fig. 54).

Distance from the apex of the bladder to the ventral body wall

Table 32: Distance from the apex of the bladder to the ventral body wall pre- and post-insufflation

	Pre-Insufflation Median (Range) in cm	Post-Insufflation Median (Range) in cm	P value
VDR	0 (0-0.54)	1.39 (0-2.08)	0.036
VDT	0 (0)	1.34 (0-1.62)	0.007
LL	0.94 (0.65-1.52)	1.78 (0.7-3.52)	0.043
RL	0.29 (0-1.38)	1.29 (0.28-3.64)	0.066

There was a statistically significant increase in the distance from the ventral body wall to the ventral apex of the bladder in the VDR, VDT and the LL positions when comparing the PrI and PoI scans. However, the RL showed a trend towards an increasing distance between the body wall and the apex of the bladder when comparing the PrI and PoI scans (Fig. 54).
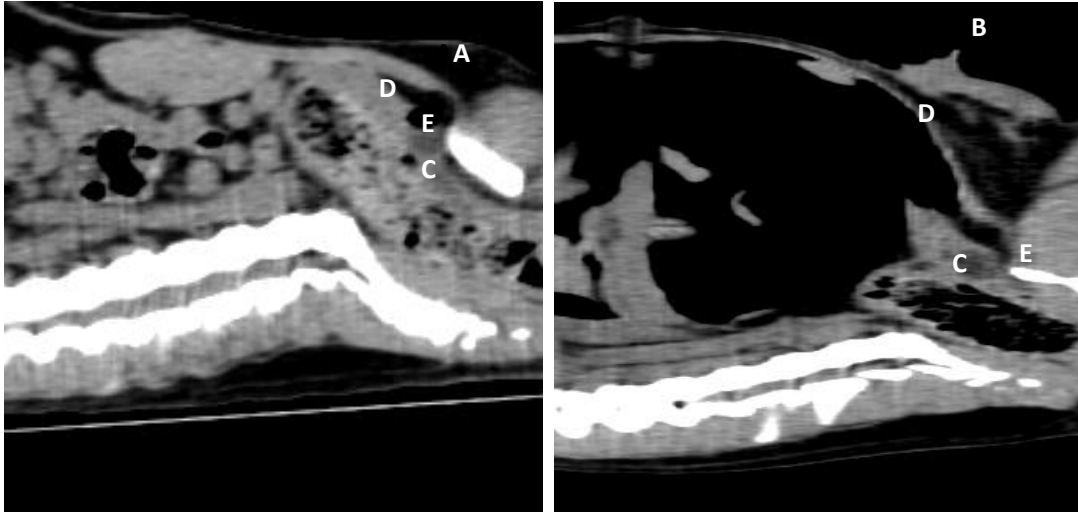
Figure 54 – A series of VDT PrI and PoI parasagittal images showing the relationship between the bladder and the body wall

The bladder (C) is visible in the PrI (A) and its relationship to the body wall (D) and the rim of the pubis (E). The same relationship is seen in the PoI VDR (B).

4.9 Uterus and ovaries

It was not possible to visualise the entire uterus in all animals in all positions. The lateral positions provided the best view of the uterine horns. These could be seen on the non-dependent side in a parasagittal plane separate from the soft tissue of the intestines and connected to the ovary. The uterine body was visible in the pelvic canal and in most cases could be followed cranially dorsal to the bladder and ventral to the colon.

The ovaries were best visualised in the lateral positions, in a parasagittal plane. They were identified caudal to the caudal pole of the respective kidney. It was possible to see the ovaries in the ventro-dorsal positions but not as readily as in the lateral positions.

Cross sectional diameter of the uterus at the level of the pelvic inlet

Table 33: Cross sectional diameter of the uterine body pre- and post-insufflation

	Pre-Insufflation Median (Range) in cm	Post-Insufflation Median (Range) in cm	P value
VDR	1.75 (1.05-3.18)	1.78 (1.2-3.4)	0.977
VDT	1.61 (0.9-1.75)	1.78 (0.95-2.09)	0.435
LL	1.55 (1.15-2.21)	1.38 (1.13-2.18)	0.593
RL	1.44 (0.92-2.09)	1.56 (1.2-2.1)	0.435

There was no statistically significant change in the cross sectional diameter of the uterus when comparing the PrI and PoI scans.

Cross sectional length and width of the ovary

Table 34: Left ovarian length and width pre-and post-insufflation

	Pre-Insufflation		Post-Insufflation			
	Length Median (Range) in cm	Width Median (Range) in cm	Length Median (Range) in cm	Width Median (Range) in cm	P value length	P value width
VDR	1.29 (0.76-1.44)	0.54 (0.34-1.09)	1.44 (0.37-1.55)	0.56 (0.25-1.22)	0.975	0.619
VDT	1.3 (0.5-1.67)	0.66 (0.3-1.1)	1.27 (1.07-1.36)	0.8 (0.49-1.04)	0.863	0.393
LL	1.12 (0.97-1.6)	0.82 (0.6-1.02)	1.16 (1.03-1.61)	0.7 (0.36-1.25)	0.376	0.931
RL	1.15 (1.01-1.28)	0.6 (0.4-1.01)	1.21 (0.99-1.59)	0.78 (0.5-0.96)	0.357	0.445

There was no statistically significant change in the length or the width of the left ovary when comparing the PrI and PoI scans in all positions.

Table 35: Right ovarian length and width pre- and post-insufflation

	Pre-Insufflation		Post-Insufflation			
	Length Median (Range) in cm	Width Median (Range) in cm	Length Median (Range) in cm	Width Median (Range) in cm	P value length	P value width
VDR	1.6 (0.8-1.69)	0.83 (0.3-1.28)	1.34 (0.58-1.24)	0.8 (0.3-1.1)	0.421	0.890
VDT	1.28 (1.04-1.98)	0.87 (0.67-1.18)	1.4 (0.97-1.55)	0.87 (0.37-0.96)	0.269	0.329
LL	1.29 (0.97-1.69)	0.78 (0.35-1.2)	1.54 (1.14-1.8)	0.76 (0.6-1.1)	0.321	0.976
RL	1.28 (1.06-1.36)	0.52 (0.3-0.72)	1.31 (0.7-1.4)	0.55 (0.32-0.67)	0.694	0.897

There was no statistically significant change in the length or width of the ovary between PrI and PoI scans in all positions.

Length of visible uterus from the mid-pubic symphysis and both uterine horns

Table 36: Visible length of the uterine body pre- and post-insufflation

	Pre-Insufflation Median (Range) in cm	Post-Insufflation Median (Range) in cm	P value
VDR	1.8 (1.2-3.23)	1.74 (1.05-3.29)	0.9
VDT	1.35 (0.45-3.6)	1.13 (0.6-3)	0.765
LL	1.63 (0.9-1.95)	1.5 (0.9-3.9)	0.636
RL	1.56 (0.75-2.25)	1.8 (0.9-2.4)	0.686

There was no statistically significant change in the length of uterine body visible in all of the positions when comparing PrI and PoI scans.

Table 37: Visible length of the left uterine horn pre- and post-insufflation

	Pre-Insufflation Median (Range) in cm	Post-Insufflation Median (Range) in cm	P value
VDR	1.32 (1.3-4.76)	3.03 (1.6-4.8)	0.165
VDT	1.07 (0.6-5.54)	1.58 (0.3-4.82)	0.838
LL	2.95 (0.15-3.58)	1.75 (0.32-4.89)	0.682
RL	2.46 (0.3-3.65)	2.82 (0.75-4.58)	0.534

There was no statistically significant change in the visible length of the left horn of the uterus in all positions when comparing the PrI and PoI scans.

Table 38: Visible length of the right uterine horn pre- and post-insufflation

	Pre-Insufflation Median (Range) in cm	Post-Insufflation Median (Range) in cm	P value
VDR	2.55 (1.01-4.8)	2.12 (1.8-4.6)	0.703
VDT	1.77 (1-3.67)	2.03 (1.01-4.77)	0.594
LL	2.07 (0.45-2.92)	2.1 (0.3-5.2)	0.996
RL	2.71 (0.9-3.45)	0.63 (0.3-4.05)	0.489

There was no statistically significant change in the visible length of the right uterine horn in all positions when comparing the PrI and PoI scans.

Length of contact / distance between uterine body and colon

Table 39: Distance of contact between the uterus and colon pre- and post-insufflation

	Pre-Insufflation Median (Range) in cm	Post-Insufflation Median (Range) in cm	P value
VDR	1.8 (1.05-2.1)	1.74 (1.05-2.2)	0.901
VDT	1.35 (0.6-3.6)	1.13 (0.6-3)	0.767
LL	1.63 (0.9-1.95)	1.5 (0.9-3.9)	0.731
RL	1.56 (0.75-2.25)	1.8 (0.9-2.4)	0.687

There was no statistically significant change in the contact distance between the uterus and the colon in any of the positions when comparing PrI and PoI scans (Fig. 55).
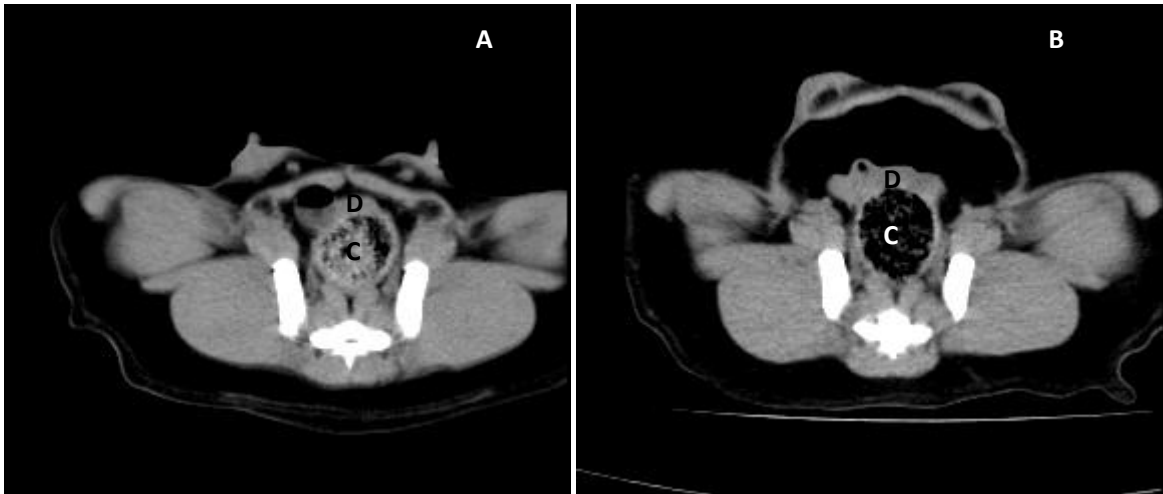
Figure 55 – A series of VDT PrI and PoI transverse images showing the relationship between the colon and the uterus

The PrI (A) shows the colon (C) and the uterus (D). The same relationship is seen in the PoI (B).

Distance from the caudal pole of the kidney to the cranial pole of the ovary

Table 40: Distance from the caudal pole of the left and right kidney to the cranial pole of the left and right ovary respectively pre- and post-insufflation

	Pre- Insufflation		Post- Insufflation			
	Left Median (Range) in cm	Right Median (Range) in cm	Left Median (Range) in cm	Right Median (Range) in cm	P value left	P value right
VDR	0.25 (0.3-1.17)	0.25 (0.15-0.84)	0.5 (0.37-0.96)	0.62 (0-1.33)	0.537	0.268
VDT	0.33 (0-1.07)	0.33 (0.22-0.76)	0.45 (0-0.78)	0.45 (0.1-0.53)	0.701	0.101
LL	0.36 (0-1.37)	0.93 (0-2.83)	0.73 (0-1.39)	0.91 (0.51-1.9)	0.498	0.969
RL	0.56 (0.22-1.39)	0.9 (0.9-1.45)	0.96 (0.57-1.1)	0.91 (0-1.2)	0.197	0.425

There was no statistically significant change in the distance from the left ovary to the kidney when comparing the PrI and PoI scans in all positions. However, there was a trend towards an increase in the distance between the kidney and the ovary in all positions when the PrI and PoI scans were compared (Fig. 56).

There was no statistically significant change in the distance of the right ovary from the right kidney when comparing the PrI and PoI scans in all positions. However, there was a trend towards an increase in the described distance in the VDR and the VDT when comparing the PrI and PoI scans (Fig. 57).
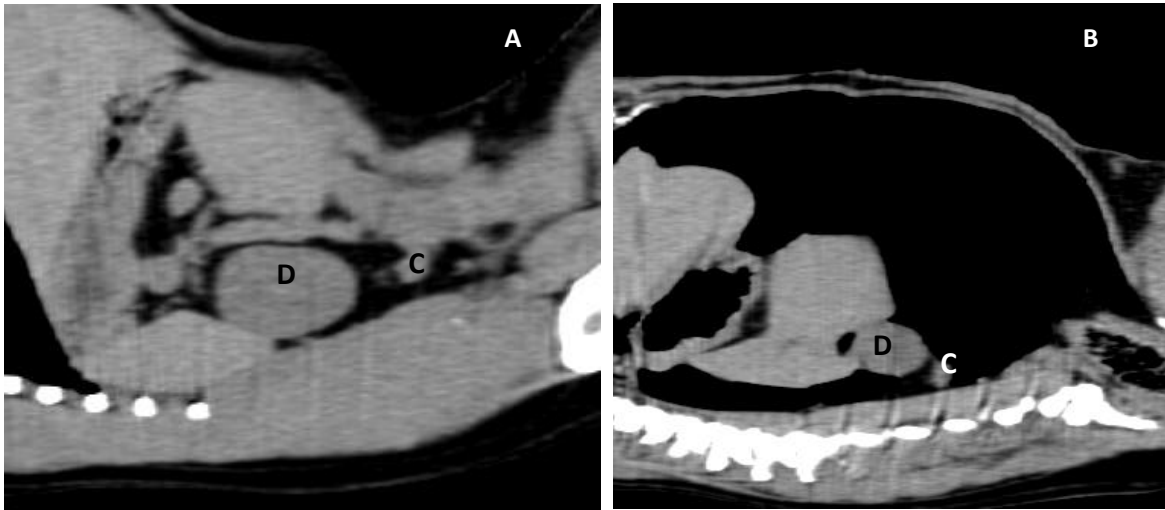
Figure 56 – A series of VDT PrI and PoI parasagittal images showing the distance from the left ovary to the caudal pole of the left kidney

The PrI (A) shows the distance from the left ovary (C) to the caudal pole of the left kidney (D) when compared to the PoI (B).
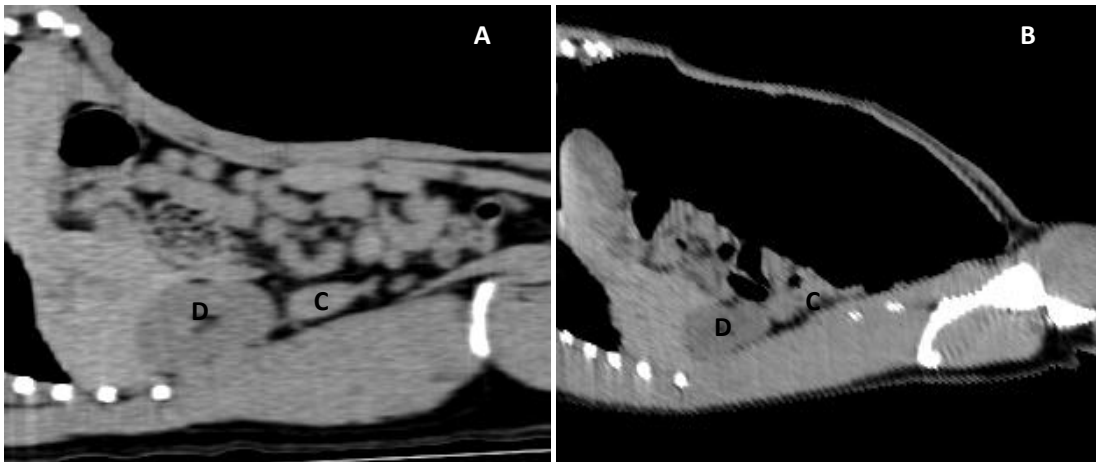
Figure 57 – A series of VDT PrI and PoI parasagittal images showing the distance from the right ovary to the caudal pole of the right kidney

The PrI (A) shows the distance from the right ovary (C) to the caudal pole of the right kidney (D) when compared to the PoI (B).

CHAPTER 5: DISCUSSION

The hypothesis was how does the introduction of air/gas into the peritoneal cavity alter the topographic anatomy for the laparoscopic approach to the abdominal organs. It was clearly seen that there were changes in the position of the organs dependant on position and gravity. Given this it was possible to determine the best position to provide the best exposure each abdominal organ system, thus proving the hypothesis.

5.1 Extra-abdominal Structures

Oesophagus

In all positions there was an increase in both the short and long axis oesophageal diameter when the PrI and PoI scans were compared. In the short axis diameter this was statistically significant in the RL and the LL. The VDR and VDT showed a trend towards an increase. In the long axis diameter there was a statistically significant increase in the RL and LL but only a trend in the VDR and VDT towards an increase. This can be explained by the increased pressure on the stomach due to the increased intra-abdominal pressure caused by the insufflation of carbon dioxide. This increased pressure on the serosal surface of the stomach was transferred through the stomach wall to the contents of the stomach, which in starved animals was mainly fluid and air. This pressure seemed to be higher than the pressure maintained at the cardia or lower oesophageal sphincter and led to the reflux of gastric content. The ability of the cardia to resist this reflux was further decreased by the animal being under general anaesthesia. This explained the changes in content of the oesophagus when the PrI and PoI scans were compared. In the PrI scans, 21 of 24 showed no visible oesophageal content. Of the three that had visible content, two contained air and one fluid. The one with fluid can be explained as 'normal' reflux under anaesthesia and an abnormal physiological position. In the PoI scans the oesophagus was empty in only one of the 24 scans, with 12 scans containing air and 11 containing some fluid. All animals were intubated and hence there was no possibility of aerophagia. This air and fluid in all cases represented reflux. This reflux was confirmed by the increases in height and cross-sectional diameter of the oesophagus as an objective measurement. There was however no statistically significant change in the cross-sectional short axis and long axis diameters of the stomach. Given that a three dimensional object was being measured in a two dimensional plane, the measurements of the stomach may not have reflected the decrease in size. The reflux was minimal and may not have caused a statistically significant decrease in the size of the stomach.

A higher incidence of reflux can be seen on the CT scans in the animals PoI. Reflux has been well documented to occur more often with intra-abdominal surgery when compared to other surgical procedures in the dog[60]. This seemed to be similar in this case as the effect of

the abdominal insufflation increased the incidence of oesophageal reflux in the study population when comparing PrI and PoI scans. This was not seen to be linked to a specific position, but to insufflation or no insufflation. This can lead to oesophagitis and possible permanent damage to the oesophagus due to stricture formation. It may be prudent to institute prophylactic treatment for reflux oesophagitis during laparoscopy. However, this needs to be further evaluated clinically in patients undergoing laparoscopic procedures.

Cranial extent of the diaphragmatic cupula in relation to the body of the thoracic vertebrae

There was always contact between some part of the ventral midline diaphragm and the cardiac silhouette. This was similar to what is routinely seen on thoracic radiographs and is considered normal for most dogs. It was expected that this contact would not be lost in the PoI scans as the diaphragm would have moved forward from the increased intra-abdominal pressure. This was seen to be the case in all the dogs.

It was not possible in the PoI scans to determine if one crus was further cranial than the other. This was due to the fact that the diaphragm became a dome-shaped structure due to the increased intra-abdominal pressure. However the most, cranial point of the diaphragm always moved cranially in all animals PoI.

The positioning of the animal had no significant difference on how far the diaphragm moved cranially. The only observation that could be made from this was that there was significant cranial movement due to the insufflation of intra-abdominal carbon dioxide and the subsequent increase in intra-abdominal pressure and that it was not possible to accurately distinguish the right and left crura from one another.

Gas in the pelvic canal / Peritoneal reflections visible

The peritoneal reflections were not visible in any of the scans. These reflections acted as a barrier to prevent gas from moving into the pelvic cavity. This resulted in these thin suspensory reflections being compressed against the pelvic fat, making them invisible. All that was seen was the transition from gas to pelvic fat, so their position could be extrapolated. In one of the dogs in the RL there was a small amount of gas visible in the pelvic canal on the non-dependent side not seen in any of the other dogs. This dog had a caesarean section a year earlier and damage to the peritoneal reflections due to surgical handling was suspected.

Abdominal parenchymatous organ height % of abdominal height at umbilicus

The VDR and VDT showed a trend towards a decrease in the parenchymatous organ height. This can be explained by the compression on the soft tissue mass of the intestines which are relatively mobile compared to the rest of the organs in the abdominal cavity. The difference between the ventro-dorsal positions and the lateral positions was due to the effect of the

gas cap acting laterally to the soft tissue mass. There was more area for the tissues to move into and thus it gave the impression of an increase in the parenchymatous organ height. However, the increased expansion of the lateral body wall and the taking of the measurement from the highest point of the lateral body wall seems to even this out. It was seen that there was no statistically significant difference between the ventro-dorsal and the lateral positions. Had this been measured from the umbilicus in the lateral view a substantial increase would have been seen as the organs would have been up against the umbilicus, even in the PoI scans. This would be due to the organs lying in the dependent half of the abdominal cavity and thus close to the umbilicus. However, this had little clinical significance and was not measured.

The abdominal height increased dramatically and this was due to the stretching of the abdominal muscles by the effects of the gas cap only in the ventro-dorsal positions and by the gas cap and the pressure on the soft tissue mass in the lateral positions. This explains why the lateral positions show a slightly higher abdominal height than the ventro-dorsal positions. The increases were dramatic as the abdominal height was increasing and the soft tissue height decreasing, thus amplifying the change. The clinical significance of this is that there is a large area ventral or lateral, depending on the positioning of the animal, to the soft tissues of the abdomen after insufflation which would be the initial working space for laparoscopic procedures. No organs, except for the kidneys, ovaries and uterine horns of the non-dependent side in the lateral views will be present in this space. The mass of soft tissue containing intestines, large and small bowel, spleen, urogenital, vascular and lymphatic structures seem to act as one mass and are compressed by the gas cap and gravity.

5.2 Liver

Distance from the caudal xiphoid to the liver

In all positions there was a significant increase in the distance from the dorsal surface of the xiphoid cartilage to the ventral serosal surface of the liver. This was to be expected as there are no peritoneal reflections or ligaments that attach to the ventral surface of the liver. The remnant of the umbilical artery which forms the falciform ligament plays a very small role in suspending the liver. In the VDR and VDT prior to insufflation the liver fell dorsally. The suspending ligaments of the liver tend to lie dorsally so the greater distance was explained by the liver collapsing on itself in the ventro-dorsal positions. In the VDT the liver pushed up against the diaphragm which tended to make the distance slightly less than in a true ventro-dorsal position. In both lateral views with the liver being suspended by its dorsal ligaments, the degree of collapse was less. This was supported by the lesser distance that was seen in both lateral positions. The RL showed the least change in the described distance. This was due to the large caudate process of the caudate lobe on the right hand side. This creates a

larger mass of liver tissue on the right which will support the liver mass more, allowing less collapse and a smaller distance from the xiphoid to the liver.

The clinical applications of this are that to get surgical exposure to the liver a straight VDR allows maximum space to access the liver and billary system. However, the liver can be accessed from all positions depending on which part of the liver pathology was suspected.

Percentage contact between the liver and the body wall at T11

When comparing the PrI and PoI scans there was a substantial decrease in the amount of liver in contact with the body wall in the PoI scans. The largest decrease in the contact was seen in the VDT. This was once again due to the measurement being taken in cross-section at a specific point. With the liver having mainly dorsal suspensory attachments, it tended to collapse on itself. Positioning in the VDT allowed the liver to slide cranially resulting in less contact with the ventral and lateral body walls. There was a smaller change in the contact in the VDR as there was less cranial movement of the liver. In the RL given the small increase in the distance from the xiphoid to the ventral liver, one would have expected a small decrease in the contact distance. However, this position showed the largest change in contact with the body wall out of all of the positions. It can only be suspected that due to the dorsal attachments of the liver, it pulls away from the lateral and ventral body wall, collapsing around the right medial and lateral lobes. In the LL it was suspected that due to the increased size of the right half of the liver it remained in contact with the body wall to a greater degree when compared to the RL. This was due to fact that the larger half was now situated in the non-dependent abdomen, causing the liver to fan out and cause a greater degree of contact when compared to the RL. When the animal was in RL, the larger half was in the dependent part of the abdomen and this allowed it to collapse on itself leading to less contact of the liver with the body wall.

Distance from the apex of the gallbladder to the right abdominal wall

The VDR and VDT positions showed the largest increases in the distance from the right body wall to the apex of the gallbladder. This was unexpected as one would assume that the LL would show the largest increase given the right position of the gallbladder within the liver. It can be explained by the bile duct running in the lesser omentum, otherwise known as the gastro-hepatic ligament. This is situated close to the dorsal margin of the liver which is where the main attachments for the liver are. As seen commonly in a celiotomy, this area has a very low degree of mobility when compared to the rest of the liver. The gallbladder was attached to the right medial liver lobe which was dorsal and medial and seemed to have a low degree of mobility. Thus it was suspected that the movement of the gallbladder would be minimal and hence the distance from the body wall would be about the same in the RL and LL.

In the VDR and VDT positions, however, it was suspected that the carbon dioxide cap together with position of the animal would shift the liver medially. This was due to the liver being in the dependent part of the abdominal cavity and hence the gas dissecting laterally to the liver between the liver and the body wall adding to the medial displacement caused by positioning. In other words the liver would tend to collapse on itself towards the midline of the body due to its attachments. There was no effect of gravity on the lateral abdominal wall in the VDR and VDT positions and thus there was an increase in abdominal diameter when compared to the LL. This was due to the gas cap raising the abdominal wall thus increasing the distance to the gallbladder from the body wall. This was why the distance was thought to be greater in the VDR and VDT scans as opposed to the LL as would have been expected.

In the RL, as expected, the pressure from the gas cap and the position forced the gallbladder into contact with the lateral body wall. This was the only position where the distance decreased significantly and the apex was in contact with the body wall in the PoI scans. This once again reinforces the approach to the gallbladder being easiest in the VDR and VDT positions but mainly the VDR.

The % contact of hepatic parenchyma to the gallbladder and % of gallbladder exposed

Gallbladder diameter remained much the same between PrI and PoI scans, indicating that there was little change in shape or size from compression by the increased intra-abdominal pressure or surrounding structures. All positions showed a significant decrease in the amount of hepatic tissue in contact with the serosal surface of the gallbladder when comparing PrI and PoI scans. This was due to the collapse of the liver onto the dorsal body wall and the increased separation of the liver lobes. This decreased contact allows exposure of the gallbladder in all positions except the RL where the exposed portion of the gallbladder lies against the body wall. The surrounding liver tissue in the RL remains in contact with the gallbladder as it lies on the dependent side now and the force of gravity and the increased intra-abdominal pressure results in much the same contact and little exposure. The RL cannot be recommended for surgical approach to the gallbladder. Given that the most exposure and least contact was seen in the VDT, this should be considered the position of choice for an approach to the gallbladder. However, it would be easy to approach the gallbladder from a LL or VDR position if the need arose.

Separation of the liver lobes

In all the views there was a significant increase in the number of liver lobe fissures that opened from the PrI to the PoI. There was no PoI position that provided a statistically significantly higher degree of lobe separation. Manual retraction of the liver lobes with laparoscopic fan retractors will be essential in laparoscopic surgery of the liver.

Distance of lesser curvature of the stomach to the caudal part of the caudate lobe of the liver

There was no significant change in the distance from the lesser curvature of the stomach to the caudal liver in the VDR. This distance was representative of the lesser omentum or the gastro-hepatic ligament. This showed that this was a relatively immobile abdominal area. This fits in with the above mentioned movement of the gallbladder from the body wall. In the VDT there was a trend towards a slight decrease in the distance described. This showed that the stomach was more mobile than the liver as the effect of gravity allowed cranial displacement of the stomach to a greater degree than the liver with its dorsal attachments. There was no significant decrease in the RL as the liver and stomach were supported by the larger liver mass on the right side and thus less collapse was seen.

With exposure of the lesser omentum and more importantly the structures in the lesser omentum, i.e. the cystic duct, the LL appears to be the best. The RL was less ideal as the overlying structures would be in the way en route from the left body wall. However the gallbladder was best exposed in the VDT, which as seen here, causes cranial movement of the stomach to possibly cover the lesser omentum as does the LL. Given that the best visibility of the cystic duct is seen in the LL above, this once again implies that internal retraction would be essential for performing surgery of the liver and the billary tract. There appears to be no position that gives a better exposure of the billary system in all aspects over another and it would be expected that the VDT would be the best position to use together with manual retraction.

Distance from the head of the spleen to the left lateral liver lobe

The spleen appeared to be a relatively mobile organ except for the head which is attached to the gastric fundus by the gastro-splenic ligament. This carries important blood supply to the gastric fundus in the form of the short gastric arteries and veins. It would be expected that the spleen would move in a similar manner as the stomach due to this attachment. In all the positions except the RL there was a trend towards a decrease in the distance from the head of the spleen to the LL lobe of the liver. This showed more change than the distance from the lesser curvature to the liver. This was as a result of the spleen being attached to the fundus which is a very mobile part of the stomach as can be seen in the gastric dilatation volvulus syndrome. This decrease was expected in all the views as the effect of gravity and increased intra-abdominal pressure would push the head of the spleen cranially to lie closer to the relatively less mobile liver. In the RL the mobile fundus and spleen were more influenced by gravity than the increased intra-abdominal pressure and tended to fall away from the liver thus increasing the described distance even though it can

only be described but was not significant. However, there was still merit in describing this change.

The clinical implications may seem obvious, but to allow the best exposure of the left lobes of the liver the animal should be positioned in RL. This will allow the spleen and stomach to fall away from the area of interest. It will also allow better access to the hiatus for complex procedures of the terminal oesophagus such as repair of a hiatal hernia.

Cystic duct visibility

The insufflation of carbon dioxide appeared to have no benefit in increasing visualisation of the cystic duct of the gallbladder. All views, except the LL, had mixed successes in allowing visualisation of the cystic duct. The LL however allowed the best CT view of the cystic duct of all the positions and there was no change when comparing the PrI and PoI scans.

This suggested that abdominal insufflation does not affect exposure of the cystic duct, but rather that the position the animal was placed in for the surgery does. One has to conclude that the best position for procedures of the cystic duct was the LL position. This could have been better examined using CT angiography which was used to differentiate the cystic duct from the hepatic vasculature in that area. This was beyond the scope of this study.

Distance between the vena porta and the vena cava

These vascular structures are situated caudal to the liver in the dorsal abdominal cavity and aid in suspending the liver. The coronal ligaments attach the liver to the dorsal body wall. It was suspected that movement of these structures would be minimal. The portal vein was more mobile than the vena cava given that it has fewer attachments and runs in the lesser omentum. As described earlier there was a medial shift of the liver in the VDR and VDT positions and this explains the trend towards a decrease in the distance of the portal vasculature. The liver will be compressed by gravity and the dissection of gas laterally, thus shifting the portal vein closer to the vena cava. In the VDT there was no change in the distance. It may be assumed that the effect of gravity may apply cranial traction on the liver and hence the portal vein cancelling out the medial movement seen in the VDR. As expected in the LL the effect of gravity plays a greater role and the portal vein moves away from the vena cava. In the RL the same was true except the movement due to gravity was towards the vena cava thus decreasing the distance. However, the movement was not considered to be statistically significant.

Clinically the most common ailment affecting this area would be an extra-hepatic porto-caval shunt. However, one has to take into account the anatomy of the greater omentum and the omental bursa formation when approaching a portocaval shunt. Most of these shunts lie in the omental bursa cranial to the phrenico-abdominal vein. It would be very difficult to approach this through a LL or RL position. One can assume that the VDT would be the position of choice as it would allow slight cranial displacement of the stomach, thus

allowing access to the omental bursa through the ventral leaf of the greater omentum. The vascular structures would not be forced closer together as in the VDR making dissection around the shunt more difficult. However retraction would still form an essential part of the surgical procedure. The advantages to a VDT approach shown in this study make it a better position to approach this area. However, given that both approaches will require manual retraction, surgeon preference may determine which position is used.

5.3 Spleen

Percentage of spleen in contact with the body wall

The spleen, being a highly mobile organ, would be expected to move dependent on gravity. The parietal splenic length showed no significant change when comparing the PrI and PoI scans except in the RL which showed a significant change. This was expected as the organs including the spleen would be under the effects of gravity and would move to the dependent left side thus decreasing contact with the body wall. The LL showed a trend towards increasing the contact. This was due to the shape of the spleen, which on the dependent side flattened out against the lateral body wall increasing the contact with the body wall in PoI. The VDR and VDT showed a trend towards a decrease in the contact distance. This was due to the pressure applied from the gas cap sitting on top of the soft tissue mass. This caused the spleen to fold on itself and decrease the contact of the lateral surface with the body wall in PoI.

Hilar access

If a laparoscopic surgery was to be performed on the spleen, the RL would provide the best approach to the spleen. However as was seen from the access to the hilar measurement, no position, PrI or PoI, provided easy access to the splenic hilus. It can be assumed that the hilar area of the spleen was less mobile than other parts of the spleen from the above measurements. However, it is essential to ligate the splenic vessels when performing a splenectomy. Once again manual retraction will be required to gain access. With the spleen being a mobile organ, manual retraction becomes easy and splenectomy possible via a modified laparoscopic approach.

Distance from the pelvis of the left kidney to the caudal portion of the head of the spleen

All views showed an increased distance from the pelvis of the left kidney to the spleen. The left kidney has been thought to be more mobile than the right kidney as the right kidney is attached to the liver. The left kidney has no attachment to any of the surrounding organs and hence is more mobile. This was evident in most of the images.

The distance between the spleen and the left kidney would be expected to decrease as they would have moved closer together and the spleen was considered to be more mobile than the left kidney. However, the spleen slides down the LL body wall with the straight distance from the pelvis to the head of the spleen increasing. This was true for the VDR and VDT and explains the increased distance. In the LL the spleen falls in contact with the body wall and slides ventrally away from the kidney thus increasing the distance. In the RL, not only does the spleen collapse to the right side of the abdomen but there was substantial movement of the left kidney ventrally and to the right thus creating the largest distance between the two organs. This was unexpected, but can be attributed to the relative mobility of the left kidney. The implications for the spleen were that the best position for access to the parietal surface of the spleen is the RL position as all the organs fall out of the way and expose the spleen.

Contact distance between spleen and the stomach

The contact distance of the spleen with the stomach showed a trend towards decreasing in the VDR and the RL. The VDT and the LL showed no real change when the PrI and PoI images were compared. The spleen and the stomach share a close association as discussed previously. The clinical implications are minimal from this observation.

5.4 Gastro-intestinal system

Position of the pylorus in relation to the vertebral column / Distance of the cranial duodenal flexure to the gallbladder

In the VDR there was a trend towards a decrease in the distance from the duodenal flexure to the gallbladder. The position of the pylorus moved caudally in most dogs in the PoI scans. The only explanation for this may be that with the liver attachments being located dorsally, the liver tends to collapse on itself in the dependent part of the abdomen. This 'collapse' may bring the gallbladder closer to the duodenum by shifting it caudally and ventrally. The initial starting point of the gall bladder was in a cranioventral-dorsocaudal orientation in the PrI scans, changing to a caudoventral-dorsocranial position in the PoI scans. This collapse shifted the pylorus and the cranial duodenal flexure caudally. This decreased the distance, as the duodenum was less mobile due to the attachments of the lesser omentum and the duodenal colic ligament.

In the VDT there was the added effect of cranial pull of gravity by the elevated pelvis. In this position we saw a trend towards an increase in the distance from the gallbladder to the cranial duodenal flexure. Caudal movement of the pylorus was still seen. This showed that the pylorus and duodenum were restricted in movement by the attachments discussed and

tended to fall into the same position in the ventro-dorsal positions. The cranial force of gravity on the liver in the VDT causes less collapse of the liver over itself and allowed collapse of the liver in a cranial direction thus maintaining the normal orientation of the gallbladder. This view in theory exposes the duodenum and associated structures best as they will shift caudally and the liver shifts cranially. This will in turn expose the pancreas and the pylorus and would be the position of choice for these surgical procedures.

In the LL there was a trend towards a decreased distance due to the cranial movement of the pylorus in all dogs. This position showed the greatest decrease in the described distance and can be attributed to the collapse of the right side of the liver, containing the gallbladder. Once again this collapse occurred over itself with the orientation of the apex of the gallbladder shifting caudally. With the cranial movement of the pylorus, one can assume that movement in the medio-lateral plane of the pylorus was greater than movement in the cranio-caudal plane. The pylorus, due to gravity and the increased pressure of the insufflation, tended to fall cranially and to the left. Both points move closer to each other, thus shortening the distance the most out of all of the positions. This creates a difficult approach to these areas in question and hence the need for manual retraction. The approach is not impossible but from the above there are easier ways to approach these areas laparoscopically.

In the RL there was no real significant change in the distance with only slight caudal movement of the pylorus. Given the position prior to insufflation one would expect the area to see little change as the mass of organs is compressed on the right side and the insufflation causes little organ compression. The slight caudal movement of the pylorus can be linked to the relative immobility of this area and possible displacement by more mobile organs. This position cannot be recommended as a surgical approach to these areas.

Stomach cross section long axis and short axis

In the VDR there was a trend towards an increase in the long axis of the stomach and a decrease in the short axis of the stomach. In the VDR the stomach lies at 90˚ to the vertebral column. With the increased pressure on the stomach from surrounding organs and the insufflation, the stomach flattened out thus increasing the long axis diameter and decreasing the short axis diameter. Overall it was suspected that there was a decrease in the volume of the stomach as we saw reflux into the oesophagus. The reflux volumes were not been measured in this study. In the VDT there was a significant decrease in the long axis diameter of the stomach with no significant change in the short axis diameter. One can assume that this was due to the effects of gravity drawing the stomach cranially. The pressure from the organs caudally may tend to support the caudal aspect of the stomach thus propping it up in a way as not to decrease the short axis diameter. The long axis is decreased due to the cranial traction which lengthens the stomach in a cranio-caudal direction and not a medio-lateral direction. Obviously there has to be a compromise made

for this cranial movement and the long axis diameter decreases. Once again one would suspect a decrease in total volume as oesophageal reflux was again prominent.

In the lateral positions there was a trend towards an increase in the long axis diameter but no statistically significant change in the short axis diameter. Given the C shape of the stomach at 90˚ to the spinal column once again there is a flattening out of the stomach due to the pressures acting on it resulting in an increase in the long axis diameter. Both positions showed reflux into the oesophagus. It was expected that the volume would decrease but given that the stomach is a large three dimensional structure it may be that measurement was at fault here. It was impossible to measure at the same point in both the PrI and PoI scans resulting in measurement errors. A better method would have been to measure total volume of the stomach. Given the limited clinical applications that size of the stomach would have, this was considered unnecessary. Surgical procedures of the stomach such as gastrotomy, gastropexy and pyloroplasty, all of which have been described using laparoscopy, tend not to be affected by the size of the stomach[27]. Most animals would have been starved for at least 8 hours prior to surgery, so a massively distended stomach would be a rarity unless there was pathology of the stomach such as gastric dilatation volvulus syndrome. Unless the stomach can be deflated, a laparoscopic gastropexy may be impossible to perform in these situations.

Distance of the mid descending duodenum from the body wall

In all the views except for the LL PoI there was contact of the duodenum with the right body wall.

In the LL the effect of gravity was clearly seen as the duodenum fell away from the body wall and came to lie on top of the mass of soft tissue. This once again indicates the mobility of the duodenum in certain directions. With most of the attachments of the duodenum being on the right side of the body it would be expected to gravitate to this position in the LL. The effect is enhanced over the PrI by the effects of the gas cap exaggerating the effect of gravity and increasing the abdominal diameter as leading to an increased in the distance.

Distance from the pelvis of the right kidney to the descending duodenum

In the normal animal as the duodenum runs past from the cranial pole of the right kidney it is nearly in contact with the kidney. When it passes the caudal pole it tends to lie a distance ventral to the kidney. In the VDR there was a trend towards a decrease in the distance from the pelvis of the kidney to the descending duodenum. This was expected due to the effect of gravity and insufflation leading to a decrease in the distance.

In the VDT a similar situation was seen and was expected. However the distances were larger even though the trend was the same. This could be explained by the cranial force of gravity on other organs in the abdomen leading to a bigger soft tissue mass between the kidney and the duodenum. Even though there was still a decrease in the distance, the

distance remained larger than in the VDR as there was more tissue in the dependent part of the abdomen.

In the LL there was a marked increase in the distance from other positions. This was caused by the right kidney being relatively immobile. When the position was changed to a LL all the organs fell away from the right kidney exposing the kidney on its own. This explains the increase as the duodenum comes to lie on top of the soft tissue pile on the dependent side of the abdomen. The surgical implications were that this position gave excellent exposure to the right kidney. The right kidney and associated retro-peritoneal structures become isolated from all other organs in the abdomen. This would be the position of choice for surgical procedures of the right kidney.

In the RL it would be expected that the distance would decrease due to the forces of gravity and the increased intra-abdominal pressure on the organs above the duodenum. However, the decrease was slight and not significant. What was seen in this view was that other organs, mainly the intestines, make their way in between the kidney and the duodenum, so there was movement but it was not reflected in this measurement as the straight line distance remained much the same. This position provided no real exposure of the structures of interest and cannot be recommended.

5.5 Pancreas

The right limb of the pancreas was the most easily visualised limb in all scans and was seen in the highest number of dogs. This was due to its close association with the descending duodenum. The VDT was the best position to visualise the right limb of the pancreas on a CT image. This was followed by the VDR and the LL. However this does not say that these were the best positions for laparoscopic visualisation of the pancreas. The RL was the position with the worst visibility of the pancreas on a CT image. However in the RL the right limb of the pancreas was still visible in a high percentage of dogs on CT images (Graph 13). Insufflation did not seem to increase the visualisation of the right limb of the pancreas. The VDT position caused cranial traction on the organs in the abdomen. The duodenum is a relatively immobile organ in the cranio-caudal direction due to its hepatic and colic attachments. With the cranial traction from gravity, the organs surrounding the duodenum and the pancreas moved away providing less soft tissue in the area. This allowed better differentiation of the pancreas from the surrounding tissue in the VDT on the CT image.

The body of the pancreas was the second most identified part of the pancreas. This was due to its association with the cranial duodenal flexure which as described was a relatively immobile area and easy to identify. The PrI scans of the VDT, LL and RL provided the best visualisation of this area on a CT image (Graph 13). However, this was not drastically higher

than the PoI scans of the same positions. This tended to suggest that insufflation, if anything, makes visualisation no better but may actually hinder it when looking for the pancreas on CT. This was seen in the RL PoI view showing the worst visualisation of the body of the pancreas. This was due to the increased pressure from the gas cap bringing all the soft tissue closer together in that area. This decreased the contrast provided by the omental fat and decreased the ability to differentiate the pancreas from surrounding soft tissue structures.

The left limb of the pancreas was the most difficult to identify. This was in part due to its position in the abdomen. When compared to the right limb and body the left limb was not as closely associated with an organ such as the duodenum. Its position in the omentum at the greater curvature of the stomach made it less visible as it became difficult to distinguish it from surrounding soft tissue. The VDR and RL PrI provided the best visibility of the left limb of the pancreas. The VDR allowed all the organs to sit spread out dorsally in the abdominal cavity. This allowed visualisation of the splenic hilus up against the parenchymatous organ mass. The hilus seemed to provide the best marker in finding the left limb of the pancreas. However, it had to be differentiated from the vasculature of the spleen which was the same HU. This was done on the direction of the vasculature and how it entered the spleen. The RL PrI provided good visualisation and this cannot be explained as it would have been expected to provide the worst visibility as the surrounding soft tissue would make identification of the pancreas difficult. This was seen in the RL PoI and was suspected to be due to the gas cap compressing the soft tissue thus eliminating the contrast provided by omental fat leading to poor visualisation of the left limb (Graph 13).

The VDR and VDT provided the best visualisation of all parts of the pancreas on the CT images. It is essential when performing laparoscopy of the pancreas that all lobes are explored. The left limb of the pancreas was visible in LL as the pancreas was lying "on top" of the mass of soft tissues in the abdomen in the CT images. This could be used as an approach to the pancreas during laparoscopy. The only concern would be the left limb as it courses from medial to lateral into the soft tissue mass. This may require extensive retraction of organs to fully explore the surface of the pancreas. Given that the VDR and VDT provide the best CT visualisation and would make ease of finding the pancreas during surgery as they would expose it best, they would be considered the positions of choice for surgery of the pancreas.

The RL gave the worst visibility of the pancreas and cannot be recommended for a surgical approach in most circumstances.

5.6 Kidneys

Cross sectional diameter of the kidneys

There was no change in the cross sectional dorso-ventral diameter of the kidneys in the study. This indicated that the compression of the soft tissues by the insufflation of the carbon dioxide was not significant.

Distance from the cranial pole of the right kidney to the renal fossa of the liver

The cranial pole of the right kidney remained in contact with or very close to the renal fossa in all scans but the LL. This confirmed the short, strong attachment between these two organs that was responsible for the relative immobility of the right kidney. However in the LL the distance was significantly increased in the PoI scans. The effect of gravity and the gas cap in creating a space in the previous potential space of the abdominal cavity and created the opportunity for movement. Even though the movement was small, it showed that there was a degree of mobility to the right kidney and when the support of the soft tissue mass of intestines was lost, it moved to a small degree. When approaching the right kidney, the LL is the best position as it provided the greatest exposure of all surfaces of the right kidney and the surrounding structures.

Distance from the cranial and caudal halves of the kidneys to the aorta

Relatively speaking, the left kidney is known to be more mobile than the right and this was seen in the descriptive results. Even though there are no statistically significant changes in the movement of the left kidney there was a trend in the VDR and the LL to an increased distance. In the RL the trend was a decrease in the distance. The distance in the LL was expected to increase as the kidney lay in the dependent part of the abdomen and the pull of gravity would tend to separate the left kidney from the aorta. The relative rigidity of the renal vasculature which forms the main attachment of the left kidney was the reason for the small change which could not be seen as significant. In the RL the trend was towards a decrease and this was for similar reasons as the left kidney now lay in the non-dependent part of the abdomen and the pull of gravity decreased the distance to the aorta as the kidney fell towards it. The distance is once again a small change that cannot be considered significant as the vasculature is relatively rigid and this caused the kidney to flip over. This lead to a small decrease as the distance from the medial hilus of the kidney to the aorta had not really changed. The VDR showed a trend towards an increase in the distance and this was due to the pressure of the organs ventrally to them being greater in the PoI scans as the gas cap provided the increased pressure leading to the lateral movement of the kidneys away from the aorta. The trend towards a decrease in the VDT was speculated to be due to

the cranial pull on the kidney added to the increased pressure from the overlying organs which possibly pushed the kidney medially and hence closer to the aorta.

The relevance is that the approach to the left kidney should be through a RL, as even though it is more mobile, it is still maintained in the non-dependent side of the abdomen with the rest of the soft tissue falling away making surgical procedures easiest in this position.

There was a trend towards a decrease in the distance in the VDR and the VDT. This was due to the increased pressure from the parenchymatous organ mass and the gas cap on the kidneys which led to a medial displacement of the kidneys. This led to the decrease in the distance. There was a statistically significant decrease in the LL and RL in the distance from the right kidney to the aorta when comparing the cranial and caudal halves in the PrI and PoI scans. In the LL the distance showed a statistically significant decrease which was expected as the kidney would sit in the non-dependent part of the abdomen and gravity would pull the kidney closer to the aorta thus decreasing the distance. The RL showed a statistically significant decrease in the distance. This was unexpected as the right kidney lay in the dependent part of the abdomen and the effect of gravity would be to pull the right kidney away from the aorta. This could be linked to the relatively immobile right kidney, as discussed, being less affected by the effects of gravity and thus not moving relative to the vascular structures. So it would have been expected to increase. This effect cannot be explained. However, it still supports that the LL approach is the best surgical approach to the right kidney as it remains in the non-dependent side of the abdomen fully exposed.

Distance from the tip of the transverse process of L2 to the nearest surface of each kidney

There was no statistical difference in any of the positions. In the LL there was a trend towards decreasing the distance. This was due to the effect of gravity pulling the kidney to the dependent side thus decreasing the distance to the tip of the transverse process. The opposite change in the distance was seen in the RL for the same effect of gravity on the right kidney, thus pulling it away from the tip of L2 transverse process.

The left kidney showed a trend towards a decreased distance in the VDR and VDT positions and the LL position. In the VDR the effect of compression from the soft tissue mass by gravity and the pressure from the gas cap was seen more in the left kidney due to less attachments and being relatively more mobile than the right kidney. This moved the left kidney medially and decreased the distance in the VDR. The effect of gravity in the VDT added a cranial pull to the kidney. Due to the vascular attachments of the kidney this force tended to transmit into a medial force, thus decreasing the distance further than the VDR. In the LL it was expected that the distance would increase but a decrease was seen. This could be due to the left kidney being supported by the soft tissue mass surrounding it, propping it up against the dorso-lateral body wall. In the RL there was marked displacement of the left kidney. There was a statistically significant difference in the PrI and PoI scans. The left kidney falls medially and ventrally in the RL due to the effects of gravity and the space

provided by the gas cap in the non-dependent side. This provided excellent exposure of the left kidney for all surgical procedures in the RL position.

Distance from the lateral peritoneal surface of the body wall to the mid lateral serosal surface of the kidney

In the RL there was a significant increase in the distance from the lateral body wall to the left kidney. This was due to the effect of gravity and the space created by the gas cap. The interesting factor was the ventro-medial flipping over of the left kidney. This was probably due to the weak attachments of the left kidney when compared to the right kidney and these attachments being mostly on the medial aspect of the left kidney. This led to relatively more movement compared to the right kidney. The VDR and VDT positions showed an increasing trend and this fitted in with the medial movement of the left kidney that decreased the distance from the kidney to the aorta in the above results. The LL, as expected, showed a trend towards a decrease in the distance as the kidney moves closer to the body wall due to the effects of gravity and the soft tissue mass on top of the kidney. This was less than in the RL as the main attachments to the left kidney are on the medial margin being its vascular supply. There are weak peritoneal attachments to the dorsal body wall that influenced movement. This vascular supply can fold over and move medially more than it can move laterally as it cannot stretch to a marked degree, thus lateral movement would have been less than medial movement.

In the LL there was a significant increased distance from the right kidney to the right body wall when comparing the PrI and PoI scans. This increase was less than that of the left kidney in RL. As described above, the effect of gravity and the space created by the gas cap lead to this effect. The smaller distance was due to the increased rigidity of the right kidney compared to the left kidney due to the attachments to the renal fossa of the liver. In the VDR and VDT there was a trend towards medial movement of the right kidney less so than the left kidney and this was repeated throughout the kidney measurements and fully discussed.

5.7   Adrenals

Distance from the closest aortic wall to the medial surface of the mid-body of the adrenal

There was no statistically significant change in the distance from the left or right adrenals to the aorta in all positions. The left adrenal was statistically closer to the aorta in all positions compared to the right adrenal. These glands are covered on the ventral surface by the peritoneum and have the phrenico-abdominal artery and vein crossing over them. This all

contributed to the adrenals being one of the most fixed organs in the abdominal cavity. Thus it was expected to see very little movement of these glands. These glands were readily visible in all positions in most of the dogs and this may hold clinical implications for diagnostic imaging of pathology of the adrenals in dogs.

5.8   Bladder

Cross sectional diameter of the bladder

There was no statistically significant change in any of the positions. This is expected in all the scans as the diameter of the bladder is accounted for by the water used to inflate the bulb of the Foleys catheter. This amount of water was kept constant at 3 ml. However, the PrI scan of the VDR showed an increase compared to the PoI and all the other scans. This was explained by the possibility that once the catheter was placed and the dog was connected to the urine collection system, time was needed to drain all the urine out even though this increase was not statistically significant. The first scan was done as soon as the patient was stable and ready. This means that urine was still present in the bladder during the first scan in this animal. This gave the higher value for the VDR cross sectional diameter of the bladder compared to all the other scans.

It would have been interesting to set up a manometer connected to the bulb in the Foleys catheter and evaluate the degree of pressure transferred onto the abdominal organs due to the insufflation. This however fell outside of the scope of the study.

Distance from the caudal aspect of the bladder to the rim of the pubis

In the VDR there was a trend towards a decreased distance from the rim of the pubis to the caudal surface of the bladder. This was unexpected as the distance would be expected to increase with the insufflation of carbon dioxide. Bearing in mind that the bladders were relatively empty and thus situated at the cranial border of the pelvic canal which gave the bladder an intra-pelvic position. What was seen in the VDR was the bladder moved closer to the pubic rim with insufflation. This indicated compression of the pelvic structures by the carbon dioxide. This fitted in well with the lack of carbon dioxide penetrating the pelvic canal. The effect of this on surgery of the bladder was thought to be minimal as the bladder would be grasped with an atraumatic forceps for surgical manipulation and possibly then exteriorised by a mini-celiotomy. All of this would be easily achievable in the VDR.

The VDT showed a similar trend but the distances remained larger than in the VDR. This was due to the effect of gravity when the pelvic limbs were elevated above the head. This tended to draw the bladder cranially, thus increasing the distances seen.

In the LL the same was seen as above for the same reasons. However, the RL showed the opposite trend in that the distance increased. A plausible reason for this was that in this position the colon lies in the pelvic cavity and prevents compression of the bladder. The bladder may be displaced under the effect of gravity over the dorsal aspect of the colon thus increasing the distance. This was however speculation as it cannot be proven.

Distance from the apex of the bladder to the ventral body wall

In all positions except the RL there was a statistically significant increase in the distance from the ventral body wall to the apex of the bladder when comparing the PrI and PoI. However the RL showed a trend to wards an increase which was approaching a significant change. It should be considered that even the RL was not statistically significant and it needs to be discussed with the other positions as one can clearly see the trend on PrI and PoI scans. The reason for this was twofold. The bladder appears to be compressed into the pelvic cavity as a result of the increased intra-abdominal pressure from the insufflation. The peritoneal reflections that separate the pelvic cavity from the abdominal cavity are attached to the bladder, the uterus and the colon. These tend to hold the distal bladder neck in place thus causing it to be compressed into the pelvic cavity. The insufflation of carbon dioxide caused an increase in abdominal diameter, thus increasing the distance from the body wall to the apex of the bladder further.

The surgical implications are that the gas cap creates a space for one to work in. The bladder lies in the caudal part of this space, but is well exposed for surgical manipulation as it lies ventrally to the soft tissue mass and is thus encountered first of all the organs of the caudal abdominal cavity.

5.9   Uterus and Ovaries

Cross sectional diameter of the uterine body at the pelvic inlet

There was no change in the size of the uterine body which was expected as the effects of the increased intra-abdominal pressure did not cause any hollow organ compression in any other organ systems.

Cross sectional length and width of the ovary

There was no change in the size of either ovary.

Length of visible uterus from the mid-pubic symphysis and both uterine horns

The lateral positions provided the best view of the uterus and ovaries due to the space created by the gas cap around the kidney. The displacement of the organs to the dependent

side by gravity meant that the left ovary and uterine horn were best seen in RL and vice versa for the right ovary and uterine horn. The attachment of the ovary to the caudal pole of the kidney via the suspensory ligament allows the ovary and hence the uterus, due to its attachment to the ovary via the proper ligament, to remain in the non-dependent side and not be affected by gravity. Even though visibility was not statistically different in the lateral positions from the ventro-dorsal positions, separation of the uterine body was clearly seen in the lateral positions. This was not measured for statistical analysis. However the surgical indications are that a lateral approach or lateral 45˚ oblique position to each respective ovary was proven to be the best approach for an ovariohysterectomy and is in use today[27]. The patient will have to be rotated on the surgical table so draping will have to accommodate this. The cervix would have to be approached through a ventral approach and preferably a VDT position, as this moves the soft tissue mass cranially exposing the uterine body. This was difficult to see in the CT images as the uterus was the same shape and opacity as empty intestine, but all other indications for the VDT have shown cranial movement of the soft tissue mass. With the cervix being attached to the vagina, the cranial movement was restricted, thus leaving it exposed for surgical exposure. This cannot be proved by this study but can be assumed from the other changes seen in the soft tissue mass.

Length of contact / distance between uterine body and colon

The uterine body and colon remained in contact for the entire length that the uterine body was visible. This was due to the close association between these two organs and their peritoneal attachment. There was no further change after insufflation as the gas cap seemed to compress the pelvic cavity rather than dilate it.

Distance from the caudal pole of the kidney to the cranial pole of the ovary

This distance was essentially a measurement of the suspensory ligament length. In all positions regarding the right suspensory ligament, there was a trend towards an increase between the PrI and PoI length. This was to be expected. However, the left only showed increases in the VDR and VDT. At the OVAH we teach students that when they start spaying to always start with the left ligament as it is longer than the right and easier to expose. This was not the case seen here. The right kidney may lie further cranial and hence the right ovary, giving the impression of a shorter suspensory ligament. In this study however the right suspensory ligament appears to be longer or more lax than the left.

CHAPTER 6: CONCLUSION

In conclusion the two main forces acting on the organs in the abdominal cavity are gravity due to patient position and the pressure and space created by the insufflated gas. Gravity has to be considered the main force as changes are seen with changes in position. The gas cap creates a space for the organs to gravitate to the dependant part of the abdomen or remain in their normal positions due to their peritoneal attachments. The effects of pressure from gas could be seen more on the extra-abdominal structures than the intra-abdominal structures. The position of organs can be manipulated by moving the patient around into different positions allowing easier access to organs laparoscopically. However, the need for manual intra-abdominal retraction will be essential in all laparoscopic procedures and cannot be replaced by positional changes.

In conclusion the best positions for the following organ systems are the following: the VDR, which provides the best exposure to the liver (all lobes), gall bladder and the pancreas; the VDT provides the best exposure to the stomach, pancreas, pylorus, bladder, cervix and can be used as a secondary position for the liver; the LL provides the best approach to the liver (right lobes), cystic duct, duodenum, right kidney, right ovary and uterine horn and as a tertiary position for the gallbladder; the RL provides the best approach to the liver (left lobes), spleen, left kidney and left ovary and uterine horn.

All patients undergoing laparoscopy should be prophylactically treated for reflux until studies, showing that no increase in the incidence of reflux oesophagitis in animals undergoing laparoscopy, are performed.

Limitations of the study

This was a CT based study and in certain positions, given the ability of CT to prevent superimposition of organs on one another, it became very difficult to evaluate three-dimensionally the route to an organ from the skin. This would be the case in a laparoscopic approach to an organ. This was evident with the pancreas and is the main limitation of this study. Only beagles were used and given the variations in the anatomy of the different dog breeds this may not be representative of the extremes of the population such as the bulldog.

The data was only reviewed by one of the authors, who was not blinded to the position which the dog was in or the type of scan, PrI or PoI. This may have left the study open to bias.

REFERENCES

1. Gutt CN, Oniu T, Schemmer P,et al. Fewer adhesions caused by laparoscopic surgery? *Surg Endosc* 2004;18:898-906.

2. Sanchez-Margallo FM, Loscertales B, Diaz-Guemes I, et al. Technical feasibility of laparoscopic Finney pyloroplasty examined in a canine model. *Surg Endosc* 2007;21:136-139.

3. Rivero MA, Vazquez JM, Ramirez JA, et al. CT-soft tissue window of the cranial abdomen in clinically normal dogs: an anatomical description using macroscopic cross-sections with vascular injection. *Anat Histol Embryol* 2008 ;38:18-22.

4. Hathcock JT, Stickle RL. Principles and concepts of computed tomography. *Vet Clin North Am: Small Anim Pract* 1993;23:399-415.

5. Stickle RS, Hathcock JT. Interpretation of computed tomographic images. *Vet Clin North Am: Small Anim Pract* 1993;23:417-435.

6. Tidwell AS. Advanced imaging concepts: a pictorial glossary of CT and MRI technology. *Clin Tech Small Anim Prac* 1999;14:65-111.

7. Tidwell AS. Principles of computed tomography and magnetic resonance imaging, In. Thrall D E, ed. *Textbook of veterinary diagnostic radiology*. 5th ed. Missouri: Saunders Elsevier, 2007;50-77.

8. Wink NM, McNitt-Gray MF, Solberg TD. Optimization of multi-slice helical respiration-correlated CT: the effects of table speed and rotation time. *Physic Medic Biol* 2005;50:5717-5729.

9. Zwingenberger AL, Schwarz T. Dual-phase CT angiography of the normal canine portal and hepatic vasculature. *Vet Radiol Ultrasound* 2004;45:117-124.

10. Frank P, Mahaffey M, Egger C, et al. Helical computed tomographic portography in ten normal dogs and ten dogs with a portosystemic shunt. *Vet Radiol Ultrasound* 2003;44:392-400.

11. Winter MD, Kinney LM, Kleine LJ. Three-dimensional helical computed tomographic angiography of the liver in five dogs. *Vet Radiol Ultrasound*. 2005;46:494-499.

12. LeBlanc AK, Daniel GB. Advanced imaging for veterinary cancer patients. *Vet Clin North Am: Small Anim Pract*. 2007;37:1059-1077.

13. Sugimoto M, Yasuda H, Koda K, et al. Virtual CO_2 MDCT pancreatography: a new feasible technique for minimally invasive pancreatectomy in intraductal papillary mucinous neoplasm's. *Hepatogastroenterol* 2008;55:270-274.

14. Caceres AV, Zwingenberger AL, Hardam E, et al. Helical computed tomographic angiography of the normal canine pancreas. *Vet Radiol Ultrasound* 2006;47:270-278.

15. Probst A, Kneissl S. Computed tomographic anatomy of the canine pancreas. *Vet Radiol Ultrasound* 2001;42:226-230.

16. Samii VF, Biller DS, Koblik PD. Normal cross-sectional anatomy of the feline thorax and abdomen: comparison of computed tomography and cadaver anatomy. *Vet Radiol Ultrasound* 1998;39:504-511.

17. Teixeria M, Gil F, Vazquez JM, Cardoso L, et al. Helical computed tomographic anatomy of the canine abdomen.*Vet Journal* 2007;174:133-138.

18. Zwingenberger AL, McLear RC, Weisse C. Diagnosis of arterioportal fistulae in four dogs using computed tomographic angiography. *Vet Radiol Ultrasound* 2005;46:472-477.

19. Rozear L, Tidwell AS. Evaluation of the ureter and uretervesicular junction using helical computed tomographic excretory urography in healthy dogs. *Vet Radiol Ultrasound* 2003;44:155-164.

20. Fife WD, Samii VF, Drost T, et al. Comparison between malignant and non-malignant splenic masses in dogs using contrast-enhanced computed tomography. *Vet Radiol Ultrasound* 2004;45:289-297.

21. Panebianco V, Grazhdani H, Iafrate F, et al. 3D CT protocol in the assessment of oesophageal neoplastic lesions: can it improve TNM staging? *Eur Radiol* 2006;16:414-421.

22. Russell ST, Kawashima A, Vrtiksa TJ, et al. Three-dimensional CT virtual endoscopy in the detection of simulated tumours in a novel phantom bladder and ureter model. *J Endourol* 2005;19:188-192.

23. Ezzeddine D, Ezzeddine B, Mckenzie R, et al. Virtual gastroscopy: Initial attempt in North American patients. *J Gastroenter Hepatol* 2006;21:219-221.

24. Jackowski C, Bolliger S, Thali MJ. and unexpected findings in mummies from ancient Egypt and south America as revealed by CT. *RadioGraphics* 2008;28:1477-1492.

25. Bajka M, Manestar M, Hug J, et al. Detailed anatomy of the abdomen and pelvis of the visible human female. *Clin Anat* 2004;17:252-260.

26. Taken from "Siemens dual slice CT manual 2007" Siemens Erlangen, Germany.

27. Monnet E, Lhermette P, Sobel D. Rigid endoscopy: laparoscopy. In, Lhermette P, Sobel D, eds. *Canine and feline endoscopy and endosurgery*. 1st ed. Gloucester: British Small Animal Veterinary Association, 2008;158-174.

28. Monnet E, Twedt DC. Laparoscopy. *Vet Clin North Am: Small Anim Pract* 2003;33:1147-1163.

29. Richter KP. Laparoscopy in dogs and cats. *Vet Clin North Am: Small Anim Pract* 2001;31:707-727.

30. Vaden SL . Renal biopsy of dogs and cats. *Clinc Tech Small Anim Prac* 2005;20:11-22.

31. Webb CB, Trott C. Laparoscopic diagnosis of pancreatic disease in dogs and cats. *J Vet Intern Med* 2008;22:1263-1266.

32. Freeman LJ. Gastrointestinal laparoscopy in small animals. *Vet Clin North Am: Small Anim Pract* 2009;39:903-924.

33. Brisson BA, Holmberg DL, House M. Comparison of mesenteric lymphadenography performed via surgical and laparoscopic approaches in dogs *Am J Vet Res* 2006;67:168-173.

34. Mathon DH, Dossin O, Palierne S, et al. A laparoscopic-sutured gastropexy technique in dogs: mechanical and functional evaluation. *Vet Surg* 2009;38:967-974.

35. Machado MAC, Galvao FHF, Pompeu E, et al. A canine model of laparoscopic segmental liver resection. *J Laparo Ad Surg Tech* 2004;14:325-328.

36. Rawlings CA, Mahaffey MB, Bement S, et al. Prospective evaluation of laparoscopic-assisted gastropexy in dogs susceptible to gastric dilatation. *J Am Vet Med Assoc* 2002;221:1576-1581.

37. Mayhew PD. Advanced laparoscopic procedures (hepatobillary, endocrine) in dogs and cats. *Vet Clin North Am: Small Anim Pract* 2009;39:925-939.

38. Sanchez- Margallo FM, Soria-Galvez F, Ezquerra-Calvo LJ, et al. Comparison of the ultrasonographic characteristics of the gastroduodenal junction during pyloroplasty performed laparoscopically or via conventional abdominal surgery in dogs. *Am J Vet Res* 2003;64:1099-1104.

39. Lew M, Jalynski M, Brzeski W. Laparoscopic removal of gastric foreign bodies in dogs—comparison of manual suturing and stapling viserosynthesis. *Pol J Vet Sci* 2005;8:137-153.

40. Chandler JC, Kudnig ST, Monnet E. Use of laparoscopic-assisted jejunostomy for faecal diversion in the management of rectocutaneous fistula in a dog *J Am Vet Med Assoc* 2005;226:746-751.

41. Hewitt SA, Brisson BA, Sinclair MD, et al. Evaluation of laparoscopic-assisted placement of jejunostomy feeding tubes in dogs. *J Am Vet Med Assoc* 2004;225:65-71.

42. Davidson EB, Moll HD, Payton ME. Comparison of laparoscopic ovariohysterectomy and ovariohysterectomy in dogs. *Vet Surg* 2004;33:62-69.

43. Devitt CM, Cox RE, Hailey JJ. Duration, complications, stress, and pain of open ovariohysterectomy versus a simple method of laparoscopic-assisted ovariohysterectomy in dogs. *J Am Vet Med Assoc* 2005;227:921-927.

44. Austin B, Lanz OI, Hamilton SM, et al. Laparoscopic ovariohysterectomy in nine dogs. *J Am Anim Hosp Assoc* 2003;39:391-396.

45. Hankock RB, Lanz OI, Waldron DR, et al. Comparison of the post operative pain after ovariohystererectomy by harmonic scalpel-assisted laparoscopy compared with median celiotomy and ligation in dogs. *Vet Surg* 2005;34:273-282.

46. Dupre G, Fiobianco V, Skalicky M, et al. Laparoscopic ovariectomy in dogs: comparison between single portal and two-portal access. *Vet Surg* 2009;38:811-817.

47. Van Goethem B, Schaefers-Okkens A, Kirpensteijn J. Making a rational choice between ovariectomy and ovariohysterectomy in the dog: a discussion of the benefits of either technique. *Vet Surg* 2006;35:136-143.

48. Miller NA, Van Lue SJ, Rawlings CA. Use of laparoscopic-assisted cryptorchidectomy in dogs and cats. *J Am Vet Med Assoc*. 2004;224:875-878.

49. Rawlings CA. Resection of inflammatory polyps in dogs using laparoscopic-assisted cystoscopy. *J Am Anim Hosp Assoc* 2007;43:342-346.

50. Rawlings CA, Mahaffey MB, Barsanti JA, et al. Use of laparoscopic-assisted cystoscopy for removal of urinary calculi in dogs. *J Am Vet Med Assoc* 2003;222:759-761.

51. Salomon JF, Coitard JP, Viguier E. Management of urethral sphincter mechanism incompetence in a male dog with laparoscopic-guided deferentopexy. *J Small Anim Prac* 2002;43:501-505.

52. Prince DT, Chari RS, Neighbours JD, et al. Laparoscopic radical prostatectomy in the canine model. *J Laparoendosc Surg* 1996;6:405-412.

53. Kovak J, Buote NJ. Complications and need for conversion to laparotomy in small animals. *Vet Clin North Am: Small Anim Pract* 2009;39:941-951.

54. Duerr FM, Twedt DC, Monnet E. Changes in pH of peritoneal fluid associated with carbon dioxide insufflations during laparoscopic surgery in dogs. *Am J Vet Res* 2008;69:298-301.

55. Evans HE. The digestive apparatus and abdomen. In; Evans HE, Miller ME, eds. *Millers anatomy of the dog*. 3rd ed. Philadelphia: WB Saunders Co, 1993; 385-462.

56. Evans HE, Christensen GC. The urogenital system. In; Evans HE, Miller ME, eds. *Millers anatomy of the dog*. 3rd ed. Philadelphia: WB Saunders Co, 1993; 494-598.

57. Laflamme DP. Development and validation of body condition score for dogs. *Canine Pract.* 1997;22:10-15.

58. Gayer G, Jonas T, Apter S, et al. Postoperative pneumoperitoneum as detected by CT: prevalence, duration, and relevant factors affecting its possible significance. *Abdom Imaging* 2000;25:301-305.

59. Mastrangelo MJ, Adrales G, McKinley R, et al. Inclusion of 3-D computed tomography rendering and immersive VR in a third year medical student surgery curriculum. *ST Heal T* 2003;94:199-203.

60. Galatos AD, Raptopoulos D. Gastro-oesophageal reflux during anaesthesia in the dog: The effect of age, positioning and type of surgical procedure. *Vet Rec* 1995;137 513-516.

APPENDIX 1 – Experimental Dog Data

	Dog 1	Dog 2	Dog 3	Dog 4	Dog 5	Dog 6	Dog 7
Date of birth	14/05/06	14/05/06	16/06/08	14/05/06	18/06/08	18/01/06	14/05/06
Weight	10.7kg	13kg	11kg	12kg	10.4	11kg	13
BCS	3	4	3	3	3	3	4
Microchip	978006000 0740473	978000000 739831	978000001 549333	978800000 0769061	978000001 566777	978000000 743734	978000000 740072
Blood smear abnormalities		Eosinophilia	Monocytosis		Mild left shift	Mild left shift Mild monocytosis	Mild left shift
De-worming date	03/06/10	03/06/10	03/06/10	03/06/10	03/06/10	03/06/10	03/06/10
Urinalysis	pH-6 SG-1.030	pH-6 SG-1.015	pH-7 SG-1.025	pH-7 Blood 1+ SG-1.028	pH-7 SG-1.020	pH-7 Blood 4+ SG-1.022	pH-8 SG-1.030
Abdominal ultrasound abnormalities		Right adrenomegally 7.8mm mild ventral bladder wall thickening					
Inclusion into study	Yes	Yes	Yes	Yes	Yes	Yes	Reserve animal

APPENDIX 2-CT Scan Data

	Dog 1	Dog 2	Dog 3	Dog 4	Dog 5	Dog 6
Slice collimation	2.5mm	2.5mm	2.5mm	2.5mm	2.5mm	2.5mm
Slice thickness	3mm	3mm	3mm	3mm	3mm	3mm
Pitch	2	2	2	2	2	2
Field of view	263mm	285mm	279mm	316mm	316mm	300mm
kV	110kV	110kV	110kV	110kV	110kV	110kV
mAs total	16206	18156	17424	21598	17998	17295
Tube rotation time	0.8s	0.8s	0.8s	0.8s	0.8s	0.8s
Kernel	B41s medium +	B41s medium +	B41s medium +	B41s medium +	B41s medium +	B41s medium +
Window Width / level	300/40	300/40	300/40	300/40	300/40	300/40
CTDI	14.95	16.29	15.06	18.89	15.35	15.33
Scan date	04/06/10	05/06/10	05/06/10	05/06/10	05/06/10	05/06/10
Start time	15h00	07h35	09h05	10h28	11h45	12h55
Finish time	16h40	08h35	10h00	11h15	12h25	13h55

APPENDIX 3- Data Capture Sheets

Data Capture Sheets

Animal no.

Scan Type.   **VDR**   **VDT**   **LL**   **RL**

Extra-abdominal measurements and general abdominal measurements

	Routine scan	Post Insufflation	Comments
Oesophageal short axis diameter			
Oesophageal long axis diameter			
Oesophageal content			
Cranial extent of the diaphragmatic cupula			
Gas in the pelvic cavity / pixel value			
Peritoneal reflections visible			
Abdominal parenchymatous organ height % of abdm height at umbilicus	PO AH	PO AH	

Liver measurements

	Routine	Post Insufflation	Comments
Distance from the caudal xiphoid to liver			
The % contact between liver and body wall T11	AD LC	AD LC	
Distance of apex of gallbladder to right abdm wall			
The % contact of hepatic parenchyma to gallbladder	HGBC GBD	HGBC GBD	
% gallbladder exposed	GBE GBD	GBE GBD	
Separation of liver lobes			
Distance of lesser curvature of stomach to caudal portion of			

the caudate lobe of the liver		
Distance from the head of the spleen to the left lateral lobe of the liver		
Cystic duct visibility		
Distance between the vena porta and vena cava		

Splenic measurements

	Routine	Post insufflations	Comments
% Contact of the spleen with body wall	BWC LSL	BWC LSL	
Hilar access			
Distance from pelvis of left kidney to the caudal portion of the head of the spleen			
Contact distance between spleen and the stomach			

Gastro-intestinal measurements

	Routine	Post Insufflation	Comments
Position of the pylorus in relation to the vertebral column			
Stomach cross section long axis and short axis	*LA* *SA*	*LA* *SA*	
Distance of the mid descending duodenum from the body wall			
Distance of cranial duodenal flexure to the gallbladder			
Distance from pelvis of the right kidney to the descending duodenum			

Pancreas measurements

	Routine	Post Insufflation	Comments
Visible length of the right limb along descending duodenum	L	L	
Visible length of the body of the pancreas at cranial duodenal flexure	L	L	
Visible length of the left limb of the pancreas caudal to the greater curvature	L	L	

Kidney measurements

	Routine	Post Insufflation	Comments
Cross sectional diameter of kidneys	R L	R L	
Distance from the cranial pole of the right kidney to the renal fossa of the liver			
Distance from the cranial and caudal halves of the kidneys to the aorta	RCr RCd LCr LCd	RCr RCd LCr LCd	
Distance from tip of transverse proc of L2 to the nearest surface of the kidney	R L	R L	
Distance from the lateral peritoneal surface of the body wall to the mid lateral serosal surface of the kidney	R L	R L	

Adrenal measurements

	Routine	Post Insufflation	Comments
Distance from the closest aortic wall to medial surface of the mid-body of the adrenal	R L	R L	

Bladder

	Routine	Post Insufflation	Comments
Cross sectional diameter of the bladder			
Distance from the caudal aspect of the bladder to the rim of the pelvis			
Distance from the apex of the bladder to the ventral body wall			

Uterus and Ovarian measurements

	Routine	Insufflation	Comments
Cross sectional diameter of uterus at the level of the pelvic inlet			
Cross sectional length and width of the ovaries	R L	R L	
Length of visible uterus from the mid-pubic symphsis and along both uterine horns	LH RH UB	LH RH UB	
Length / contact distance between the uterine body and colon			
Distance from caudal pole of the kidney to the cranial pole of the ovary	R L	R L	